

A Novel Control Strategy for a Static Interphase Power Controller

Khalid Ibrahim Elamari

A Thesis

In the Department

Of

Electrical and Computer Engineering

Presented in Partial Fulfillment of the Requirements

For the Degree of

Doctor of Philosophy (Electrical and Computer Engineering) at

Concordia University

Montréal, Québec, Canada

October 2018

© Khalid Ibrahim Elamari, 2018

CONCORDIA UNIVERSITY
SCHOOL OF GRADUATE STUDIES

This is to certify that the thesis prepared

By: Khalid Ibrahim Elamari

Entitled: A Novel Control Strategy for a Static Interphase Power Controller

and submitted in partial fulfillment of the requirements for the degree of

Doctor Of Philosophy (Electrical and Computer Engineering)

complies with the regulations of the University and meets the accepted standards with respect to originality and quality.

Signed by the final examining committee:

_____	Chair
Dr. Catherine Mulligan	
_____	External Examiner
Dr. Ilhan Kocar	
_____	External to Program
Dr. Marius Paraschivoiu	
_____	Examiner
Dr. Shahin Hashtrudi Zad	
_____	Examiner
Dr. Chunyan Lai	
_____	Examiner
Dr. Jacques Brochu	
_____	Thesis Supervisor
Dr. Luiz A.C. Lopes	

Approved by

Dr. Mustafa Mehmet Ali, Graduate Program Director

December 13,
2018

Dr. Amir Asif, Dean
Gina Cody School of Engineering and Computer Science

Abstract

A Novel Control Strategy for a Static Interphase Power Controller

Khalid Ibrahim Elamari, PhD.

Concordia University, 2018

With the rapid increase of electricity demand, the possibility of overloading the existing power transmission lines increases. Building new transmission lines can be avoided or delayed, provided that fast and accurate means for controlling active and reactive power are made available. There are a number of Flexible AC Transmission System (FACTS) devices that can help meeting these goals. Among them is the Interphase Power Controller (IPC), which presents an important characteristic: Active power regulation in a transmission line with a highly variable transmission angle. Its original implementation is based on mechanically controlled phase-shifting transformers, which are relatively slow and only allow active and reactive power flow control in a discrete range. Static IPCs can be realized with three Voltage Source Converters (VSCs) in a configuration called dual Unified Power Flow Controller (UPFC). However, this Unified IPC (UIPC) has been controlled as a Static Phase Shifter (SPS) and does not make use of all the flexibility offered by the dual UPFC.

This thesis discusses the operation of the dual UPFC of the UIPC with all its features: Phase shifting and reactive power compensation, series and shunt. The complexity of the control logic increases since the number of control variables increases from two to four. To address this issue, a control strategy based on the sharing of the real and imaginary components of the desired transmission line current among the capacitive and inductive branches of the UIPC is proposed. The control variables are then computed with an optimization algorithm that minimizes the apparent power of the VSCs of the capacitive and inductive branches for increased efficiency. The superior performance of the proposed scheme over the conventional one is demonstrated based on analytical expressions.

The performance of the proposed control scheme is also investigated in the time domain. For that, dynamic models of the system required for designing the control loops of the currents in the inductive branch, capacitive branch, shunt branch and DC bus voltage are derived. Proportional plus Integral (PI) type controllers in the dq (rotating reference) frame and Proportional Resonant (PR) controller in the abc (stationary reference) frame are designed. The dynamic performance of the system is verified by means of simulation using PSCAD/EMTDC. Besides, a reduced-scale prototype controlled with a rapid prototyping real-time control hardware was built to further validate the performance of the system experimentally.

ACKNOWLEDGMENTS

I would like to express my gratitude to my supervisor, Dr. Luiz Lopes who was abundantly helpful and offered invaluable assistance, support and guidance.

I would like to acknowledge the Libyan Ministry of Higher Education and Scientific Research and Concordia University for their financial support.

I would also like to thank my other distinguished professor, Pragasen Pillay and my colleagues in the Power Electronics and Energy Research (PEER) group. A very special thanks to my colleagues, Ahmad Malkawi, for his motivation and encouragement during my study.

Last, but not least, I would like to express my love and gratitude to my beloved parents, Fatima and Ibrahim for endless giving and tender. I also wish to express my gratitude to my brothers and sisters for their support. I would like to express gratitude to my wife, Zainab, for her understanding and patient through the duration of my study, and my three wonderful children, Janan, Alaa, and Musab, who provide unending inspiration.

I cannot close without express my sincere gratitude to my close relatives and friends for their steady support and encouragement.

Table of Contents

List of Figures	ix
List of Tables	xiii
Nomenclature	xiv
CHAPTER 1. INTRODUCTION	1
1.1. Introduction.....	1
1.2. Flexible AC Transmission System (FACTS) Devices	3
1.3. The Basic Interphase Power Controller (IPC).....	4
1.3.1. The Phase Shifting Transformer (PST).....	5
1.3.2. The Limitations of the Basic Interphase Power Controller (IPC).....	7
1.4. Literature Review of the Static Interphase Power Controller.....	8
1.5. The Unified Interphase Power Controller (UIPC).....	10
1.6. The Scope of the Research Work	12
1.7. Outline of the Thesis.....	14
1.8 List of Publications	15
CHAPTER 2. COMPARISON OF CONVENTIONAL AND PROPOSED CONTROL STRATEGY OF THE UIPC	16
2.1. Introduction.....	16
2.2. The Unified Interphase Power Controller (UIPC).....	16
2.2.1. The Unified Power Flow Controller (UPFC).....	17
2.2.2. The Operation Principle of the UPFC.....	17
2.2.3. The operations principle of the Unified Interphase Power Controller (UIPC).....	18
2.3. The Conventional (SPS-based) UIPC.....	20
2.3.1. Mathematical Model of the SPS-based UIPC.....	21
2.3.2. Calculation of the Control Parameters of the SPS-based UIPC	23
2.4. The Proposed (UPFC-based) UIPC	23
2.4.1. Mathematical Model of the UPFC-based UIPC	24
2.4.2. Control Limits of the UPFC-based UIPC	24
2.4.3. Calculation of the Control Parameters of the UPFC-UIPC	25
2.4.4. Parameter Calculation by Means of Optimization.....	26

2.5. Case Study	27
2.5.1. The Unity Power Factor (UPF) Case (PF = 1).....	28
2.5.2. PF = 0.8/ Leading Case.....	31
2.5.3. PF = 0.8/ Lagging Case.....	34
2.5.4. Comparison of the Simulation Results of the SPS-UIPC and the UPFC-based UIPC.....	37
2.6. Summary.....	39
CHAPTER 3. SIMULATION VERIFICATION OF THE UPFC-BASED UIPC.....	40
3.1. Introduction.....	40
3.2. The Unified Interphase Power Controller (UIPC) Model in PSCAD/EMTDC	40
3.2.1. The Model of the Dual UPFC on the PSCAD/EMTDC	41
3.2.2. The Parameters of the UPFC-based UIPC	42
3.3. The Mathematical Model and Control Strategy of the Shunt Converter (VSC3) of the UPFC-Based-UIPC	45
3.3.1. The Mathematical Model of the Inner Current Loop of the Shunt Branch in the dq Frame	46
3.3.2. The Mathematical Model for the Outer Voltage Control Loop of the Shunt Branch (DC Voltage Controller)	48
3.4. Realizing the Proposed Control Strategy for the Series VSCs of the UPFC-based UIPC	52
3.4.1. Proportional Resonant (PR) Controller.....	53
3.4.2. The Mathematical Model of the Series Branches of the UPFC-Based-UIPC in the abc Stationary Frame	54
3.4.3. Realizing the Current References in abc-Frame for the PR Controllers.....	56
3.5. Case Study	58
3.6. Simulation Results	59
3.6.1. Simulation Results to Investigate the Performance of PR Controllers of the Series Branches.....	59
3.6.2. Simulation Results to Investigate the Performance of the Shunt Branch Controller.....	67
3.7. Summary.....	69
CHAPTER 4. THE SYNCHRONOUS REFERENCE FRAME (DQ) CONTROLLER.....	70
4.1. Introduction.....	70
4.2. The Mathematical Model of the Series Branches of the UPFC-based-UIPC in dq Frame	70

4.2.1. The Mathematical Model for the Inductive Branch of the UPFC-based-UIPC.....	71
4.2.2. The Mathematical Model of the Capacitive Series Branch of UPFC-based-UIPC	73
4.2.3. Realizing the Current and Voltage References for the dq Controllers	78
4.3. Case Study	81
4.4. Simulation Results	81
4.3.1. Simulation Results of the UPF Case ($\phi_{ITL} = 0^\circ$)	81
4.3.2. Simulation Results of the Leading PF Case (0.8 and $\phi_{TL} = 36.87^\circ$)	85
4.3.3. Simulation Results of the Lagging PF Case (0.8 and $\phi_{ITL} = - 36.87^\circ$).....	88
4.4.4 Comparison of the Simulation Results of the UPFC-based UIPC Between the PR Controller and dq Controller in the Steady State Condition	91
4.5. Summary	92
CHAPTER 5. THE EXPERIMENTAL IMPLEMENTATION OF THE UPFC-BASED UIPC.....	94
5.1. Introduction.....	94
5.2. The Modification of the Electric Circuit with the UIPC	94
5.2.1. The Scaled-Down System for Experimental Verification	95
5.2.2. Redefining the Reference Voltage to V_{RS}	96
5.2.3. The Components of the Experimental Set-up:.....	96
5.3. Control Strategy for the Series VSCs of the UPFC-UIPC.....	100
5.4. Simulation and Experimental Results.....	101
5.4.1. UPF Case	103
5.4.2. Leading PF Case	106
5.4.3. Lagging PF Case	107
5.5. Summary	107
CHAPTER 6. CONCLUSION AND THE FUTURE WORK	108
6.1. Conclusion	108
6.2. Future Work.....	112
REFERENCES.....	113
APPENDICES	118

List of Figures

Figure 1-1: Interconnected transmission power system.....	1
Figure 1-2: classification of the FACTS devices based on their connections to the transmission system	3
Figure 1-3: The generic circuit of the IPC	4
Figure 1-4: (A) The winding connections of the indirect-symmetrical PST (B) The phasor diagram [28].....	6
Figure 1-5: Schematic diagram of the basic IPC (PST-based IPC).....	8
Figure 1-6: Schematic diagram of the TC-based IPC.....	9
Figure 1-7: Schematic diagram of the SSSC-based IPC.....	10
Figure 1-8: Schematic diagram of the UIPC.....	11
Figure 2-1: Single-line schematic diagram of the UIPC.....	16
Figure 2-2: Simple diagram of the UPFC	17
Figure 2-3: The considered operations modes of the UPFC (SPS, and UPFC mode) for the UIPC application.....	18
Figure 2-4: Schematic diagram of the UIPC showing the three VSCs and the voltages and currents in the various nodes and branches, respectively	19
Figure 2-5: The equivalent circuit of the UIPC controlled as two SPSs.	21
Figure 2-6: The 2-node transmission system with the UIPC connected at the sending end.....	27
Figure 2-7: Comparison of the results (A) $V_{injL-SPS}$ and $V_{injL-UPFC}$ (B) $V_{injC-SPS}$ and $V_{injC-UPFC}$; for different values of I_{TL} and δ and the UPF case ($PF=1$).	29
Figure 2-8: Comparison of the results (A) The absolute values of I_{L-SPS} & I_{L-UPFC} , and I_{TL} (B) The absolute values of I_{C-SPS} & I_{C-UPFC} and I_{TL} ; for different values of I_{TL} , δ , and $PF=1$	30
Figure 2-9: Comparison of the results (A) $S_{injL-SPS}$ and $S_{injL-UPFC}$ (B) $S_{injC-SPS}$ and $S_{injC-UPFC}$; for different values of I_{TL} and δ and $PF=1$	30
Figure 2-10: Comparison of the results (A) V_{L-SPS} and V_{C-SPS} (B) V_{L-UPFC} and V_{C-UPFC} ; for different values of I_{TL} and δ and for $PF = 1$	31
Figure 2-11: Comparison of the results (A) $V_{injL-SPS}$ and $V_{injL-UPFC}$ (B) $V_{injC-SPS}$ and $V_{injC-UPFC}$; for different values of I_{TL} and δ and for $PF=0.8/leading$	32
Figure 2-12: Comparison of the results (A) The absolute values of I_{L-SPS} & I_{L-UPFC} , and I_{TL} (B) The absolute values of I_{C-SPS} & I_{C-UPFC} and I_{TL} ; for different values of I_{TL} and δ and $PF=0.8/leading$	33
Figure 2-13: Comparison of the results (A) $S_{injL-SPS}$ and $S_{injL-UPFC}$ (B) $S_{injC-SPS}$ and $S_{injC-UPFC}$; for different values of I_{TL} and δ and $PF=0.8/leading$	33
Figure 2-14: Comparison of the results (A) V_{L-SPS} and V_{L-UPFC} (B) V_{C-SPS} and V_{C-UPFC} ; for different values of I_{TL} and δ and $PF=0.8/leading$	34

Figure 2-15: Comparison of the results (A) $V_{injL-SPS}$ and $V_{injL-UPFC}$ (B) $V_{injC-SPS}$ and $V_{injC-UPFC}$; for different values of I_{TL} and δ and $PF=0.8$ /lagging	35
Figure 2-16: Comparison of the results (A) Absolute values of I_{L-SPS} and I_{L-UPFC} and I_{TL} (B) Absolute values of I_{C_SPS} and I_{C-UPFC} , and I_{TL} ; for different values of I_{TL} and δ and $PF=0.8$ /lagging	35
Figure 2-17: Comparison of the results (A) $S_{injL-SPS}$ and $S_{injL-UPFC}$ (B) $S_{injC-SPS}$ and $S_{injC-UPFC}$; for different values of I_{TL} and δ and $PF=0.8$ /lagging	36
Figure 2-18: Comparison of the results (A) V_{L-SPS} and V_{C-SPS} (B) V_{L-UPFC} and V_{C-UPFC} ; for different values of I_{TL} and δ and for $PF=0.8$ /lagging	37
Figure 3-1: The Schematic diagram of the UIPC Model	40
Figure 3-2: The connection of the three VSCs to realize the structure of the Dual UPFC.....	41
Figure 3-3: The connection of three single phase, two winding, and transformers to form the series coupling transformers (T1 or T2) for each branch of the UPFC-based-UIPC	42
Figure 3-4: The considered UIPC circuit for the control design	45
Figure 3-5: The circuit of the shunt branch	46
Figure 3-6: The equivalent circuit of the shunt branch (A) d circuit (B) q circuit	47
Figure 3-7: The block diagram for the design of the PI-type controller of the shunt branch (inner current loop).....	48
Figure 3-8: The circuit of the DC link	48
Figure 3-9: The block diagram for the design of DC voltage control	50
Figure 3-10: Schematic diagram of the outer and inner control block of the shunt VSC3.....	51
Figure 3-11: Bode Diagram (A) ideal PR controller with, $K_p = 1$, $K_i = 100$, $\omega_o = 2\pi 60$ (rad/s), (B) non-ideal PR controller with $K_p = 1$, $K_i = 100$, $\omega_o = 2\pi 60$, $\omega_c = 10$ (rad/s).....	53
Figure 3-12: The single line diagram of the inductive branch.....	54
Figure 3-13: The single line diagram of the capacitive branch	55
Figure 3-14: Schematic diagram of the proposed control scheme for the UPFC-UIPC with optimal current sharing factors and PR controllers, Eq are (3.31 and 3.32).....	57
Figure 3-15: Simulation waveforms for UPF case: (A) $I_{TL} = 0.5$ pu (B) $I_{TL} = 1$ pu. Top: I_{TL} , I_L and I_C . Bottom: I_{TL} and V_R	60
Figure 3-16: the active power (P_r), reactive power (Q_r), and the power factor (PF), at the receiving end side	60
Figure 3-17: The actual and reference current waveforms for phase A of the inductive and capacitive branches, for UPF case	61
Figure 3-18: Simulation waveforms for PF/Leading case: (A) $I_{TL} = 0.5$ pu and (B) $I_{TL} = 1$ pu. Top: I_{TL} , I_L , and I_C . Bottom: I_{TL} and V_R	62
Figure 3-19: the active power (P_r), reactive power (Q_r), and the power factor (Pf), at the receiving end side	63

Figure 3-20: The actual and reference current waveforms for phase A of the inductive and capacitive branches, for PF/leading case	64
Figure 3-21: Simulation waveforms for PF/Lagging case: (A) $I_{TL} = 0.5$ pu and (B) $I_{TL} = 1$ pu. Top: I_{TL} , I_L , and I_C . Bottom: I_{TL} and V_R	65
Figure 3-22: the active power (P_r), reactive power (Q_r), and the power factor (Pf), at the receiving end side	66
Figure 3-23: The actual and reference current waveforms for phase A of the inductive and capacitive branches, for PF/leading case	66
Figure 3-24: (A) The actual and references dq currents of shunt branch, (B) current waveforms for phase A of the shunt branch (C) The actual and reference of the DC voltage across the DC sharing the link, for the lagging PF case.....	68
Figure 3-25: The active power; P_{VSC1} and P_{VSC2} , - ($P_{VSC1} + P_{VSC2}$), and P_{VSC3} for DC bus voltage regulation.	69
Figure 4-1: The single line diagram of the inductive branch circuit.....	71
Figure 4-2: The equivalent circuits of the inductive branch (A) The circuit of the d axis (B) The circuit of the q axis.....	71
Figure 4-3: The block diagram for the design of the PI-type controller of the inductive branch.	72
Figure 4-4: The single line diagram of the capacitive branch	73
Figure 4-5: (A) The circuit of d axis (B) The circuit of q axis	76
Figure 4-6: The block diagram for the design of the PI-type controller of the inductive branch.	77
Figure 4-7: Bode plots of the plant, controller, and LTF of the capacitive branch	78
Figure 4-8: The schematic control diagram of the series branches of the UPFC-based-UIPC	80
Figure 4-9: Simulation waveforms for UPF case: (A) $I_{TL-des} = 0.5$ pu and (B) $I_{TL-des} = 1$ pu. Top: I_{TL} , I_L , and I_C . Bottom: I_{TL} and V_R	82
Figure 4-10: (A) the actual and references dq currents, (B) The actual and reference current waveforms for phase A, of the inductive branch for the UPF case.	83
Figure 4-11: (A) the actual and reference dq voltage (B) The actual and reference voltage waveforms for phase A, of the capacitive branch for the UPF case.....	84
Figure 4-12: The actual and reference current waveforms for phase A of the capacitive branch for UPF case	84
Figure 4-13: Simulation waveforms for Lead PF case: (A) $I_{TL-des} = 0.5$ pu and (B) $I_{TL-des} = 1$ pu. Top: I_{TL} , I_L , and I_C . Bottom: I_{TL} and V_R	85
Figure 4-14: the actual and references dq currents, (B) The actual and reference current waveforms for phase A, of the inductive branch for the leading PF case	86
Figure 4-15: (A) the actual and reference dq voltage (B) The actual and reference voltage waveforms for phase A, of the capacitive branch for the PF leading case	87

Figure 4-16: The actual and reference current waveforms for phase A of the capacitive branch for leading PF case	87
Figure 4-17: Simulation waveforms for lagging PF case: (A) $I_{TL-des} = 0.5$ pu and (B) $I_{TL-des} = 1$ pu. Top: I_{TL} , I_L , and I_C . Bottom: I_{TL} and V_R	89
Figure 4-18: the actual and references dq currents, (B) The actual and reference current waveforms for phase A, of the inductive branch for the lagging PF case	90
Figure 4-19: (A) The actual and reference dq voltage (B) The actual and reference voltage waveforms for phase A, of the capacitive branch for the PF lagging case	90
Figure 4-20: The actual and reference current waveforms for phase A of the capacitive branch for lagging PF case	91
Figure 5-1: The 2-node transmission system with the UIPC connected at the sending end.....	94
Figure 5-2: The equivalent single-source system used in the experimental set-up	96
Figure 5-3: The layout of the experimental set-up.....	98
Figure 5-4: The picture of the experimental set of the porotype of the UIPC based UIPC.....	99
Figure 5-5: The series VSC 1 and VSCs and the emulated shunt VS	99
Figure 5-6: Schematic diagram of the proposed control scheme for the UPFC-UIPC with optimal current sharing factors and PR controller	101
Figure 5-7: Lookup table with the optimization results (α and β) considering different cases (values of δ , I_{TL-des} , and ϕ_{TL-des}).	102
Figure 5-8: Simulation waveforms for UPF: (A) $I_{TL} = 0.5$ pu and (B) $I_{TL} = 1$ pu. Top: I_{TL} , I_L , and I_C . Bottom: I_{TL} and V_R	103
Figure 5-9: Actual and reference current waveforms of (A) The capacitive branch (B) the inductive branch for UPF case and I_{TL-des} varying from 0.5pu to 1pu.	104
Figure 5-10: Experimental waveforms for UPF: (A) $I_{TL} = 0.5$ pu and (B) $I_{TL} = 1$ pu. Top: I_{TL} (red), I_L (blue) and I_C (green). Bottom: I_{TL} (red) and V_{RS} (green).....	105
Figure 5-11: Actual and reference current waveforms of (A) the capacitive branch (B) the inductive branch for UPF case and I_{TL-des} varying from 0.5pu to 1pu.	105
Figure 5-12: Experimental waveforms for: (A) $I_{TL} = 0.5$ pu and (B) $I_{TL} = 1$ pu. Top: I_{TL} (red), I_L (blue) and I_C (green). Bottom: I_{TL} (red) and V_{RS} (green).....	106
Figure 5-13: Experimental waveforms for: (A) $I_{TL} = 0.5$ pu and (B) $I_{TL} = 1$ pu. Top: I_{TL} (red), I_L (blue) and I_C (green). Bottom: I_{TL} (red) and V_{RS} (green).....	107

List of Tables

Table 1-1: Overview of the IPC's types and basic comparison of their features	11
Table 2-1: The System parameters	27
Table 2-2: The transmission line current control range for different δ	27
Table 2-3: The Comparison OF Maximum Values Obtained with the SPS-based UIPC and the UPFC-based UIPC	38
Table 2-4: The Injected Active and Reactive Power of both Series VSCs at $\delta = 30^\circ$ and $I_{TL} = 1.3$ pu.....	38
Table 3-1: The parameters of the series coupling transformer (3-phase)	42
Table 3-2: The parameters of the shunt-coupling transformer (3-phase)	42
Table 3-3: DC side and the VSCs parameters	42
Table 3-4: The size of L_L and C_c	43
Table 3-5: Values of α and β , I_L , ϕ_L , I_C , and ϕ_C , for the two considered value of I_{TL-des} for the UPF case.....	59
Table 3-6: Values of α and β , I_L , ϕ_L , I_C , and ϕ_C for the two considered values of I_{TL-des} for the PF/leading case	62
Table 3-7: Values of α and β , I_L , ϕ_L , I_C , and ϕ_C , for the two considered values of I_{TL-des} for the PF/lagging case	64
Table 4-1: Comparison of errors values for the PR controllers and for dq controllers in different values of I_{TL} and ϕ_{TL}	92
Table 5-1: parameters of the single source system	96
Table 5-2: values of the sharing factors α and β for the desired current magnitudes and angles (I_{TL} and ϕ_{TL})	102

Nomenclature

APST	Assisted Phase Shifting Transformer
DG	Distributed Generations
DI	Decoupling Interconnector
FACTS	Flexible AC Transmission System
FCLT	Fault Current Limitation Transformer
IPC	Interphase Power Controller
PFC	Power Flow Control Technologies
PF	Power Factor
PR	Proportional Resonant
PST	Phase Shifting Transformer
RESs	Renewable Energy Sources
SPS	Static Phase Shifter
SPWM	Sinusoidal Pulse Width Modulation
SSSC	Static Series Synchronous Compensator
STATCOM	Static Synchronous Compensator
TSO	Transmission System operator
TC-PST	Thyristor Controlled Phase Shifting Transformer
UIPC	Unified Interphase Power Controller
UPFC	Unified Power Flow Controller
UPF	Unity Power Factor
VSC	Voltage Source Converter

CHAPTER 1. INTRODUCTION

1.1. Introduction

The demand for electricity has been increased continuously and rapidly over the world. The growth in the demand requires more power to be transmitted from the generation side to the consumer side. The transmission systems of today tend to be highly interconnected to reduce the odds of not being able to deliver electricity at key substations, in case a given transmission line is disconnected due to a fault or for maintenance purposes. This characteristic is represented in Figure 1-1 [1]. Other benefits included proper using of the installed capacities, improving the system frequency control, sharing reserve capacities, and facilitating the large-scale integration of renewable energy sources (RESs). The interconnection of neighboring grids is achieved by tie transmission lines [2].

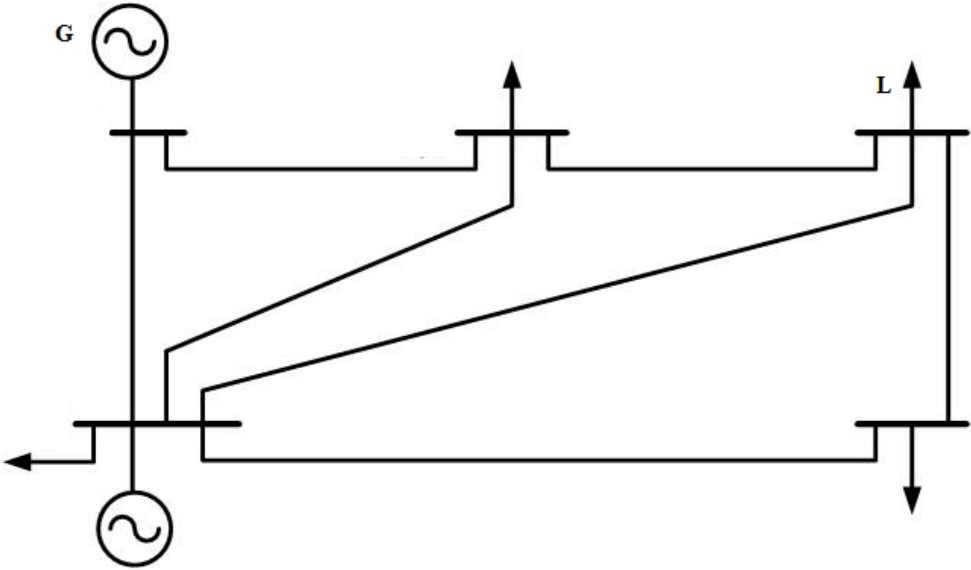


Figure 1-1: Interconnected transmission power system [1]

In recent years, there has been a global trend to increase the productions of the electricity using RESs. The use of RESs as wind and solar can mitigate climate change since they are environmental friendly, sustainable sources and readily available [3]. Large scale of RESs (100's of MW) are usually integrated into the transmission system level. However, since RESs are variable and fluctuating sources, they could adversely affect the power flow through the transmission system, and increase the load on certain transmission lines unpredictably [4].

The path of the electricity in a transmission line depends directly on its impedances and the angle difference between the voltages at its two ends. In an interconnected system, power will flow more in the transmission lines with low impedances, and less in transmission lines with high impedances [5]. Consequently, some transmissions lines will be overloaded, and other will be underloaded. This leads to ineffective use of the power transmission system and leads to a known issue in the power system, which is the congestion in the transmission systems. Furthermore, the deregulation of the electricity market in recent years has caused a primary change within the operation of the transmission system. It leads to the creation of contractual paths to deliver power from sources to loads very far apart. The contractual path of electricity can be seen as a “straight line” from the generation side to the consumer. However, a common issue in the power system, a loop flow, has been raised since the flows of the electricity follows Kirchhoff’s voltage laws and not contractual paths [6].

The nature of power flow through the transmissions lines or tie lines is not only the concern of the Transmission System Operator (TSO). The integration of high penetrations of RESs and Distributed Generations (DG) and the rapid increase of the electricity demand complicate the task of the TSO to make effective use of the power transmission system and maintain its security and loadability [7].

The conventional solution to prevent overloading of the existing transmission lines is to build new transmission lines. Building new transmission lines is costly, and their construction takes many years [8]. The environmental issues and social concerns that are raised due to the installation of the new transmission lines make this solution a difficult task, or even impossible to achieve in some cases [9]. Furthermore, the expansion of highly interconnected transmission system will increase its complexity and short circuit level. Consequently, a new issue will be introduced, which is the need for upgrading the substations equipment and the circuit breakers [10].

The alternative solution is to control the power flow of the existing transmission system using Power Flow Control (PFC) technologies [11]. Controlling the power flow in the existing transmission power system is a sufficient solution for many reasons. Using PFC is less costly, and its installation requires less time than building new lines. Moreover, PFC will increase the control flexibility in the power transmission system. Among the power flow control devices reported in the literature are the Flexible AC Transmission System (FACTS) devices.

1.2. Flexible AC Transmission System (FACTS) Devices

FACTS devices based on power electronics have been used to control the power flow and improve the voltage profiles in the transmission system. The definition of FACTS devices by IEEE is “*alternating current transmission systems incorporating power-electronic based and other static controllers to enhance controllability and increase power transfer capability*” [12]. The basic principle of FACTS devices is to employ controllable elements in series and/or in parallel with the network thus increasing the control flexibility of the transmission systems [13]. The FACTS devices can be classified, based on the type of power electronic devices, into two generations. The first generation is based on the line-commutated thyristor while the second generation is based on the self-commutated Voltage-Source Converter (VSC). FACTS devices can also be classified, based on their connections to the transmission system, into three categories as shown in the block diagram in Figure 1-2 [14, 15]:

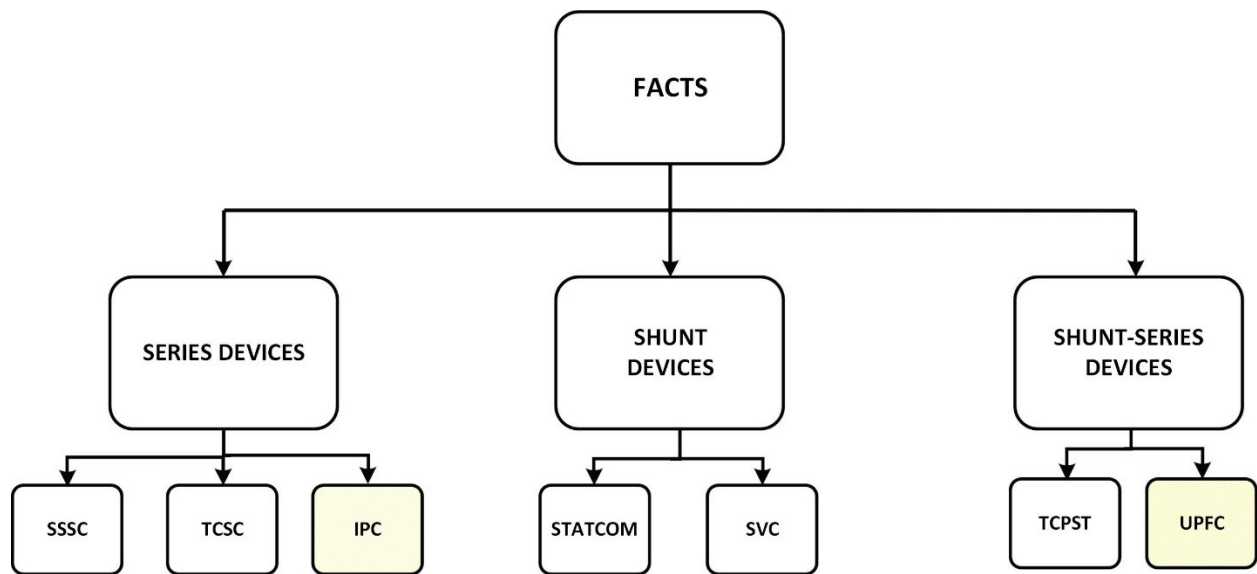


Figure 1-2: classification of the FACTS devices based on their connections to the transmission system

The series FACTS devices; Static Series Synchronous Compensator (SSSC), Thyristor Controlled Series Capacitor (TCSC), and Interphase Power Controller (IPC), are preferably used for power flow control.

The shunt FACTS devices; Static Synchronous Compensator (STATCOM) and Static Var Compensator (SVC), are preferably used for regulating the voltage of the system and keeping it within acceptable limits.

The shunt-series FACTS devices; Thyristor Controlled Phase Shifting Transformer (TCPST), and Unified Power Flow Controller (UPFC) are used for both, power flow control and regulating the voltage of the system.

In this research work, the focus will be on the IPC and the UPFC, the ones highlighted by yellow color in Figure 1-2.

1.3. The Basic Interphase Power Controller (IPC)

The IPC is a less-known series FACTS device, which presents important characteristics. These features are namely active power regulation in a transmission line with highly variable transmission angles, using minimum active control elements [16]. Conceptually, the basic IPC is a series connected device composed of two parallel branches, each consisting of an impedance (inductor or capacitor) in series with a phase shifting transformer (PST) as shown in Figure 1-3 [17].

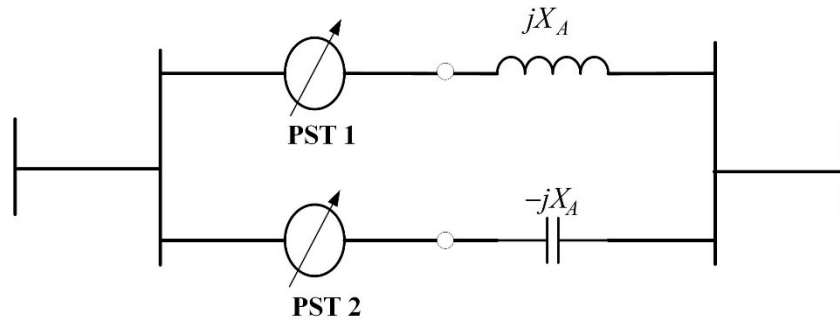


Figure 1-3: The generic circuit of the IPC

The IPC can be used in different applications. The configuration of the IPC for certain applications can be simplified by removing some of the basic components. Some examples of these applications are the Decoupling Interconnector (DI), the Fault Current Limitation Transformer (FCLT) and the Assisted PST (APST) [16].

For the DI applications of the IPC, the inductive and capacitive impedances form a parallel circuit tuned to the fundamental frequency of the network. These high impedance IPCs have their own characteristics of limiting their impact to the short circuit current and decoupling the voltage at their terminals. Each terminal of a DI behaves as controlled current sources. In normal operation condition, a DI controls the active power flow in both directions and provides support for the voltage by generating and absorbing reactive power. By controlling the tap changer of the PST,

one can obtain the desired active power. A DI provides no short-circuit contributions during perturbations. It decouples the voltage of both sides and does not transfer the impact of perturbations from one side to the other [18-21].

When a DI links two voltage levels connected in parallel with conventional transformers, it can be configured to mitigate the fault currents. This configuration of IPC is called Fault Current Limitation Transformer (FCLT). The main purpose of the FCLT is to increase the capacity of transformers in the transmission and distribution substations without increasing the Short-Circuit Levels (SCLs). The FCLT will lead to avoid any wide modification or add a new substation in or nearby the substations whose short-circuit level is already close to the ratings of the circuit breakers [22, 23].

Finally, the Assisted PST (APST) application of IPC is used to assist the existing PST for power flow control. The main purpose of the APST is to increase the normal and contingency transfer capacity of an existing PST or to implement a PST with high capacity and competitive price [23]. The first world IPC installation that is based on this application was in Plattsburgh, NY in 1999 [23, 24].

For this work, the focus will be on the applications of the phase controlled two branches DI. The reason behind that is the DI application of the IPC can achieve active and reactive power flow control, mitigate the fault current, isolate the voltage on each side and avoid transferring the impact of perturbations from one side to the other.

Since the main component of the basic IPC is the PST, as can be seen from Figure 1-3, the next two subsections will discuss the operation principles and types of the PST, and its limitations.

1.3.1. The Phase Shifting Transformer (PST)

The phase shifting transformer (PST) is a special type of transformers that inserts a phase angle (α) between its terminals. In this way, it can be used to control the power flow in a transmission line [25]. However, it can also be used as a controllable element in the basic IPC. The phase shifting angle (α) is created by adding a regulated voltage (ΔV) to one of the PST's terminals; say the source side, V_S . The voltage at the other terminal, say load side, V_L is phase shifted with respect to V_S by α . The magnitude of V_L can be equal to or not equal to the magnitude of V_S , which depends on the type of PST as will be explained in the next paragraph.

PSTs can be categorized into four types, depending on their constructions and their output voltage magnitudes with respect to their input voltage magnitudes. These types are direct-asymmetrical, direct-symmetrical, indirect-asymmetrical and indirect-symmetrical PSTs [26, 27]. The term direct or indirect means that the PST has one or two cores, respectively. The term symmetrical or asymmetrical means that the PST produces an output voltage with a magnitude that is the same or not, as that of the input waveform. Even though the indirect-symmetrical PST is the most expensive one, it should be chosen for this work, due to its great flexibility for tapping the voltage and its symmetrical property.

- **Indirect-symmetrical PST:**

Figure 1-4 (A) and (B) show the indirect-symmetrical PST winding connection and its phasor diagram, respectively.

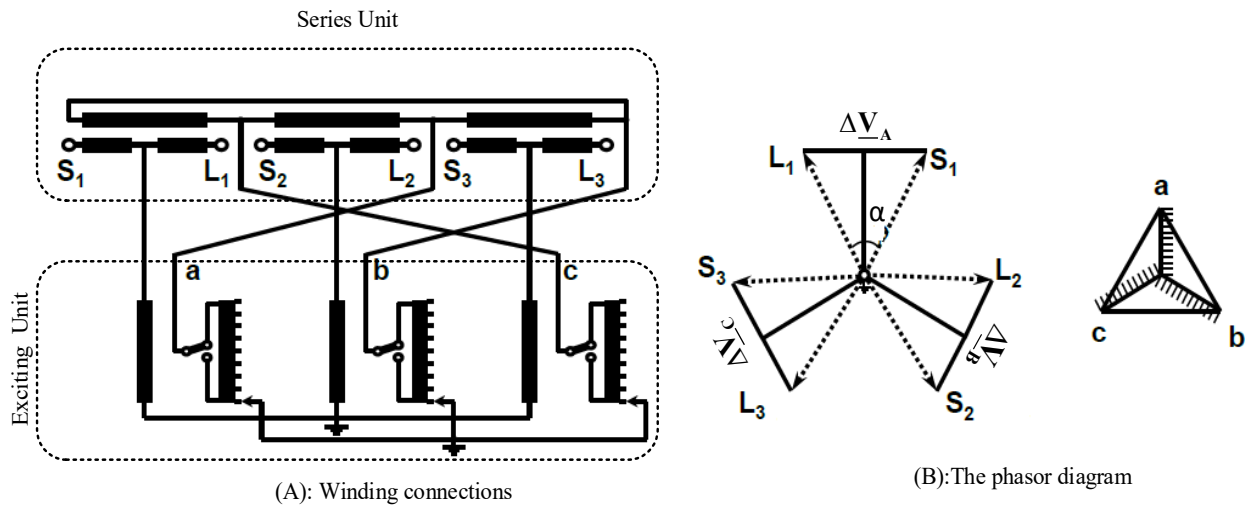


Figure 1-4: (A) The winding connections of the indirect-symmetrical PST (B) The phasor diagram [28]

As can be seen from Figure 1-4 (A), the indirect-symmetrical PST consists of series and exciting units. These units could be in one tank or two tanks for a 3-phase PST or one tank for each phase, meaning (three single-phase PSTs), depending on the power ratings, voltage level, and available space in the substations [29]. The primary winding of the series unit is connected to the source and load sides, while the primary of the exciter unit is connected to the middle of the primary winding of the series unit (the rated voltage of the primary winding of the exciter unit is the system voltage level).

To create a quadrature voltage (ΔV), each phase of the secondary winding of the series transformer is connected to the other two phases of the secondary winding of the exciter transformer as shown in Figure 1-4 (A). The way of these connections leads to create a delta connection for the secondary winding of the series transformer that leads to create the quadrature voltage (ΔV), as shown in Figure 1-4 (B). ΔV can be controlled using an On-Load Tap Changer (OLTC) in the secondary winding of the exciter unit for each phase. Each tap changer is equipped with a changeover switch (S) as shown in Figure 1-4 (A) to allow lead or lag phase shifts between input and output voltages. Both primary and secondary windings of the exciter unit are Y-N connections. The relation between the injected voltage (ΔV) and the phase angle (α) can be expressed as follows:

$$\alpha = \pm \sin^{-1} \left(\frac{\Delta V}{2V_s} \right) \quad (1.1)$$

From (1.1), one can note that the control limits of α will depend on the maximum ΔV that the PST can inject, which in turn depends on the rating of the PST.

1.3.2. The Limitations of the Basic Interphase Power Controller (IPC)

In the basic IPC, the control variables (the phase angles of the PSTs) are controlled by means of altering the OLTC's position of the PSTs. There are three types of OLTC reported in the literature, the mechanical tap changer, thyristor-assisted tap changer (or hybrid electronic tap changer), and the fully electronic (or solid-state) tap-changer [30]. The implementation complexity and high cost of the hybrid electronic and electronic tap changers, make the mechanical tap changer the common type associated with PST's. Figure 1-5 shows the schematic diagram of the basic (PST-based) IPC.

Due to the use of the mechanical switches to change the positions of OLTCs, the total operation time of the mechanical OLTC is considered high. It is between 3 s to 10 s as reported in [31]. Therefore, the low-speed response of the control of the basic IPC makes it only suitable for steady-state operation condition. The basic IPC could not be used for transient stability enhancement, dynamic voltage control, and power oscillation damping.

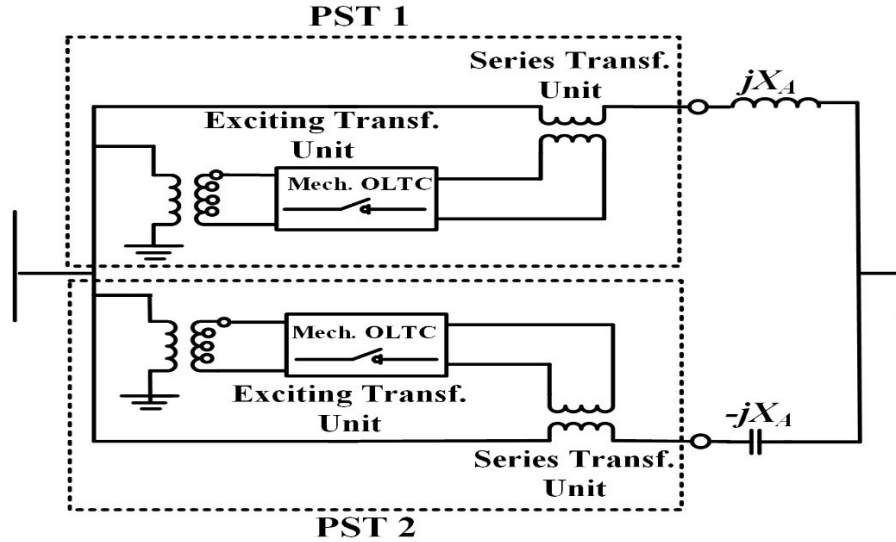


Figure 1-5: Schematic diagram of the basic IPC (PST-based IPC)

There are other essential limitations of using the basic IPC. The power control ranges by the basic IPC are limited by the maximum and minimum phases shifting angles that the PSTs can provide. This limitation of the basic IPC will decrease the flexibility of the control and may not achieve the independent control of the active and reactive power in many cases. The basic IPC, as mentioned before, can control active and reactive power flow in normal conditions, mitigate the fault and isolate the networks during the fault conditions.

1.4. Literature Review of the Static Interphase Power Controller

Adding power electronic devices to the basic IPC can make its operating range continuous and speed up the control action. The IPC with power electronics will form a static IPC (electronic-based IPC). In the literature, three types of the static IPC were introduced; the Thyristor Controlled-based IPC (TC-based IPC) [32, 33], the SSSC-based IPC [34-37], and the Unified IPC (UIPC) [38-40].

For the first type, Thyristor Controlled PSTs (TCPSTs) substitute the mechanical PSTs of the basic IPC. The windings of the TCPST are the same as the original PST, and the only difference between them is that static thyristors control the OLTC of the TCPST while the mechanical switches control the OLTC of the PST. Some references use the term ‘Static Phase Shifter’ (SPS) instead of the TCPST [41]. Figure 1-6 shows the schematic diagram of the TC-based IPC. Although

using the TC-based IPC provides a fast-speed of response for the control action, it does not increase its power control range. Therefore, the TC-based IPC is out of the scope of this research work.

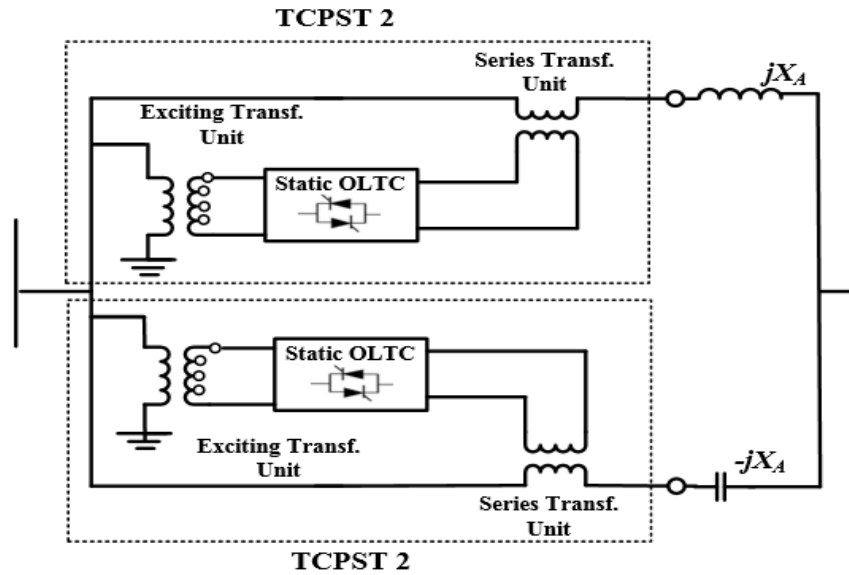


Figure 1-6: Schematic diagram of the TC-based IPC

The second and the third types of static IPC are based on the second generation of FACTS devices, which use the self-commutated Voltage-Source Converter (VSC) as the controlled devices instead of using the line-commutated thyristors of the earlier generation of the FACTS devices. Unlike in the TC-based IPC, the PSTs are replaced entirely by electronic devices in the SSSC-based IPC and the UIPC.

For the SSSC-based IPC, the two PSTs of the basic IPC are replaced by two SSSCs as it is shown in Figure 1-7. The SSSC-based IPC is not included in this work since it is restricted to its main component, the SSSC. The main limitation of the SSSC is its inability to supply or absorb active power during the steady-state condition, which will lead to limit the control range of the power flow. Moreover, the SSSC does not have the ability to regulate the voltage at its local bus [32].

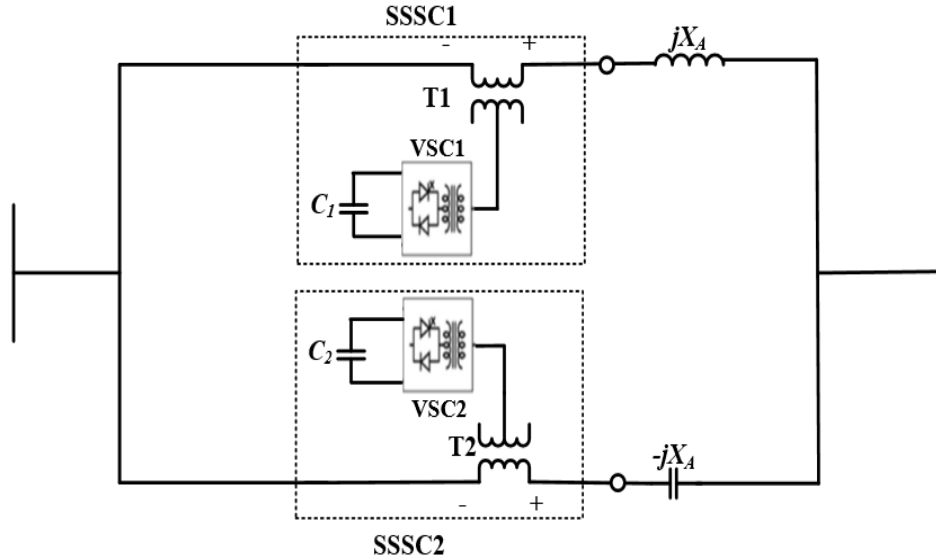


Figure 1-7: Schematic diagram of the SSSC-based IPC

For the third type of static IPC, the UIPC, the PSTs of the basic IPC is substituted by a dual UPFC [39]. This type of the static IPC has more flexibility than the first and the second types since its main component is the UPFC. Therefore, the UIPC will be the focus of this research work.

1.5. The Unified Interphase Power Controller (UIPC)

This configuration, called Unified Interphase Power Controller (UIPC) is shown in Figure 1-8 [39]. Adding the dual UPFC, with two series converters and one shunt converter, as the main component of the IPC has great advantages due to the superior capabilities of the UPFC among FACTS devices. It is the most flexible, incorporating features of other FACTS devices: Static Phase Shifter (SPS), STATCOM, and SSSC [42]. However, it is also the most complex and costly of them all.

The UIPC that has been reported in the literature did not explore the use of all incorporated features of the UPFC [39]. It only considered the features of the UPFC when it works as an SPS, which is essentially the conventional PST with continuous phase angle variations. This control strategy is called the SPS-based UIPC. Although the low-speed response of the control in the basic IPC and the inability to regulate the voltage in the SSSC-based IPC are overcome by using the SPS-based UIPC, this type does not solve the limitation in the power control range.

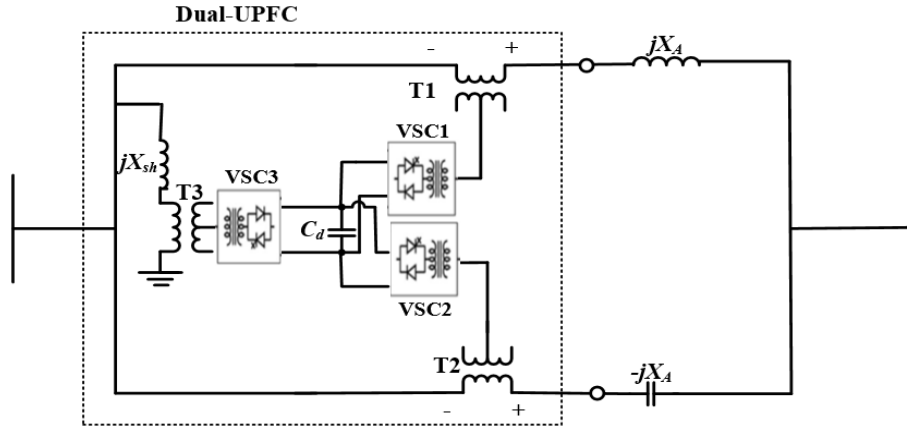


Figure 1-8: Schematic diagram of the UIPC

It should be noted that the focus of the more recent literature on the UIPC has been on its impact on the performance of distance protection relays [40] and short-circuit current limitations in wind farms [38]. The control strategy of the VSCs of the dual UPFC remains the same, as in the early days, when the IPC was mechanically controlled. As results, not all features of the UPFC were explored in the UIPC.

The Table 1-1 summarizes the features of the static IPCs that have been reported in the literature, besides the basic IPC. It should be mentioned that all IPC types included in the Table are used for the DI application. Generally, the DI IPCs can achieve active and reactive power flow control, mitigate the fault current, isolate the voltage on each side and avoid transferring the impact of perturbations from one side of the transmission line to the other. However, the performance level will be different from one type of the IPC to the other types.

Table 1-1: Overview of the IPC's types and basic comparison of their features

IPC	Device Scheme	Main component	Controlled devices	Feature of the main component	Features of the IPC type
Basic IPC		PSTs	Mechanical switching OLTC	<ul style="list-style-type: none"> ■ phase angle control. 	<ul style="list-style-type: none"> ■ Power flow control: <ul style="list-style-type: none"> - Limited control range and less flexible (two control variables) - Low-speed response of the control. - Discrete operating range. - Simple control structure. ■ Voltage regulation.
IPC	Device Scheme	Main component	Controlled devices	Feature of the main component	Features of the IPC type

TC-based-IPC		TCPSTs	Static (Thyristors) switching OLTC	<ul style="list-style-type: none"> ■ phase angle control. 	<ul style="list-style-type: none"> ■ Power flow control: <ul style="list-style-type: none"> - Limited control range and less flexible (two control variables) - Fast-speed response of the control. - Continuous operating range. - Simple control structure. ■ Voltage regulation.
SSSC-based-IPC		SSSC	VSC	<ul style="list-style-type: none"> ■ Line impedance (branch impedance) control. 	<ul style="list-style-type: none"> ■ Power flow control: <ul style="list-style-type: none"> - Limited control range and less flexible (emulate series inductive/capacitive reactance and no P exchange). - Fast-speed response of the control. - Continuous operating range ■ No voltage regulation.
SPS-based-UIPC		Dual UPFC	VSC	<ul style="list-style-type: none"> ■ UPFC works as SPSs (phase angle control). 	<ul style="list-style-type: none"> ■ Power flow control: <ul style="list-style-type: none"> - Limited control range and less flexible (two control variables). - Fast-speed response of the control. - Continuous operating range. - Simple control structure. ■ Voltage regulation: <ul style="list-style-type: none"> - Injecting/absorbing Q to its local bus is limited.

1.6. The Scope of the Research Work

The main objective of this research work is to explore full features of the dual UPFC internet in the UIPC, to control the power flow through the transmission lines, to regulate the voltage at the local bus, and to mitigate the impact of potential short-circuit faults in transmission lines. As a result, the control flexibility of the power flow in the transmission lines will increase significantly, and more efficient use of the existing transmission lines will be accomplished. Moreover, the use of a multi-functional power flow device such as the UIPC, can either avoid or delay building new transmission lines. The UIPC with the proposed control strategy (considering all incorporated features of its dual UPFC), will be named as proposed (UPFC-based) UIPC.

The use of the UIPC considering all features of its dual UPFC and all features of the basic IPC will increase the control flexibility of power flow in the transmission lines significantly. This is because the control variables of the UIPC will be doubled compared with the use of the UPFC only or the basic IPC only. Increasing the number of control variables of the UIPC will lead to

increase the control flexibility because there will be three degree of freedom (controlling the active power, reactive power at sending end and the reactive power at receiving end). Consequently, an independent control of the reactive power flows in transmission lines can be achieved. With independent control, one can maximize the flow of the active power while minimizing the flow of the reactive power, thus generating the most revenue from an AC transmission system [43].

In particular, this thesis makes the following contributions:

Proposing an approach to compute the four control parameters of the UPFC-based UIPC. The benefit of a more flexible control scheme (UPFC-based UIPC), comes with the challenge of computation of four control parameters of the series VSCs of the dual UPFC to make it work in a multi-functional mode (UPFC mode). Therefore, it is proposed to solve this issue with a simple and effective approach: Employ a current control scheme where the real and imaginary parts of the transmission line current are split among the inductive and capacitive branches as a function of sharing factors, α , and β . The use of optimization techniques is proposed to calculate α and β and also to minimize the apparent power required from the series connected VSCs, to realize a given transmission line current. The final target of using the computation approach for the UIPC with prospered control scheme and the optimization techniques will lead to design a device with low size (low power rated) compared with the UIPC when its work in conventional control scheme.

Modeling of the UPFC-based UIPC in PSCAD/EMTDC and use the Proportional Resonant (PR) in abc reference frame as current controllers for the series branches. To prove the concept of the novel proposed control scheme of the UIPC (UPFC-based UIPC), its model is developed using PSCAD/EMTDC. This is a general-purpose time domain simulation tool used for studying the transient behavior of electrical networks. The current sharing factors (α and β), which are calculated by the approach mentioned in the above paragraph, are stored in a lookup table. Then, reference currents of the inductive and the capacitive branches are obtained using an inverse Park transformation, with dq values computed from α and β . These currents are used as reference signals for the current controllers of both branches. The challenge of synthesizing a current in the capacitive branch of the UIPC with a VSC2 is overcome with a Proportional Resonant (PR) controller in the abc reference frame and Sinusoidal Pulse Width Modulation (SPWM) [44].

Development of a mathematical model of the capacitive branch in the synchronous reference frame (dq) for designing of a suitable current control loop. Although the PR controller in the abc reference frame proves the concept of the UPFC-based-UIPC, it does not have the feature to get zero error in the steady state, to a step variation of the reference signal. Therefore, this research proposes the use of the synchronous reference frame (dq) for controlling the series VSCs with a linear PI controller, to achieve a zero steady-state error. [45]. The design of the PI controller for the series VSC1, of the inductive branch of the UPFC-based UIPC, is well known and similar to the ones used for the STATCOM and the SCCC [46, 47]. On the other hand, the design of the PI controller in dq frame for the series VSC2 of the capacitive branch is not that simple and less known, since VSCs are typically connected to a power grid via a series inductance, not a series capacitance as in the capacitive branch of the UIPC. Hence, it is proposed in this work to develop mathematical models of the capacitive branch in dq frame for designing of the current control.

Implementing the UPFC-based-UIPC experimentally. It is worth mentioning that a detailed literature review has shown no reports of experimental verification of VSC-based IPCs. All works related to the UIPC have been based on simulation studies [39]. As a motivation and another contribution in this field, the UPFC-based-UIPC is implemented experimentally to prove its concept.

1.7. Outline of the Thesis

This thesis is organized as follows:

Chapter 2 presents a review of the basic control strategy of the UIPC (SPS-based UIPC) with the equations that describe their main control variables. Then, the proposed control strategy of the UIPC (UPFC-based UIPC), with equations that describe their main control variables is presented. The proposed method that is based on an appropriate sharing of the transmission line current through the capacitive and inductive branches is presented for the UPFC-based UIPC. Its performance is demonstrated using a simple power system and compared with the SPS-based UIPC.

Chapter 3 presents a simulation verification to validate the numerical results obtained in Chapter 2 and to prove the concept of the proposed control scheme of the UIPC (UPFC-based UIPC). A model of the UPFC-based UIPC is developed using PSCAD/EMTDC to achieve the simulation verification task. Then, a double loop PI control scheme is used for the shunt branch,

and PR controllers are used for the series branches. The performance of these controllers is validated using a simple power system as the one used in Chapter 2.

Chapter 4 addresses the use of the synchronous reference frame (dq) controller for controlling the inductive and capacitive branches of the UIPC, to provide a zero error in the steady state for step variations in the reference signal. Mathematical dynamic model in the dq frame for current control design, is reviewed for the inductive branch, and it is proposed for the capacitive branch. The same simple power system that is used in Chapter 3 is used to exam these dq current controllers.

Chapter 5 presents the experimental verification of the UPFC-based UIPC. First, the details concerning the sizing of a reduced-scale prototype, covering the hardware as well as the real-time controller, are discussed. Then, the experimental results of the UIPC for the same cases that were considered in the simulations results of the previous chapters are presented.

Chapter 6 draws the main conclusions from this research work and suggests prospects of this research work.

1.8 List of Publications

- K. Elamari, L. A. C. Lopes, "A Novel Control Strategy for a UPFC-Based Interphase Power Controller with Experimental Performance Verification" in IEEE Transactions on Power Delivery, submitted 2018 (under review).
- K. Elamari, L. A. C. Lopes, "Comparison of Static Phase Shifter and Unified Power Flow Control Based Unified Interphase Power Controllers," in Canadian Journal of Electrical Power and Computer (CJECE). Accepted and published in 2017.
- K. Elamari, L. A. C. Lopes, "Multi-Functional Interphase Power Controller for Power Flow Control in the Power Transmission System" in CIGRÉ Canada Conférence, 2016. Accepted and presented in October 2016.
- K. Elamari, L. A. C. Lopes, "Comparison of Phase Shifting Transformer and Unified Power Flow Control Based Interphase Power Controllers," in Electrical Power and Energy Conference (EPEC), 2016 IEEE, 2016, Accepted and presented in October 2016.

CHAPTER 2. COMPARISON OF CONVENTIONAL AND PROPOSED CONTROL STRATEGY OF THE UIPC

2.1. Introduction

This Chapter starts with a review of the conventional control strategy of the UIPC, called SPS-based UIPC, with the equations that describe their two main control variables. Then, a novel method that requires the computation of four control parameters of the series VSCs of the UPFC is proposed. This will be called UPFC-based UIPC. The steps for finding the required control parameters for both UIPC control logics are presented. Due to the complexity associated with the UPFC-based UIPC, and to achieve better performances, the use of optimization techniques is considered. A straightforward scheme based on the sharing of the real and imaginary components of the desired transmission line current is proposed. Its superior performance is demonstrated using a simple power system with a UIPC connected in series with a transmission line.

2.2. The Unified Interphase Power Controller (UIPC)

Adding power electronic converters to the basic IPC can make its operating range continuous as well as speed up the control action. Therefore, it has been suggested to replace the PSTs of the IPC with a modified (dual) UPFC, which presents two series converters and one shunt converter. This configuration is called Unified Interphase Power Controller (UIPC) [39].

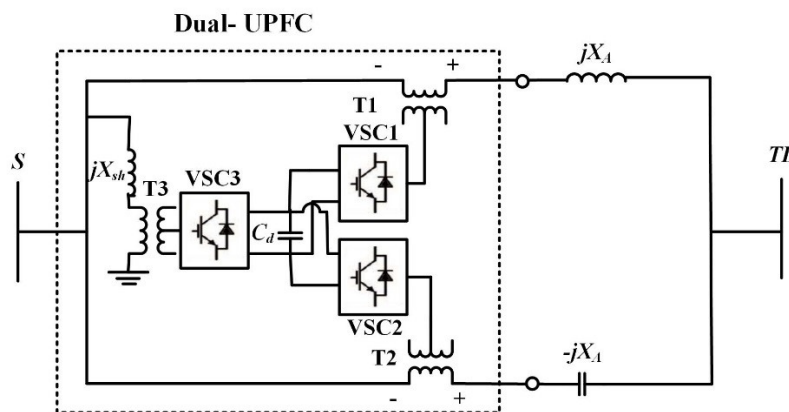


Figure 2-1: Single-line schematic diagram of the UIPC

As shown in Figure 2-1, the UIPC presents two branches: One inductive and the other capacitive. The inductive branch consists of VSC1 connected in series with an inductor through a series-coupling transformer T1. The capacitive branch consists of VSC2 connected in series with

a capacitor through a series-coupling transformer T2. VSC1 and VSC2 share the same DC link with VSC3, which is connected in shunt with the sending end through shunt coupling transformer T3. The UIPC is of the tuned type like the basic IPC. That is, $X_{LA} = -X_{CA} = X_A$.

For this type of IPC, the main component is the dual UPFC. Therefore, a review of the UPFC and its use in the UIPC application is addressed in the following subsection.

2.2.1. The Unified Power Flow Controller (UPFC)

The UPFC is a multi-functional FACTS device based on the back-to-back voltage source converter (VSC) configuration and was introduced by Gyugi in 1991[48]. One VSC is connected in shunt while the other is connected in series with a transmission line as shown in Figure 2-2. The UPFC can control the most important power flow parameters (voltage, angle, and line impedance) simultaneously or selectively. As a result, the flow of active and reactive powers in the line can be controlled independently by the UPFC. This feature is the main reason for adding the adjective “Unified” to the name of this FACTS device to form its abbreviations ‘UPFC’ [15].

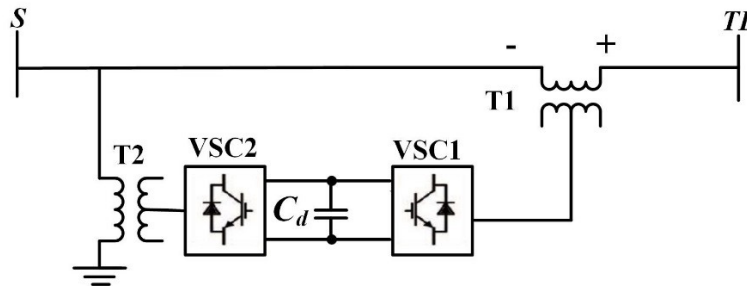


Figure 2-2: Simple diagram of the UPFC

2.2.2. The Operation Principle of the UPFC

Referring to Figure 2-2, the VSC1 of the UPFC will inject a voltage in series with the transmission line. In this way, one can create a voltage at the sending end of the transmission line, different from the one of the sending end bus, what allows the power flow through the transmission line to be controlled. The shunt VSC2 will inject/absorb reactive power to regulate the voltage magnitude at the sending end bus and provide a path for the active power exchanged between the series VSC1 and the transmission line.

The power flow control and the voltage regulation can be achieved by varying the control variables of the UPFC. These are the magnitude, and the angle of the series injected voltage, V_{inj} .

and ρ , and the magnitude and the angle of the shunt injected voltage, V_{sh} , and δ_{sh} . Varying the control variables of the UPFC in a certain way will lead to making the UPFC work in different operation modes. It can work as STATCOM, SSSC, SPC, or a combination of them all (multi-functional mode or UPFC mode) [42]. For this work, only two operation modes will be considered, the SPS operation mode and the UPFC operation mode. Brief descriptions of these two modes of the UPFC are presented below:

- 1- Symmetrical or ideal Static Phase shifter (SPS) mode, see Figure 2-3 (A). This operation mode results in the same voltage magnitude at the two sides, like the symmetrical PST. The only change will be on the angle of the voltage.
- 2- The multi-functional (UPFC) mode, see Figure 2-3 (B): In this mode, the UPFC can control the angle, reactance, and voltage magnitude simultaneously.

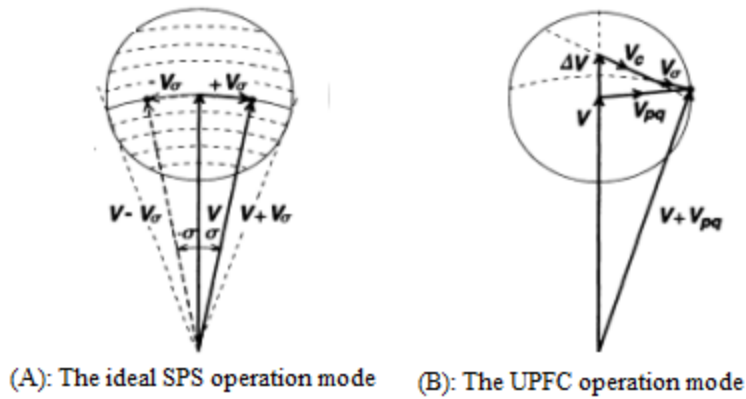


Figure 2-3: The considered operations modes of the UPFC (SPS, and UPFC mode) for the UIPC application [42]

2.2.3. The operations principle of the Unified Interphase Power Controller (UIPC)

As can be seen from Figure 2-4, the series VSC1 will inject a voltage in the inductive branch, \underline{V}_{injL} , and the series VSC2 will inject a voltage in the capacitive branch, \underline{V}_{injC} . The shunt VSC3 will inject /absorb a shunt current, \underline{I}_{sh}

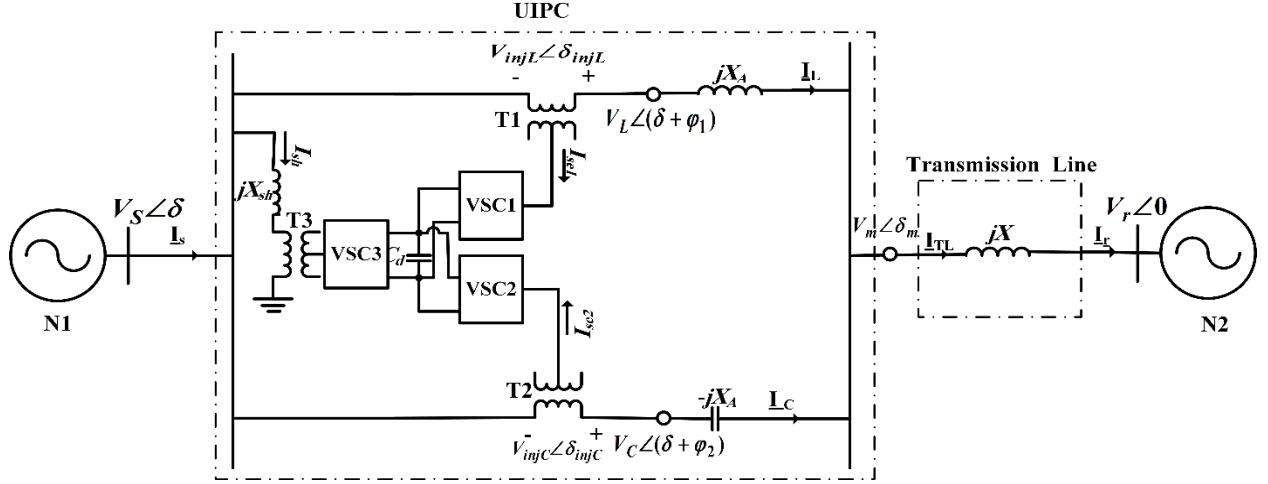


Figure 2-4: Schematic diagram of the UIPC showing the three VSCs and the voltages and currents in the various nodes and branches, respectively

The injected voltages of series VSC1 and VSC2 in their complex forms can be expressed as:

$$\underline{V}_{injL} = V_{injL} \angle \delta_{injL} = V_{injL} \angle (\delta + \rho_1) \quad (2.1)$$

$$\underline{V}_{injC} = V_{injC} \angle \delta_{injC} = V_{injC} \angle (\delta + \rho_2) \quad (2.2)$$

Where V_{injL} and V_{injC} are the magnitudes of the injected voltage of series VSC1 and VSC2 respectively. The angles δ_{injL} and δ_{injC} are the phase angles of the injected voltages of VSC1 and VSC2 respectively with respect to the reference voltage (V_r in this study). The angles δ_{injL} and δ_{injC} can be substituted by $(\delta + \rho_1)$ and $(\delta + \rho_2)$ respectively. Where, δ is the phase angle of the sending end voltage, \underline{V}_s , and ρ_1 and ρ_2 are the angles of \underline{V}_{injL} and \underline{V}_{injC} with respect to \underline{V}_s . Since δ is an uncontrollable but measurable parameter, it is preferable to use ρ_1 and ρ_2 as the control variable angles of the injected voltages instead of angles, δ_{injL} , and δ_{injC} that include δ .

The injected voltages, \underline{V}_{injL} , and \underline{V}_{injC} by the two series VSCs will be resulting in new voltages, \underline{V}_L , and \underline{V}_C , at the connection points between the coupling transformers, T1 and T2, and the series reactance, X_A of both branches of the UIPC. They are equal to:

$$\underline{V}_L = V_L \angle (\delta + \varphi_1) = \underline{V}_s + \underline{V}_{injL} \quad (2.3)$$

$$\underline{V}_C = V_C \angle (\delta + \varphi_2) = \underline{V}_s + \underline{V}_{injC} \quad (2.4)$$

Where, $(\delta + \varphi_1)$ and $(\delta + \varphi_2)$ are the angles of \underline{V}_L and \underline{V}_C with respect to the voltage reference (V_r), respectively. Where φ_1 and φ_2 are the angles of \underline{V}_L and \underline{V}_C with respect to \underline{V}_s , respectively. With the assumption that the voltage magnitude of \underline{V}_s is equal to its rated value, and δ is an

uncontrollable parameter, it could be noted from (2.3) and (2.4), that the only way to control V_L and V_C and their angles are by controlling the series injected voltage magnitudes, V_{injL} , and V_{injC} , and their angles, ρ_1 and ρ_2 . Based on this statement, one could say that the angles ρ_1 and ρ_2 and the voltage magnitudes, V_{injL} , and V_{injC} , of the series, injected voltages in both branches are the main control parameters of the UIPC.

The shunt VSC3 can inject/absorb a shunt current to regulate the voltage at the sending end. The shunt VSC3 will also provide a path for the active power exchanged between the series VSCs and branches of the UIPC so as to regulate the voltage in the intermediate DC bus. Since this chapter aims to use the UIPC to control the active and reactive power flowing through the transmission line, the voltage regulation feature by the shunt VSC3 will be disregarded.

Bearing in mind that the UPFC is the main component of the UIPC, the operation modes of the UIPC will be the same as the ones mentioned for the UPFC. For this Chapter, two operation modes will be considered what leads to having two types of UIPC. The first is the ideal SPS operation mode that corresponds to the conventional approach of the UIPC, the SPS-based UIPC. The second is the UPFC operation mode that corresponds to the proposed approach for this work, the UPFC-based UIPC. In the following sections, the mathematical models, control limits and the methods for calculating the control parameters will be addressed individually for each UIPC (the SPS-based UIPC and the UPFC-based UIPC).

Before moving to the next sections, three assumptions will be made. First, the equivalent reactance of each branch, X_A , is equal to the sum of the leakage reactance of the series coupling transformer and the main reactance of each UIPC's branch; ($X_A = X_{LA} = X_L + X_{Tranf}$) and ($X_A = -X_{CA} = -X_C + X_{Tranf}$). The second one, which is following the previous works in the IPC topic by many authors, the series passive elements of the UIPC, are assumed either purely inductive or purely capacitive (lossless series elements) [16]. Finally, the series coupling transformers are assumed to be ideal transformers. These assumptions are significant to simplify the derivation of equations of the UIPC in steady-state cases.

2.3. The Conventional (SPS-based) UIPC

The basic control scheme of the UIPC concerns the operation of the dual UPFC of Figure 2-4 as simple SPSs [39, 40]. This is shown in the equivalent circuit of Figure 2-5.

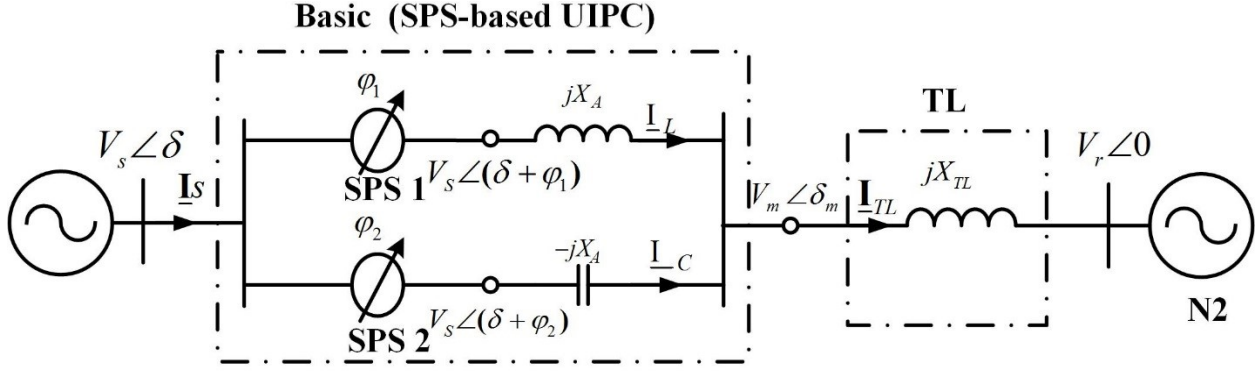


Figure 2-5: The equivalent circuit of the UIPC controlled as two SPSs.

2.3.1. Mathematical Model of the SPS-based UIPC

The conventional (SPS-based) UIPC, shown in Figure 2-5 presents two SPSs, one in each branch. They are assumed to be of the symmetrical type [26]. Therefore, the magnitude of \underline{V}_s is equal to the magnitude of \underline{V}_L and \underline{V}_C , ($V_L = V_C = V_s$). On the other hand, \underline{V}_L and \underline{V}_C are shifted with respect to \underline{V}_s , by using the SPSs of the inductive and the capacitive branches by angles φ_1 and φ_2 , respectively. The angles, φ_1 and φ_2 , are the main control variables of the SPS-based UIPC. \underline{V}_L and \underline{V}_C can be expressed as:

$$\underline{V}_L = V_s \angle (\delta + \varphi_1) \quad (2.5)$$

$$\underline{V}_C = V_s \angle (\delta + \varphi_2) \quad (2.6)$$

The relations between the shift angles, φ_1 and φ_2 and the injected voltage magnitudes of both series VSCs, V_{injL} and V_{injC} , and their angles, ρ_1 , and ρ_2 are:

$$V_{injL} = 2V_s \sin\left(\frac{|\pm\varphi_1|}{2}\right) \quad (2.7)$$

$$\rho_1 = \delta + \frac{\varphi_1}{2} \pm \frac{\pi}{2}, \text{ where "+" is for } \varphi_1 > 0^\circ \text{ and "-" is for } \varphi_1 < 0^\circ \quad (2.8)$$

$$V_{injC} = 2V_s \sin\left(\frac{|\pm\varphi_2|}{2}\right) \quad (2.9)$$

$$\rho_2 = \delta + \frac{\varphi_2}{2} \pm \frac{\pi}{2} \text{ where "+" is for } \varphi_2 > 0^\circ \text{ and "-" is for } \varphi_2 < 0^\circ \quad (2.10)$$

From Figure 2-5, the current flowing through the transmission line, \underline{I}_{TL} , is equal to the sum of the currents flowing through the inductive and the capacitive branches of the IPC, \underline{I}_L , and \underline{I}_C , respectively.

$$\underline{I}_{TL} = \underline{I}_L + \underline{I}_C \quad (2.11)$$

\underline{I}_L and \underline{I}_C can be expressed as:

$$\underline{I}_L = I_L \angle \phi_L = \frac{V_s \angle (\delta + \varphi_1) - V_m \angle \delta_m}{jX_A} \quad (2.12)$$

$$\underline{I}_C = I_C \angle \phi_C = \frac{V_s \angle (\delta + \varphi_2) - V_m \angle \delta_m}{-jX_A} \quad (2.13)$$

Where I_L and ϕ_L are the magnitude and the angle of inductive branch current. I_C and ϕ_C are the magnitude and the angle of capacitive branch current. V_m and δ_m are the magnitude and the angle of the input voltage to the transmission line.

By substituting (2.12) and (2.13) into (2.11), \underline{I}_{TL} becomes:

$$\underline{I}_{TL} = I_{TL} \angle \phi_{TL} = \frac{V_s \angle (\delta + \varphi_1) - V_s \angle (\delta + \varphi_2)}{jX_A} = 2V_s \sin\left(\frac{\varphi_1 - \varphi_2}{2}\right) \angle \left(\delta + \frac{\varphi_1 + \varphi_2}{2}\right) \quad (2.14)$$

Where, I_{TL} and ϕ_{TL} are the magnitude and angle of the transmission line current.

Then, one can compute \underline{V}_m and the active and reactive power at the receiving end (P_R and Q_R) as:

$$\underline{V}_m = V_m \angle \delta_m = \frac{X_{TL}}{X_A} \left[2V_s \sin\left(\frac{\varphi_1 - \varphi_2}{2}\right) \angle \left(\delta + \frac{\varphi_1 + \varphi_2}{2}\right) \right] + V_r \angle 0 \quad (2.15)$$

$$P_R = \frac{2V_s V_r}{X_A} \sin\left(\frac{\varphi_1 - \varphi_2}{2}\right) \cos\left(\delta + \frac{\varphi_1 + \varphi_2}{2}\right) \quad (2.16)$$

$$Q_R = \frac{2V_s V_r}{X_A} \sin\left(\frac{\varphi_1 - \varphi_2}{2}\right) \sin\left(\delta + \frac{\varphi_1 + \varphi_2}{2}\right) \quad (2.17)$$

From (2.14) to (2.17), it can be noted that all quantities are functions of the magnitude of the sending and receiving end voltages, \underline{V}_s and \underline{V}_r , their phase difference, δ , and the magnitude of the UIPC impedances, X_A . V_s , V_r , and X_A are assumed to be known and fixed while δ is variable. (2.14) to (2.17) are also functions of the main control variables of the SPS-based UIPC, φ_1 , and φ_2 .

2.3.2. Control Limits of the SPS-UIPC

In the SPS control mode, the phase shifting angle (φ) is created by injecting a voltage (\underline{V}_{inj}) in series with the transmission line. The relation between the magnitude of the injected voltage (V_{inj}) and angle φ for a symmetrical SPS is:

$$\varphi = \pm \sin^{-1}\left(\frac{V_{inj}}{2V_s}\right) \quad (2.18)$$

From (2.18), one can note that the range of φ depends on the magnitude of the maximum injected voltage ($V_{inj-max}$) of the SPS. In this work, $V_{inj-max}$ is assumed to be around 0.25pu. Thus, the limits of φ_1 and φ_2 are:

$$-14.46^\circ \leq \varphi_1 \ \& \ \varphi_2 \leq 14.46^\circ \quad (2.19)$$

2.3.2. Calculation of the Control Parameters of the SPS-based UIPC

The aim of the SPS-UIPC is to control the power flow (current flow) through the transmission line, by varying φ_1 and φ_2 , according to:

$$I_{TL} = \frac{2 V_s}{X_A} \sin\left(\frac{\varphi_1 - \varphi_2}{2}\right) \quad (2.20)$$

$$\phi_{TL} = \left(\delta + \frac{\varphi_1 + \varphi_2}{2}\right) \quad (2.21)$$

The calculated values of φ_1 and φ_2 are used to calculate the current flow in each branch of the SPS-based UIPC and the required injected voltage by each SPS according to:

$$V_{injL-SPS} = 2V_s \sin\left(\frac{|\varphi_1|}{2}\right) \quad (2.22)$$

$$V_{injC-SPS} = 2V_s \sin\left(\frac{|\varphi_2|}{2}\right) \quad (2.23)$$

Then, the magnitude of the injected apparent power by each series VSC is equal to:

$$S_{injL} = V_{injL-SPS} \times I_L \quad (2.24)$$

$$S_{injC} = V_{injC-SPS} \times I_C \quad (2.25)$$

2.4. The Proposed (UPFC-based) UIPC

In the proposed scheme (UPFC-based UIPC), the action of the dual UPFC will not be limited to phase shifting. It will inject a voltage in series with the inductive and capacitor branches that can also correspond to a virtual impedance. This approach provides more flexibility in terms of control, but the magnitude of \underline{V}_L and \underline{V}_C will not be equal to that at the sending end of the transmission line ($V_L \neq V_C \neq V_s$).

2.4.1. Mathematical Model of the UPFC-based UIPC

The series VSC1 and VSC2 of the UIPC, shown in Figure 2-4, will inject voltages, \underline{V}_{injL} , and \underline{V}_{injC} in series with the inductive and the capacitive branches resulting in new voltages, \underline{V}_L , and \underline{V}_C . The injected voltages, \underline{V}_{injL} and \underline{V}_{injC} , will not only lead to varying the angles of \underline{V}_L , and \underline{V}_C (φ_1 and φ_2) but also will lead to varying the voltage magnitudes of \underline{V}_L , and \underline{V}_C (V_L and V_C). Thus, $V_L \neq V_C \neq V_S$ in the UPFC- UIPC, unlike the SPS-based UIPC case. The following quantities can be derived for the UPFC-based UIPC:

$$\underline{I}_L = \frac{V_{injL} \angle(\delta + \rho_1) + V_S \angle \delta - V_m \angle \delta_m}{jX_A} \quad (2.26)$$

$$\underline{I}_C = \frac{V_{injC} \angle(\delta + \rho_2) + V_S \angle \delta - V_m \angle \delta_m}{-jX_A} \quad (2.27)$$

$$\underline{I}_{TL} = \frac{V_{injL} \angle(\delta + \rho_1) - V_{injC} \angle(\delta + \rho_2)}{jX_A} \quad (2.28)$$

$$\underline{V}_m = \frac{X_{TL}}{X_A} [V_{injL} \angle(\delta + \rho_1) - V_{injC} \angle(\delta + \rho_2)] + V_r \angle 0 \quad (2.29)$$

$$P_R = \frac{V_{injL} V_r}{X_A} \sin(\delta + \rho_1) - \frac{V_{injC} V_r}{X_A} \sin(\delta + \rho_2) \quad (2.30)$$

$$Q_R = \frac{V_{injL} V_r}{X_A} \cos(\delta + \rho_1) - \frac{V_{injC} V_r}{X_A} \cos(\delta + \rho_2) \quad (2.31)$$

From (2.28) -(2.31), one notes that all quantities are functions of V_r , and X_A , considered to be fixed. They are also functions of the magnitudes of the series injected voltages V_{injL} and V_{injC} , and their angles, ρ_1 and ρ_2 . These four control variables of the UPFC-based UIPC provide a more flexible way to control the current flow through the transmission line. Before studying how to calculate V_{injL} , ρ_1 , V_{injC} and ρ_2 to achieve the desired current flow through the transmission line, it is important to define their control ranges. This will be done in the next subsection.

2.4.2. Control Limits of the UPFC-based UIPC

The control range of the angles of the series injected voltages by VSC1 and VSC2, ρ_1 and ρ_2 are assumed to be within a fully controlled range, ($0 \leq \rho_1 \& \rho_2 \leq 2\pi$) [49]. The control ranges of V_{injL} and V_{injC} , are assumed to 0.25 pu same as the SPS-based UIPC [15]. As a result, the control ranges of the main control variables of the UPFC-based UIPC are:

$$(0 \leq V_{injL} \& V_{injC} \leq 0.25pu) \quad (2.32)$$

$$(0 \leq \rho_1 \& \rho_2 \leq 2\pi) \quad (2.33)$$

2.4.3. Calculation of the Control Parameters of the UPFC- based UIPC

Assuming that the desired complex current flowing in the transmission line is known, it can be used to calculate the required values of V_{injL} , ρ_1 , V_{injC} , and ρ_2 . Using (2.28), the transmission line current magnitude and angle are obtained as:

$$I_{TL} = \frac{\sqrt{V_{injL}^2 + V_{injC}^2 - 2V_{injL}V_{injC} \cos(\rho_1 - \rho_2)}}{X_A} \quad (2.34)$$

$$\phi_{TL} = \tan^{-1} \left[\frac{V_{injC} \cos(\delta + \rho_2) - V_{injL} \cos(\delta + \rho_1)}{V_{injL} \sin(\delta + \rho_2) - V_{injC} \sin(\delta + \rho_1)} \right] \quad (2.35)$$

From the (2.34) and (2.35), one can note that finding the main control variables of the UPFC-based UIPC is not as straightforward as the SPS-based UIPC case. This is because there are only two equations and four unknowns. Thus, a certain approach needs to be applied to find these unknown variables.

The proposed approach in this work is to calculate the UPFC-based UIPC control variables by splitting the real and imaginary parts of the transmission line current among the inductive and capacitive branches as a function of sharing factors, α and β , bounded between 0 and 1. That is,

$$\underline{I}_L = \alpha \times Re(\underline{I}_{TL}) + j\beta \times Im(\underline{I}_{TL}) \quad (2.36)$$

$$\underline{I}_C = (1 - \alpha) \times Re(\underline{I}_{TL}) + j(1 - \beta) \times Im(\underline{I}_{TL}) \quad (2.37)$$

These will affect the internal voltages of the UIPC as

$$\underline{V}_L = \underline{V}_m + jX_A \underline{I}_L \quad (2.38)$$

$$\underline{V}_C = \underline{V}_m - jX_A \underline{I}_C \quad (2.39)$$

$$\underline{V}_{injL} = \underline{V}_L - \underline{V}_S \quad (2.40)$$

$$\underline{V}_{injC} = \underline{V}_C - \underline{V}_S \quad (2.41)$$

Since the required equations are now based on the sharing factors, α , and β , one should be able to find a combination of the UPFC-based UIPC control variables (V_{injL} , ρ_1 , V_{injC} , and ρ_2) that realizes the desired transmission line current, ideally without violation of the injected voltage limits constraints and the bounds of α and β . This task can be done using optimization techniques, which will be discussed in the next subsection.

2.4.4. Parameters Calculation by Means of Optimization

The general form of a problem in optimization

$$\text{minimize/maximize } f(x) \text{ Subject to } x \in \Omega$$

Where, $f(x)$ is the the cost function (CF) that will be minimized or maximized, and x is the variable that will be obtained to min/max $f(x)$, and finally, Ω is the set of feasible values of variable x that meets the constraints [50].

One function worth minimizing is the apparent power injected by VSC1 and VSC2, which should lead to reduced power losses and lower stress on the switches. Therefore, the target of the optimization is:

$$CF = S_{injL}^2 + S_{injC}^2 = (V_{injL}I_L)^2 + (V_{injC}I_C)^2 \quad (2.42)$$

It is subject to two types of constraints,

1- Bound constraints

$$0 \leq \alpha \leq 1 \ \& \ 0 \leq \beta \leq 1 \quad (2.43)$$

2- Nonlinear inequality constraints

$$C_1 = V_{injL} \leq 0.25 \quad (2.44)$$

$$C_2 = V_{injC} \leq 0.25$$

Where 0.25 is the maximum value of the injected voltage magntute.

The objective function and constraints are rewritten as functions of α and β in the optimization program (MATLAB). In MATLAB's optimization toolbox, there are many built-in functions. Since the cost function is a function of two variables (α and β) and the constraints includes inequality nonlinear constraint functions, and the main task of the optimization is to minimize them, the selected built-in function is *fmincon* (Find a minimum of constrained nonlinear multivariable function) [51].

2.5. Case Study

The electrical system used for this study is a simple 2-node transmission system with the UIPC connected at the sending end shown in Figure 2-6. The system voltage is 230 kV, the rated frequency is 60 Hz, and the base power is 100 MVA. The system parameters in pu are given in Table 2-1.

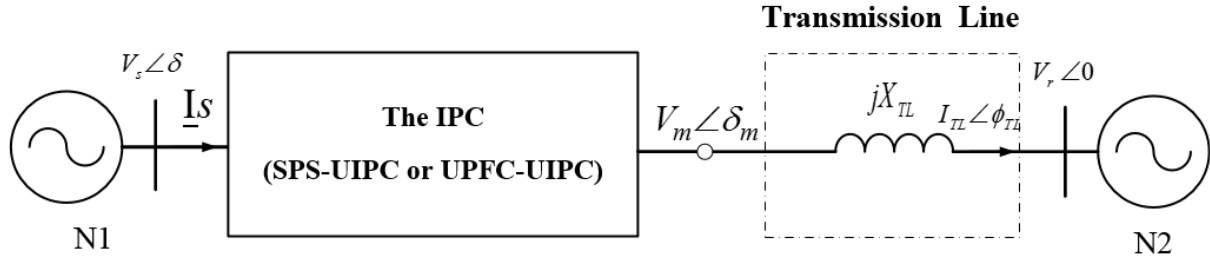


Figure 2-6: The 2-node transmission system with the UIPC connected at the sending end

Table 2-1: The System parameters

V_s	V_r	δ	X_{TL}	X_A
1pu	1pu	$0^\circ \leq \delta \leq 30^\circ$	0.4pu	0.35pu

Other important parameters that are assumed to be given as mentioned before are the desired magnitude, and the angle of the transmission line current, I_{TL-des} and ϕ_{TL-des} respectively. Table 2-2 gives the different control limits of I_{TL-des} for different values of δ .

Table 2-2: The transmission line current control range for different δ

δ ($^\circ$)	I_{TL-unc}	I_{TL-des} (max(UIPC))	I_{TL-des} (min(UIPC))	The control limit
0	0	0.6	0	$0 \leq I_{TL(UIPC)} \leq 0.6$
5	0.2181 \approx 0.2	0.6	0	$0 \leq I_{TL(UIPC)} \leq 0.6$
10	0.4358 \approx 0.4	0.6	0	$0 \leq I_{TL(UIPC)} \leq 0.6$
15	0.6526 \approx 0.6	0.7	0.1	$0.1 \leq I_{TL(UIPC)} \leq 0.7$
20	0.8682 \approx 0.9	0.9	0.3	$0.3 \leq I_{TL(UIPC)} \leq 0.9$
25	1.0822 \approx 1.1	1.1	0.5	$0.5 \leq I_{TL(UIPC)} \leq 1.1$
30	1.2941 \approx 1.3	1.3	0.7	$0.7 \leq I_{TL(UIPC)} \leq 1.3$

where I_{TL-unc} is the current magnitude for an uncompensated transmission line case (no UIPC, is connected to the transmission line).

For this work, three desired values of the transmission line current angle, ϕ_{TL-des} , are considered. These three values of ϕ_{TL-des} , which are corresponded to three Power Factor (PF) cases at the receiving end of the transmission line, are: $\phi_{TL-des} = 0^\circ$ (PF = 1), $\phi_{TL-des} = 36.87^\circ$ (PF = 0.8/leading), and $\phi_{TL-des} = -36.87^\circ$ (PF = 0.8/lagging). The results with each value of $\phi_{ITL-des}$ (PF) will be presented separately as three main cases.

These three PF cases will be used to compare the performance of the conventional (SPS-based) UIPC and the proposed (UPFC-based) UIPC when operating in a certain control range of I_{TL-des} for different values of δ . Furthermore, they will be used to compare the ability of the two control schemes to supply or absorb reactive power within a certain range. For each case, δ and I_{TL-des} will be varied based on their defined ranges, which were mentioned in Table 2-1 and Table 2-2, respectively.

In order to compare the results of the SPS-based UIPC with the results of the UPFC-based UIPC for each case, each quantity of each branch of the SPS-UIPC is presented in the same plot with the quantity that corresponds to the same branch of the UPFC-UIPC. For example, the voltage injected by VSC1 for the SPS-UIPC is denoted as $V_{injL-SPS}$ and is plotted at the same subplot as that for the UPFC-UIPC, denoted as $V_{injL-UPFC}$.

In the case of the SPS-UIPC, the desired values of I_{TL-des} and ϕ_{TL-des} are used to calculate the required angles of the 2 SPS, φ_1 and φ_2 using (2.20) and (2.21). For the case of the UPFC-UIPC, the approach is to run the optimization program to minimize the magnitudes of S_{injL} and S_{injC} using the cost function of (2.42) without exceeding the injected voltage limits of VSC1 and VSC2 and keeping α and β within their defined bounds.

2.5.1. The Unity Power Factor (UPF) Case (PF = 1)

For the UPF case ($\phi_{TL-des} = 0^\circ$), the receiving end of the power system shown in Figure 2-6 does not supply nor absorb reactive power ($Q_r = 0$ pu). Therefore, the reactive power absorbed by the transmission line has to be supplied by the UIPC and the sending end of the system.

The figures below show the results of different quantities; those required by the SPS-UIPC and UPFC-UIPC to achieve different desired control ranges of I_{TL-des} for different values of δ for the UPF case ($\phi_{ITL} = 0^\circ$).

From Figure 2-7 (A) and (B), one sees that the values of $V_{injL-UPFC}$ and $V_{injC-UPFC}$ did not exceed the maximum limit (0.25pu, the red line). Figure 2-7 (A) shows that $V_{injL-SPS}$ is higher than $V_{injL-UPFC}$ in many cases. Although $V_{injL-UPFC}$ is higher than $V_{injL-SPS}$ for few cases, it is still within its defined limit. Figure 2-7 (B) shows that $V_{injC-SPS}$ is higher than $V_{injC-UPFC}$ for all values of δ and all current values defined within its control range.

The overall comparison of the injected voltages by both UIPCs shows that both series VSCs of the UPFC-UIPC are required to inject less voltage than the ones corresponding to the SPS-UIPC.

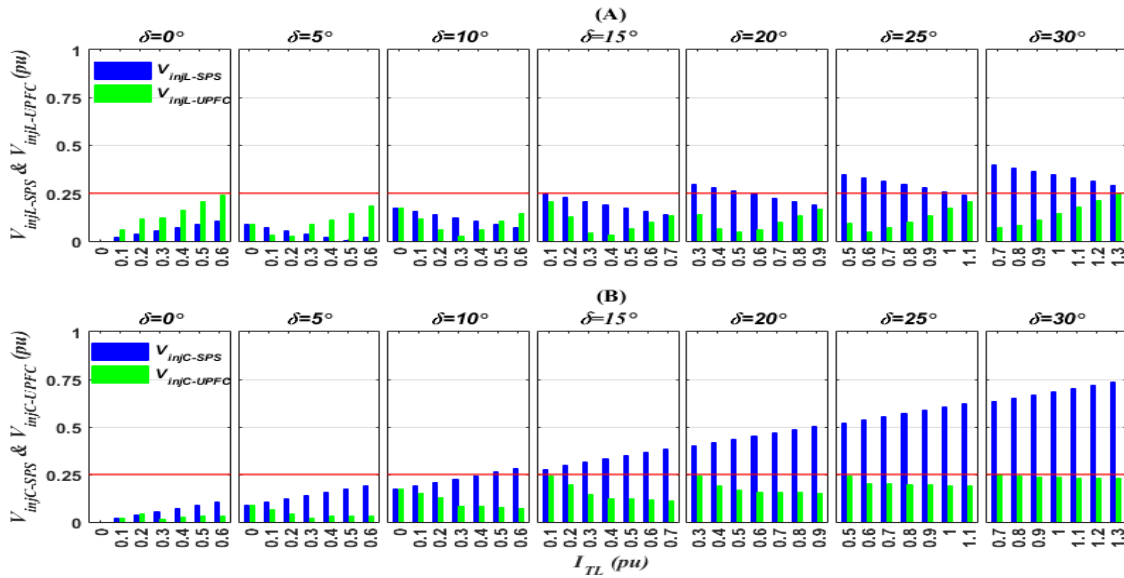


Figure 2-7: Comparison of the results (A) $V_{injL-SPS}$ and $V_{injL-UPFC}$ (B) $V_{injC-SPS}$ and $V_{injC-UPFC}$; for different values of I_{TL} and δ and the UPF case ($PF=1$).

Since the injected voltages of both SPSs, $V_{injL-SPS}$ and $V_{injC-SPS}$, are directly related to the phase shifting angles, ϕ_1 and ϕ_2 , as per (2.22) and (2.23), no comments will be made on whether the phase shifting angles exceed the maximum value.

From Figure 2-8 (A), one can see that the currents flowing through the inductive branches of both UIPCs do not exceed the desired value of I_{TL} for all the defined control range of I_{TL} and all δ values. In many cases, I_{L-UPFC} is smaller than I_{L-SPS} . From Figure 2-8 (B), one can note that I_{C-SPS} is higher than I_{C-UPFC} . More importantly, I_{C-SPS} is higher than the desired value of I_{TL} for all the defined control range of I_{TL} and δ values. The values of I_{C-SPS} are high enough from I_{TL} to make the difference between them (which is equal to I_{L-SPS}) more than half of I_{TL-des} . On the other hand, I_{C-UPFC} is always smaller than I_{TL} for all the defined control range of I_{TL} and δ .

In short, the current values of both branches in the case of the SPS-UIPC are higher than in the UPFC-UIPC case. The high values of I_{C_SPS} and I_{L_SPS} will lead to increases power losses in both series VSCs of the SPS-UIPC.

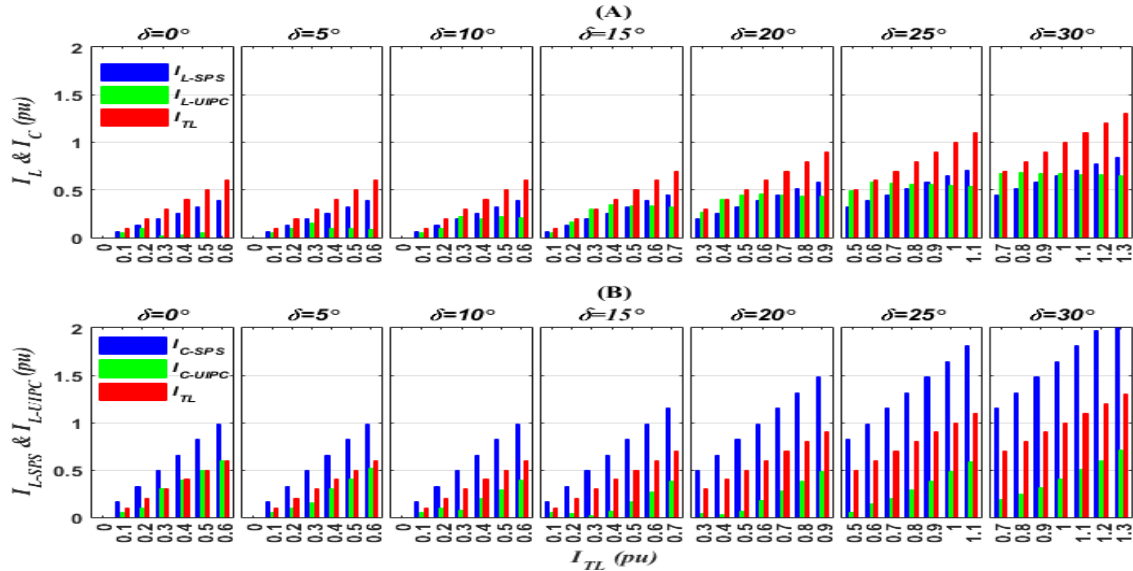


Figure 2-8: Comparison of the results (A) The absolute values of I_{L_SPS} & I_{L_UPFC} , and I_{TL} (B) The absolute values of I_{C_SPS} & I_{C_UPFC} and I_{TL} ; for different values of I_{TL} , δ , and $PF=1$

Figure 2-9 (A) shows that S_{injL_SPS} is higher than S_{injL_UPFC} in many cases. Figure 2-9 (B) shows that S_{injC_SPS} is higher than S_{injC_UPFC} for all δ values for all current values defined in its control range. In other words, the series VSCs of the SPS-UIPC injected more apparent power than the series VSCs of the UPFC-UIPC. This is expected for the capacitive branch of the SPS-UIPC since the current flowing in this branch and the injected voltage are quite high.

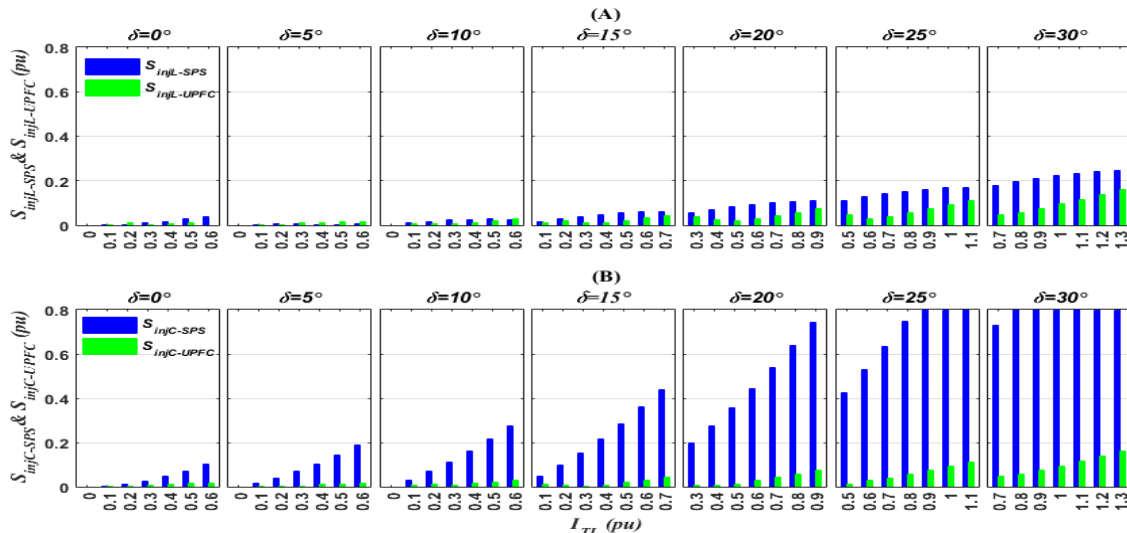


Figure 2-9: Comparison of the results (A) S_{injL_SPS} and S_{injL_UPFC} (B) S_{injC_SPS} and S_{injC_UPFC} ; for different values of I_{TL} and δ and $PF=1$

Figure 2-10 (A) and (B) show that the voltage magnitudes at the connection points between the series VSCs and the series reactance of both branches of the SPS-UIPC, V_{L-SPS} , and V_{C-SPS} , is always constant and equal to V_s . This is expected since the SPSs considered in this work are of the symmetrical type. On the other hand, V_{L-UPFC} and V_{C-UPFC} for the UPFC-based UIPC are variable, unlike V_{L-SPS} and V_{C-SPS} . Figure 2-10 (A), the values of V_{L-UPFC} increase as I_{TL} increases to high values defined within its desired control range for a given δ . These values of V_{L-UPFC} are increased to unacceptable values, above 1.1pu, in some cases. In contrast, the values of V_{C-UPFC} are still within the acceptable limits for all values of I_{TL} as can be seen in Figure 2-10 (B).

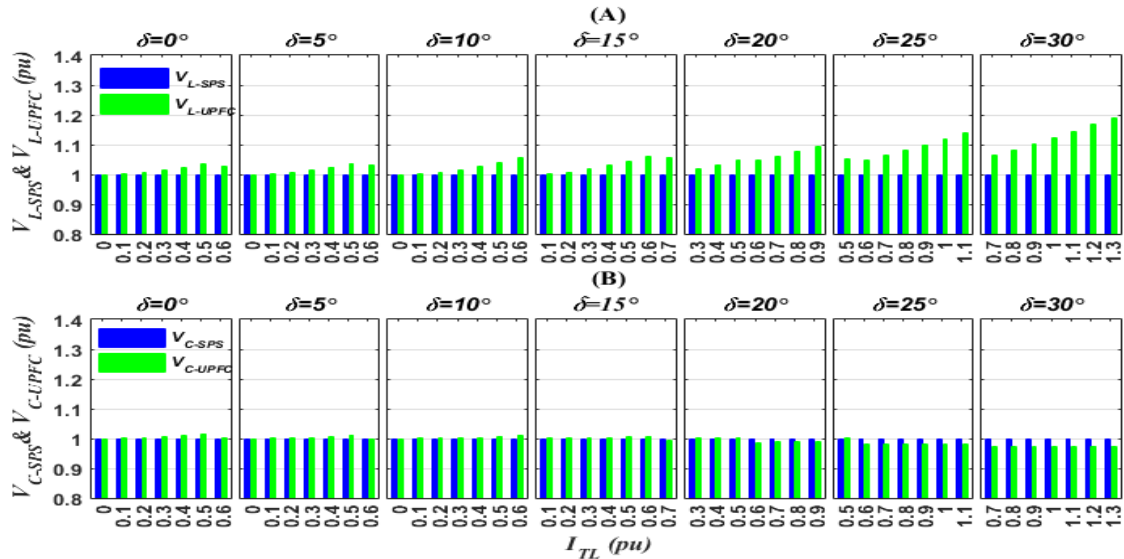


Figure 2-10: Comparison of the results (A) V_{L-SPS} and V_{C-SPS} (B) V_{L-UPFC} and V_{C-UPFC} ; for different values of I_{TL} and δ and for $PF = 1$.

2.5.2. $PF = 0.8$ / Leading Case

For the leading PF case with a value equal to 0.8 ($\phi_{ITL} = 36.87^\circ$), the receiving end of the power system shown in Figure 2-6, will supply reactive power to the transmission line. The surplus of reactive power, if any, has to be absorbed by the UIPC. The figures below show the results of different quantities; those required by the SPS-UIPC and UPFC-UIPC to achieve different desired control ranges of I_{TL} for different values of δ and for the leading PF case with a value of 0.8.

From Figure 2-11 (A) and (B), it is clear that the response of the SPS-UIPC in this case (leading PF) is different from the UPF case. This is because the UIPC might have to absorb a portion of the reactive power that is supplied by the receiving end. The values of $V_{injL-SPS}$ and $V_{injC-SPS}$ are quite high for many cases.

For the UPFC-UIPC, one can note that the limit of the injected voltages has been exceeded in a few cases. The worst value for $V_{injL-UPFC}$ is 0.282pu when $I_{TL} = 1.3pu$ and $\delta = 30^\circ$. While the worst case for $V_{injC-UPFC}$ is 0.286pu when $I_{TL} = 1.3pu$ and $\delta = 30^\circ$. Nevertheless, these values of $V_{injL-UPFC}$ and $V_{injC-UPFC}$ are still smaller than the values of $V_{injL-SPS}$ and $V_{injC-SPS}$. The angles of the SPSs, φ_1 , and φ_2 follow the variation of the injected voltages, $V_{injL-SPS}$ and $V_{injC-SPS}$.

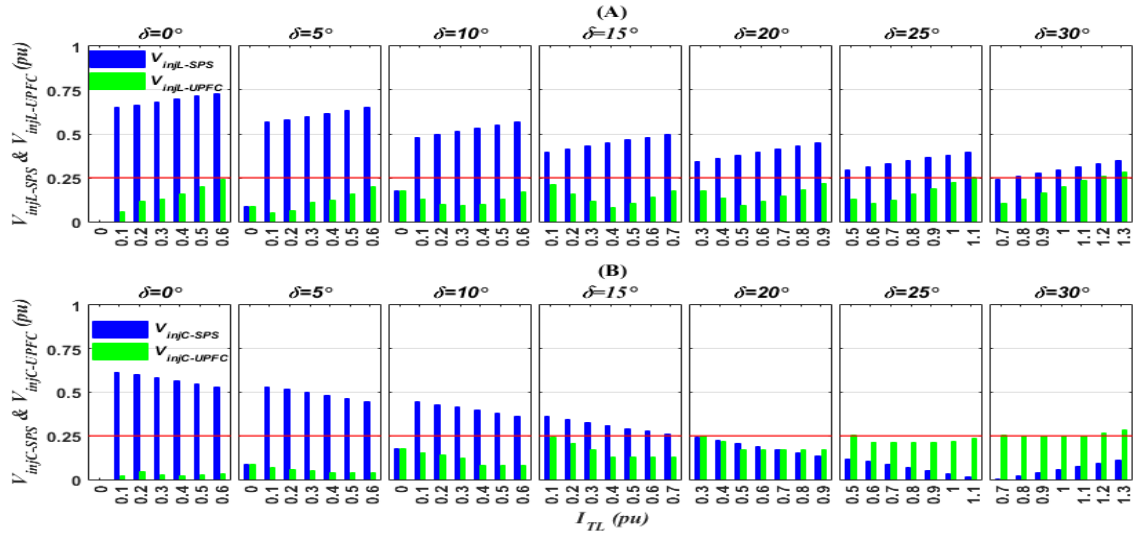


Figure 2-11: Comparison of the results (A) $V_{injL-SPS}$ and $V_{injL-UPFC}$ (B) $V_{injC-SPS}$ and $V_{injC-UPFC}$; for different values of I_{TL} and δ and for PF=0.8/leading.

From Figure 2-12 (A) and (B), one can see that I_{L-SPS} and I_{C-SPS} are higher than I_{L-UPFC} and I_{C-UPFC} , respectively. For this case (leading PF), not only I_{C-SPS} is higher than the desired value of I_{TL} but also I_{L-SPS} . On the other hand, I_{L-UPFC} and I_{C-UPFC} are always smaller than I_{TL} for all the defined range of I_{TL} and δ values. In summary, the currents of both branches in the case of the SPS-UIPC are higher than in the UPFC-UIPC case. The high values of I_{C-SPS} and I_{L-SPS} will lead to increased power losses in both series VSCs. If the UPF and leading PF cases are compared, the values of I_{L-SPS} for the leading PF case are higher than the ones for the UPF case.

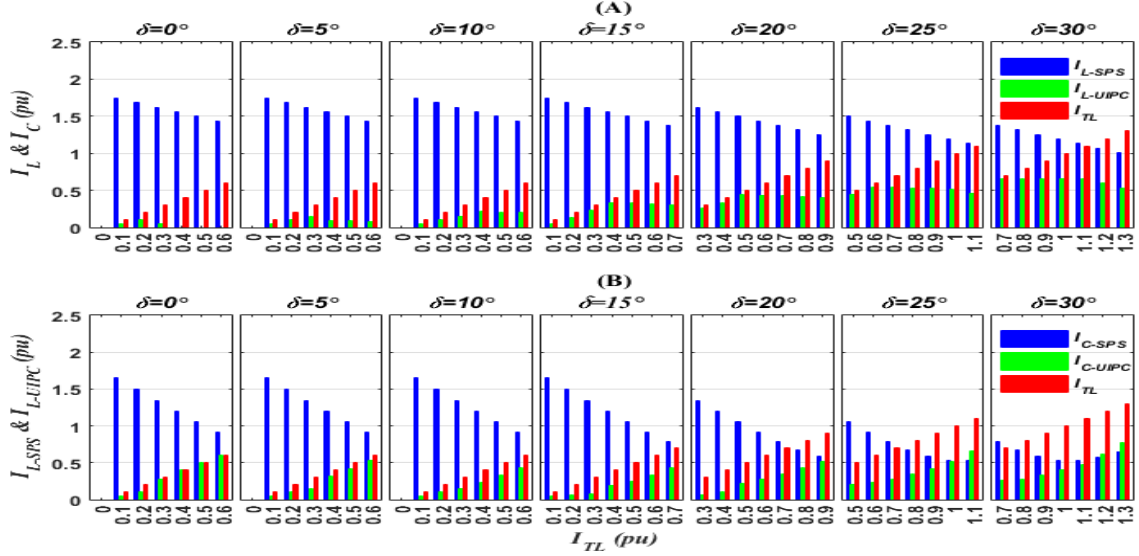


Figure 2-12: Comparison of the results (A) The absolute values of I_{L-SPS} & I_{L-UPFC} , and I_{TL} (B) The absolute values of I_{C-SPS} & I_{C-UPFC} and I_{TL} ; for different values of I_{TL} and δ and PF=0.8/leading

Figure 2-13 (A) and (B) show that $S_{injL-SPS}$ is higher than $S_{injL-UPFC}$ and that $S_{injC-SPS}$ is higher than $S_{injC-UPFC}$ in most cases. With respect to the *UPF* case, $S_{injL-SPS}$ and $S_{injC-SPS}$ are quite large for the leading *PF* case. On the other hand, $S_{injL-UPFC}$ and $S_{injC-UPFC}$ are almost like the *UPF* case.

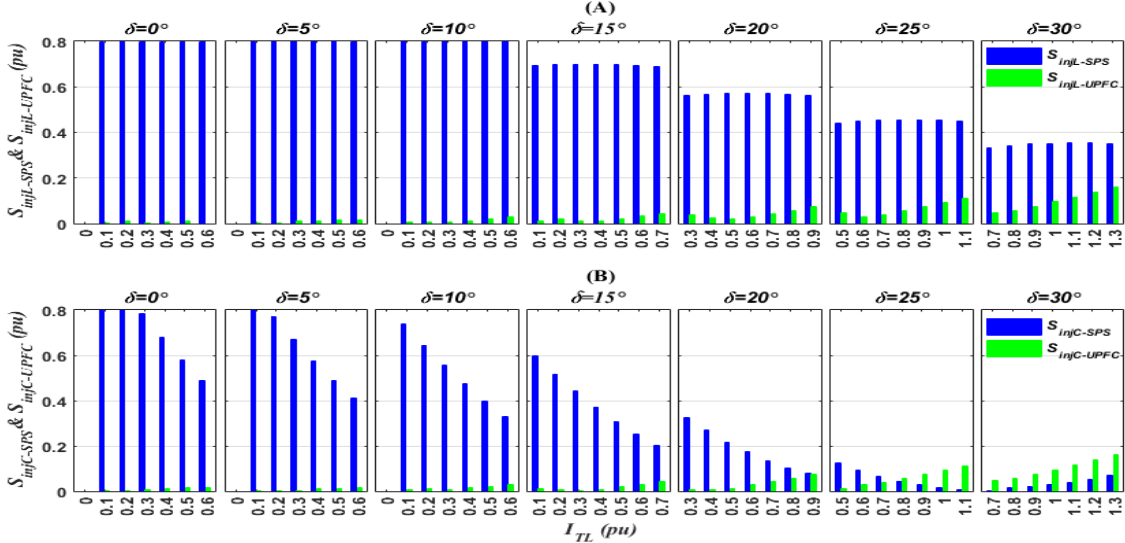


Figure 2-13: Comparison of the results (A) $S_{injL-SPS}$ and $S_{injL-UPFC}$ (B) $S_{injC-SPS}$ and $S_{injC-UPFC}$; for different values of I_{TL} and δ and PF=0.8/leading

Figure 2-14 (A) and (B) show that V_{L-SPS} and V_{C-SPS} , are always constant and equal to V_s (1pu in this case) like in the *UPF* case. On the other hand, V_{L-UPFC} and V_{C-UPFC} vary. The values of V_{L-UPFC} and V_{C-UPFC} drop below 1pu for all values of I_{TL} greater than zero. The values of V_{C-UPFC} are still within the acceptable limit. In the other hand, the values of V_{L-UPFC} are quite low and

sometimes exceed, 0.9pu, especially for high I_{TL} . Nevertheless, the UIPC components can be designed to accept certain levels of its internal voltages, V_{L-UPFC} and V_{C-UPFC} .

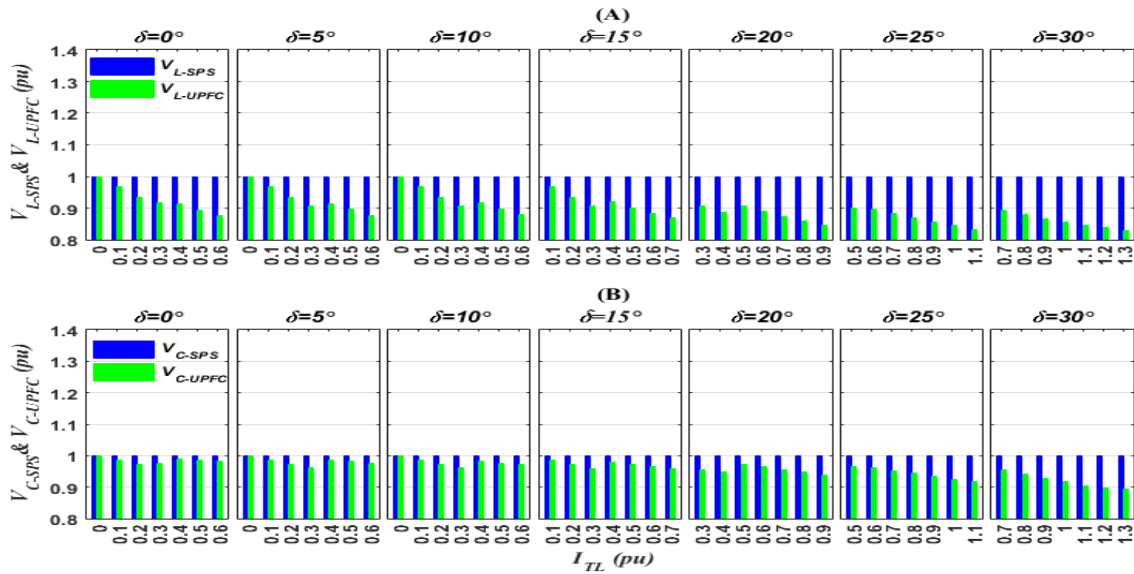


Figure 2-14: Comparison of the results (A) V_{L-SPS} and V_{L-UPFC} (B) V_{C-SPS} and V_{C-UPFC} ; for different values of I_{TL} and δ and $PF=0.8/\text{leading}$

2.5.3. PF = 0.8/ Lagging Case

For the lagging PF case with a value equal to 0.8 ($\phi_{ITL} = -36.87^\circ$), the receiving end of the power system shown in Figure 2-6 will absorb reactive power from the system. Therefore, the UIPC has to supply this absorbed reactive power by the receiving end of the system. The figures below show the results of different quantities; those required by the SPS-UIPC and UPFC-UIPC to achieve different desired control ranges of I_{TL} for different values of δ .

From Figure 2-15 (A) and (B), it is clear that the response of the SPS-UIPC to the case of lagging PF is different from the previous ones. The values of $V_{injL-SPS}$ and $V_{injC-SPS}$ are quite high for all magnitudes of I_{TL} that are defined within the desired control range for a given δ . From Figure 2-15 (A) and (B), one sees that the values of $V_{injL-UPFC}$ and $V_{injC-UPFC}$ exceed the maximum limit (0.25pu, the red line) many times. The worst case for $V_{injL-UPFC}$ is 0.345pu when $I_{TL} = 1.3\text{pu}$ and $\delta = 30^\circ$. Conversely, the worst case for $V_{injC-UPFC}$ is 0.295pu when $I_{TL} = 0.7\text{pu}$ and $\delta = 30^\circ$. Nevertheless, these values of $V_{injL-UPFC}$ and $V_{injC-UPFC}$ are still smaller than the values of $V_{injL-SPS}$ and $V_{injC-SPS}$.

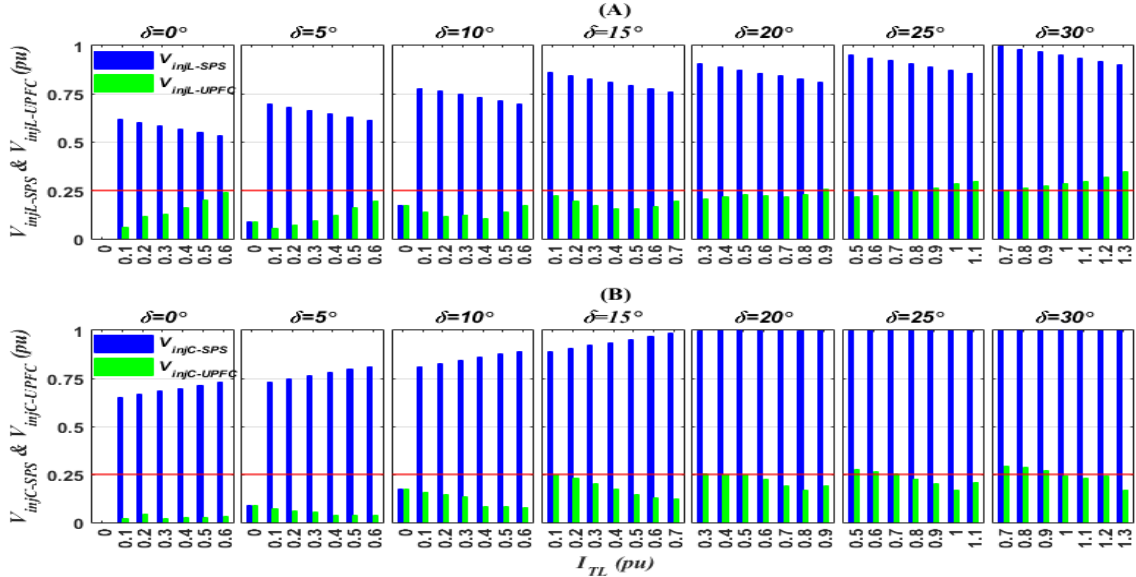


Figure 2-15: Comparison of the results (A) $V_{injL-SPS}$ and $V_{injL-UPFC}$ (B) $V_{injC-SPS}$ and $V_{injC-UPFC}$; for different values of I_{TL} and δ and $PF=0.8/lagging$

From Figure 2-16 (A) and (B), one sees that I_{L-SPS} and I_{C-SPS} are higher than I_{L-UPFC} and I_{C-UPFC} , respectively. Moreover, I_{L-SPS} and I_{C-SPS} for lagging PF are higher than the ones corresponding to the UPF and leading PF cases. The absolute values of I_{L-SPS} and I_{C-SPS} are higher than the desired value of I_{TL} for all defined control ranges of I_{TL} and all δ . On the other hand, I_{L-UPFC} and I_{C-UPFC} are always smaller than I_{TL} for all defined control ranges of I_{TL} and δ .

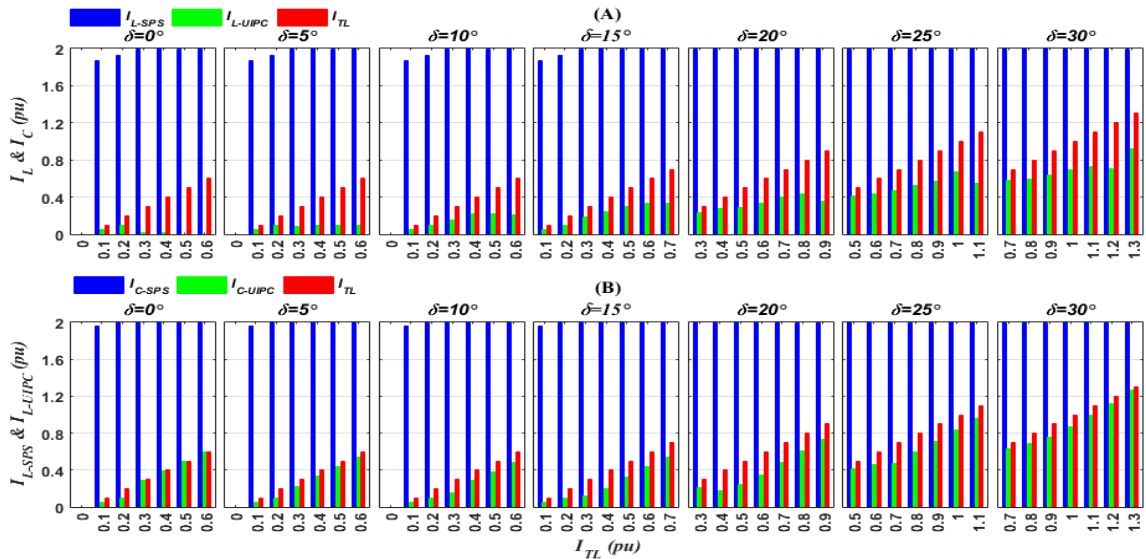


Figure 2-16: Comparison of the results (A) Absolute values of I_{L-SPS} and I_{L-UPFC} and I_{TL} (B) Absolute values of I_{C-SPS} and I_{C-UPFC} , and I_{TL} ; for different values of I_{TL} and δ and $PF=0.8/lagging$

Figure 2-17 (A) and (B) show that the same conclusion can be reached for the lagging PF case as the UPF and the leading PF cases in terms of the comparison between $S_{injL-SPS}$ and $S_{injL-UPFC}$.

UPFC or $S_{injC-SPS}$ and $S_{injC-UPFC}$. Both series VSCs of the UPFC-UIPC inject less apparent power than the SPS-UIPC. In terms of the comparison between the injected apparent powers by the same series VSC of the same IPC (SPS-UIPC or UPFC-UIPC) for the *UPF* case or leading *PF* case, and the lagging *PF* case, the results for this case are much worse for the SPS-UIPC and almost similar for the UPFC-UIPC.

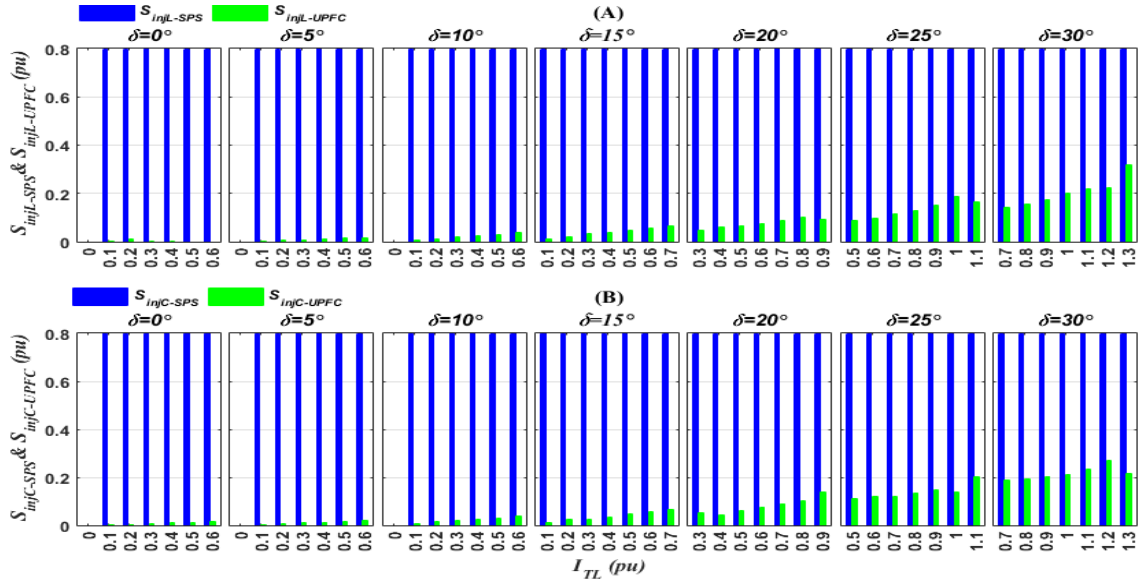


Figure 2-17: Comparison of the results (A) $S_{injL-SPS}$ and $S_{injL-UPFC}$ (B) $S_{injC-SPS}$ and $S_{injC-UPFC}$; for different values of I_{TL} and δ and $PF=0.8$ /lagging

To sum up, the values of the injected apparent power by the VSCs of both branches of the SPS-UIPC are higher than those of the UPFC-based UIPC. The high values of $S_{injL-SPS}$ and $S_{injC-SPS}$ will lead to increased power losses in both series VSCs.

Figure 2-18 (A) and (B) show that V_{L-SPS} and V_{C-SPS} , are always constant at 1pu like in the other cases. On the other hand, V_{L-UPFC} and V_{C-UPFC} vary. The values of V_{L-UPFC} raised above 1pu for all values of I_{TL} greater than zero and exceeded the acceptable limit, 1.1pu especially for high I_{TL} . The values of V_{C-UPFC} are still with the acceptable limit.

In terms of comparison between different *PF* cases, the resulting voltage in the capacitive branch of the UPFC-UIPC, V_{C-UPFC} , is usually within its acceptable limit. However, the resulting voltage in the inductive branch of the UPFC-UIPC, V_{L-UPFC} , raised to an unacceptable value (1.3 pu) for the lagging *PF* case and decreased to an unacceptable for leading *PF* case.

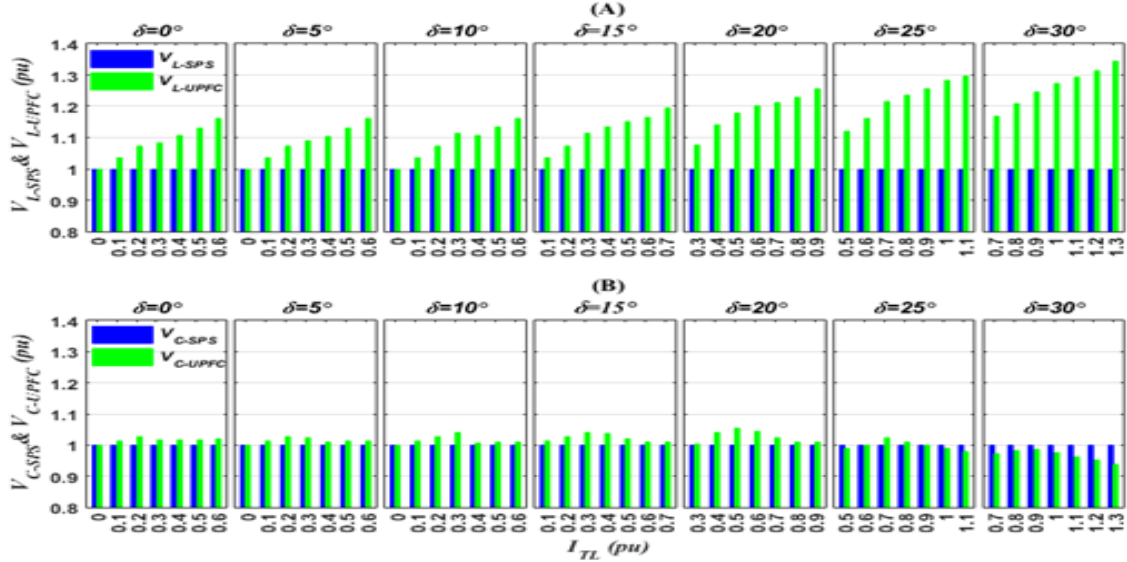


Figure 2-18: Comparison of the results (A) V_{L-SPS} and V_{C-SPS} (B) V_{L-UPFC} and V_{C-UPFC} ; for different values of I_{TL} and δ and for $PF=0.8$ /lagging

2.5.4. Comparison of the Numerical Results of the SPS-UIPC and the UPFC-based UIPC

The purpose of this subsection is to give a summary of the results, to determine the gains from using the UPFC-UIPC over the SPS-UIPC in terms of values of the injected voltage, and injected apparent power by the series VSCs that are required to achieve a certain control range of I_{TL} for different δ and for different power factors. The maximum values of the quantities mentioned above are given in Table 2-3.

From Table 2-3, one can see that the SPS-UIPC has to inject more voltage with its series VSCs than the UPFC-UIPC. If the worst cases are considered, which occur for $PF = 0.8$ lagging, the rated voltage of the series VSC in the inductive branch of the SPS-UIPC has to be almost three times that of the UPFC-UIPC. For the capacitive branch, the rated voltage of the series VSC of the SPS-UIPC has to be more than four times that of the series VSC of the UPFC-UIPC.

Table 2-3 also shows the maximum injected apparent power of both series VSCs that are required to achieve a certain range of I_{TL-des} for different δ and for different power factors. Like for the injected voltage, the worst case, $PF = 0.8$ lagging, is considered. The rated power of the series VSC in the inductive branch of the SPS-UIPC has to be almost nine times that of the UPFC-UIPC. For the capacitive branch, the result is even worse. The rated power of the series VSC of the SPS-UIPC should be more than fifteen times that of the series VSC of the UPFC-UIPC.

Table 2-3: The Comparison of Maximum Values Obtained with the SPS-based UIPC and the UPFC-based UIPC

Quantities	UIPC type	Power factor value		
		<i>UPF (PF = 1)</i>	<i>PF = 0.8/ leading</i>	<i>PF = 0.8/ lagging</i>
The injected voltage of both series VSCs				
$V_{injL-max}$ (pu)	SPS-UIPC	0.398	0.731	0.997
	UPFC-UIPC	0.247	0.282	0.345
$V_{injC-max}$ (pu)	SPS-UIPC	0.735	0.616	1.286
	UPFC-UIPC	0.248	0.286	0.295
The injected power of both series VSCs				
S_{injL} (pu)	SPS-UIPC	0.246	1.133	2.348
	UPFC-UIPC	0.160	0.221	0.271
S_{injC} (pu)	SPS-UIPC	1.572	1.017	4.991
	UPFC-UIPC	0.161	0.158	0.317

Another important aspect to consider is the real and the reactive powers injected by each VSC. The former seems to be more relevant since it will have to flow through the shunt inverter (VSC3) of the dual UPFC. The values of P_{inj} and Q_{inj} for the two series VSCs that that are required to achieve a line current of 1.3 pu at $\delta = 30^\circ$ are shown in Table 2-4. P_{injL} and Q_{injL} refer to VSC1 and P_{injC} , and Q_{injC} refer to VSC2, respectively.

Table 2-4: The Injected Active and Reactive Power of both Series VSCs at $\delta = 30^\circ$ and $I_{TL-des} = 1.3$ pu

Quantities	UIPC type	Power factor value		
		<i>UPF (PF =1)</i>	<i>PF = 0.8/ leading</i>	<i>PF = 0.8/ lagging</i>
P_{injL} (pu)	SPS-UIPC	-0.110	-0.189	-1.138
	UPFC-UIPC	0.087	-0.105	0.310
Q_{injL} (pu)	SPS-UIPC	0.220	0.289	2.053
	UPFC-UIPC	0.135	0.108	0.0235
P_{injC} (pu)	SPS-UIPC	0.285	-0.062	1.667
	UPFC-UIPC	0.087	-0.146	0.213
Q_{injC} (pu)	SPS-UIPC	-1.546	-0.036	-4.705
	UPFC-UIPC	-0.135	-0.166	-0.027

From Table 2-4 one can see that the values of P_{inj} and Q_{inj} for the proposed (UPFC-UIPC) case are smaller than for the conventional (SPS-UIPC) scheme, with the exception of the case of leading PF for VSC2, in the capacitive branch.

2.6. Summary

In this chapter, the use of the full features of the dual UPFC inherent to the UIPC was investigated, and its performance was compared with the basic control strategy, the SPS-based UIPC. For the UPFC-based UIPC, it was proposed to use an optimization technique to determine the increased number of control parameters. Then, a simple case study was used to compare the voltage, current and apparent power quantities of both UIPCs to control the transmission line current to different desired values for different values of angle δ , and for different target values of power factors at the receiving end. It was shown that in most cases, the UPFC-UIPC has to inject lower voltages and conduct lower currents in the two branches than in the SPS-UIPC, thus resulting in much lower apparent power required to impose a desired current in the transmission line. This was shown for the system operating with UPF at the receiving end as well as for $PF = 0.8$, leading and lagging. The only drawback of the proposed method (UPFC-UIPC) is a potential overvoltage in the point of intersection between the series VSC and the UIPC reactance for certain high power conditions.

CHAPTER 3. SIMULATION VERIFICATION OF THE UPFC-BASED UIPC

3.1. Introduction

This Chapter presents a simulation verification to validate the numerical results that are presented in Chapter 2 and to prove the concept of the proposed control scheme of the UIPC (UPFC-based UIPC). A model of the UPFC-based UIPC is developed by using PSCAD/EMTDC. PSCAD/EMTDC is a powerful tool for simulating power systems and studying their transient and dynamic behaviors [52]. Then, dynamic models of the system required for designing of the control loops of the series and shunt branches of the UPFC-based-UIPC are derived. The double loop PI decoupled controller is used to control the shunt branch current and to regulate the DC bus voltage of the UPFC-based-UIPC. The Proportional Resonant (PR) controllers are used to synthesize the currents of the series branches, to achieve the desired transmission line current magnitude and its angle. The performance of these controllers is demonstrated using a simple power system with a UIPC connected in series with a transmission line in the time domain.

3.2. The Unified Interphase Power Controller (UIPC) Model in PSCAD/EMTDC

As shown in Figure 3-1, the main component of the UIPC is the dual UPFC. Therefore, the focus of the implementation of the PSCAD model of the UIPC will be on its dual UPFC.

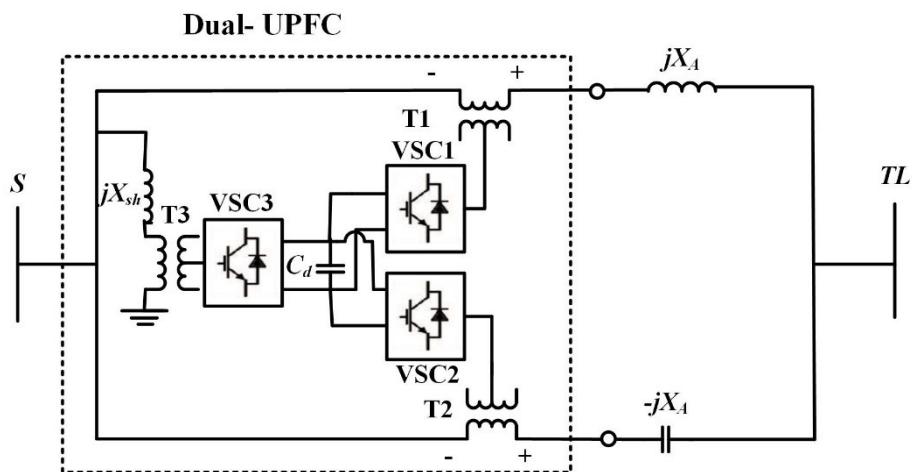


Figure 3-1: The schematic diagram of the UIPC Model

3.2.1. The Model of the Dual UPFC on the PSCAD/EMTDC

The dual UPFC, as seen in Figure 3-1, consists of two series components and one shunt component sharing a DC link. Some of these component models are taken from the PSCAD Master library or PSCAD examples library. For example, the DC capacitor link, C_d , and the 3-phase shunt-coupling transformer, T3, are available in the PSCAD Master library. The structure of three VSCs (VSC1, VSC2, and VSC3), and their gate pattern logic, which are based on Sinusoidal Pulse Width Modulation (SPWM), are imported from the PSCAD examples library [53]. These three VSCs are of the type two level six pulses (6pls) converter. They are connected to realize the structure of the dual UPFC, as shown in Figure 3-2. The series coupling transformers, T1 and T2, are modeled by using three single-phase, two winding, transformers for each branch, see Figure 3-3.

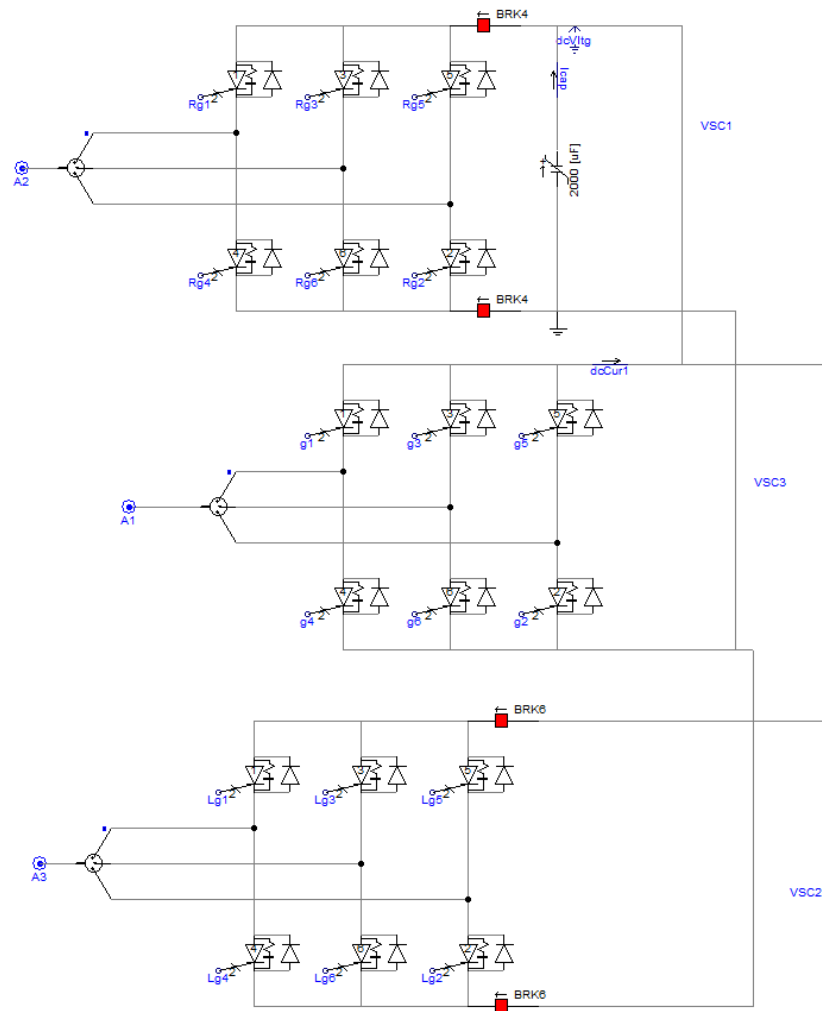


Figure 3-2: The connection of the three VSCs to realize the structure of the dual UPFC

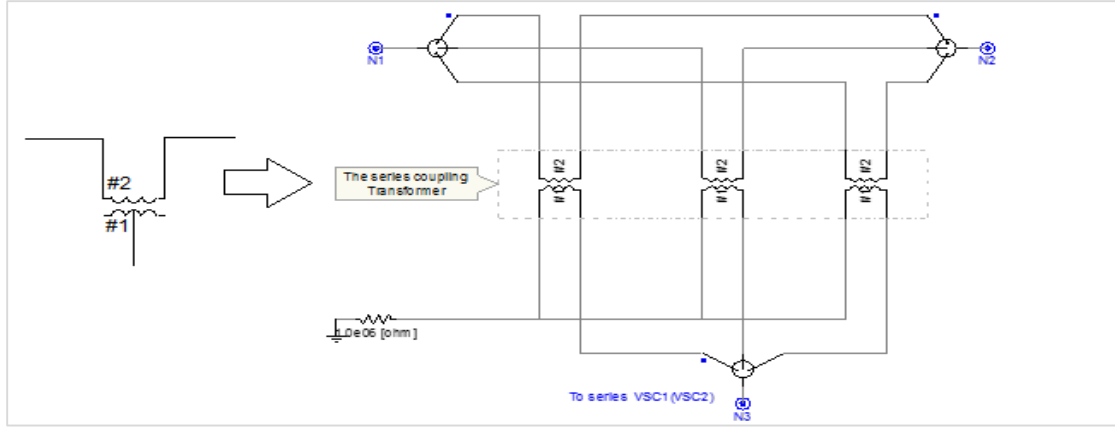


Figure 3-3: The connection of three single phase, two winding, and transformers to form the series coupling transformers (T1 or T2) for each branch of the UPFC-based-UIPC

3.2.2. The Parameters of the UPFC-based UIPC

The parameters of the UIPC that is used for this work are shown in the following tables:

Table 3-1: The parameters of the series coupling transformer (3-phase)

Parameters type	Parameters value
Rating	40MVA
The line-line voltage at the primary side (the VSC1 or VSC2 side)	14.54 kV
The line to line voltage at the secondary side (the inductive or capacitive branch side)	57.5kV
Leakage reactance	0.05pu

Table 3-2: The parameters of the shunt-coupling transformer (3-phase)

Parameters type	Parameters value
Rating	50MVA
The line to line voltage at the secondary side (the VSC3 side)	230 kV (Y)
The line-line voltage at the primary side (the sending end side)	11kV (Δ)
Leakage reactance	0.1pu

Table 3-3: DC side and the VSCs parameters

Parameters type	Parameters value
AC Line to Line voltage	14.4kV
DC rated voltage	25 kV
DC link capacitor	2000 μ F
Switching scheme	SPWM
Switching frequency (f_{sw})	(85 x 60 Hz) = 5100 Hz

The final parameters of the UIPC that need to be defined are the size of the series inductor of the inductive branch, L_L , and the size of the series capacitor of the capacitive branch, C_C . In Chapter 2, it was mentioned that the value of the equivalent reactance of each branch of the UIPC, X_A , is the sum of the reactance of each branch (X_L or X_C) and the leakage reactance of the series-coupling transformer, X_{Tranf} . For the simulation verification case, X_{Tranf} should be extracted from X_A since it is already defined in the PSCAD model of the series-coupling transformer. Then, one can find the size of L_L and C_C that need to be defined for the PSCAD model of the UIPC. The total reactance for each branch considering the tuned type UIPC ($X_{LA} = -X_{CA} = X_A$) are:

$$X_A = X_{LA} = X_L + X_{L_{Tranf}} \quad (3.1)$$

$$X_A = -X_{CA} = -X_C + X_{L_{Tranf}} \quad (3.2)$$

Recall the given values of X_A and X_{Tranf} in pu, the base impedance (Z_{base}) for the considered case study, which were already mentioned in Table 2-1 and Table 3-1, one can find L_{Tranf} , L_L , and C_C . Their values are shown in Table 3-4.

Table 3-4: The size of L_L and C_C

L_{Tranf}	L_L	C_C
0.0146 H	0.4767 H	13.912 μ F

To verify the numerical results from Chapter 2 by using PSCAD model of the UPFC-based UIPC, VSC1 and VSC2 of the series branches and VSC3 of the shunt branch should be controlled by means of close loop control. Next section will discuss the controller types and the mathematical models that will be used to design the control loops for the shunt and series branches.

Before discussing the mathematical models of the series branches and the shunt branch of the UPFC-based UIPC, general aspects that help to have a proper mathematical model will be highlighted. First, to derive the mathematical models of the shunt branch, the series inductive branch, and the series capacitive branches, their single line diagrams are extracted from the UPFC-based UIPC circuit. The circuit of the shunt branch consists of one voltage source, a sending end voltage source (V_s). On the other, hand, the circuits of the inductive and the capacitive branches consist of two voltage sources, a sending end voltage source (V_s) and a variable m-end voltage source, at the transmission line side of the UIPC, (V_m). Considering the variable V_m voltage in the model, instead of the receiving end voltage of the transmission line, will reduce the complexity of

the derivation of the dq models of the inductive and the capacitive branches by implicitly including the impact of the transmission line impedance in the variable m-end voltage source.

The second aspect that should be taken into account for the derivation of the mathematical models, specifically for the series branches of the UIPC, is the effect of the leakage inductance of the series-coupling transformer, L_{Tranf} . Since considering L_{Tranf} will not lead to a change in the order of the system of the inductive branch, its effect will be only on the value of the series inductor, L_L . However, the case is different for the capacitive branch. Unlike the inductive branch, considering L_{Tranf} for the capacitive branch will lead to not only a change in the value of the required series capacitor, C_C but also a change in the system order from first to second-order.

The third aspect that should be considered for the derivation of the mathematical models is the presence of intrinsic/parasitic resistances in of three branches of the UPFC-based UIPC (the shunt and two series branches). These resistance values were not considered in the calculations of the references currents using the optimization techniques in Chapter 2, because their values are small compared with X_A , which will not lead to a noticeable error in the calculated references. Moreover, the closed-loop current controllers will compensate for the error, if there is any. Finally, for the simulation case, the series-coupling transformers and the shunt-coupling transformer are assumed lossless like in Chapter 2. Thus, R_{tranf} is assumed to be zero, the series resistance of the inductive branch, R_L , will be equal to R_{LA} , the series resistance of the capacitive branch, R_C , will be equal to R_{CA} , and the resistance of the shunt branch will be equal to R_{sh}

Based on the aforementioned statements, the single-line circuit of the UPFC-based-UIPC can be redrawn for the derivation of the dynamic mathematical models, as shown in Figure 3-4.

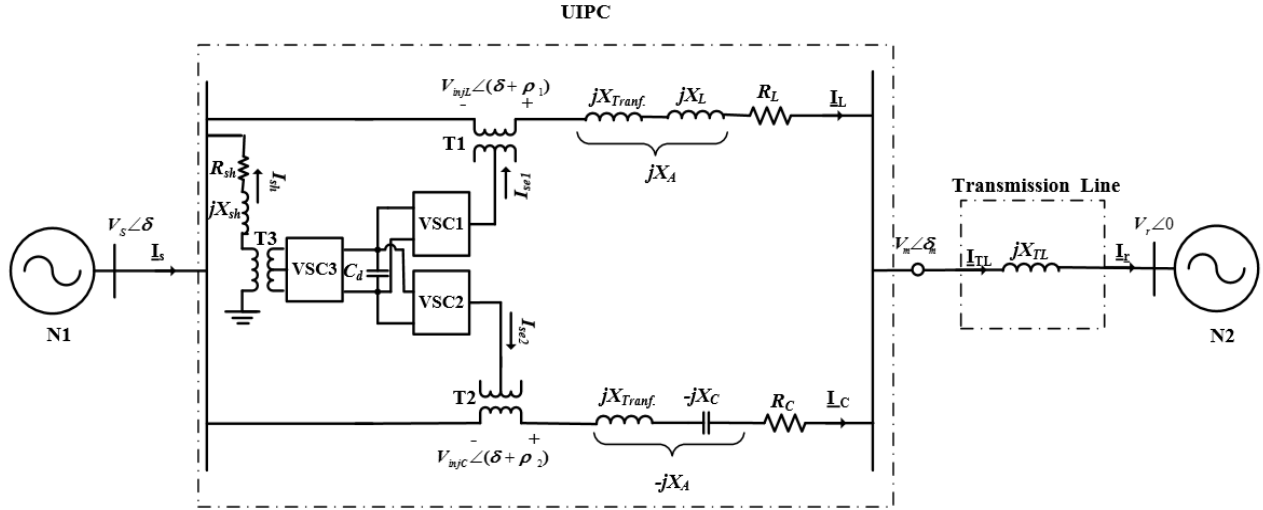


Figure 3-4: The considered UIPC circuit for the control design

3.3. The Mathematical Model and Control Strategy of the Shunt Converter (VSC3) of the UPFC-Based-UIPC

The shunt VSC3 of the shunt branch plays a significant role in the operation of the UPFC-based UIPC. It regulates the DC voltage and provides a path for the active power flow, and supply/absorb the reactive power to the system and regulate the voltage of the AC bus of the UPFC-based UIPC.

The output active and reactive power of the shunt VSC3 can be controlled independently by regulating the current in the q-axis and d-axis, respectively. Consequently, the DC voltage is controlled by the q-axis current component and the AC voltage is controlled by the d-axis current component of the shunt VSC3. The commonly used double loop PI decouple controller (the cascaded PI control) with the synchronous reference frame (dq), for the shunt branch of the UPFC (the STATCOM) is considered in this work [47, 54]. The double loop PI decoupled controller system is composed of, the outer voltage loop, and the inner current loop. In order to design these loops, the mathematical model in the dq frame of the shunt VSC3 and related grid components should be derived. Deriving the mathematical model of the shunt VSC3 in the dq frame results in the transfer functions that are important for the design of the inner and the outer loops of the double loop PI decouple control.

3.3.1. The Mathematical Model of the Inner Current Loop of the Shunt Branch in the dq Frame

The mathematical model of the shunt branch of the UPFC-based UIPC in the dq frame for the inner current loop is similar to the models that have been reported in the literature for the STACOM [55]. Thus, its derivation will not be included, and only the expressions that represent the shunt branch model and equivalent circuits, in dq frame will be presented. Figure 3-5 shows the single line diagram of the shunt branch, which is extracted from the circuit of the UPFC-based-UIPC in Figure 3-4.

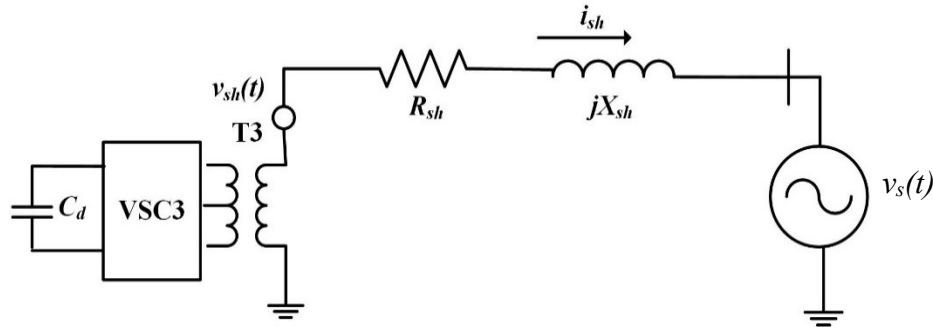


Figure 3-5: The circuit of the shunt branch

Although the derivation of the dq model of the shunt branch will not be included in this work, one should mention that the Park transformation considered in this work is the “original motor notation” [56]. There, the positive d-axis is aligned with the magnetic axis of the field winding, and the positive q-axis leads the d-axis by 90° . In such a case, the d and q components of the grid (reference) voltages are $V_d = 0$ and $V_q = -\sqrt{2} V_{\phi_rms}$.

$$\begin{aligned}
 [f_{dq0}] &= [T_{dq0}(\theta_d)][f_{abc}] \quad \text{and} \quad [f_{abc}] = [T_{dq0}(\theta_d)]^{-1} [f_{dq0}] \\
 [T_{dq0}(\theta_d)] &= \frac{2}{3} \begin{bmatrix} \cos \theta_d & \cos(\theta_d - 120^\circ) & \cos(\theta_d + 120^\circ) \\ \sin \theta_d & \sin(\theta_d - 120^\circ) & \sin(\theta_d + 120^\circ) \\ 0.5 & 0.5 & 0.5 \end{bmatrix} \\
 [T_{dq0}(\theta_d)]^{-1} &= \begin{bmatrix} \cos \theta_d & \sin \theta_d & 1 \\ \cos(\theta_d - 120^\circ) & \sin(\theta_d - 120^\circ) & 1 \\ \cos(\theta_d + 120^\circ) & \sin(\theta_d + 120^\circ) & 1 \end{bmatrix}
 \end{aligned} \tag{3.3}$$

The two main expressions that represent the shunt branch model are:

$$v_{shd} = v_{sd} + L_{sh} \frac{di_{shd}}{dt} + R_{sh} i_{shd} + \omega L_{sh} i_{shq} \quad (3.4)$$

$$v_{shq} = v_{sq} + L_{sh} \frac{di_{shq}}{dt} + R_{sh} i_{shq} - \omega L_{sh} i_{shd} \quad (3.5)$$

The equivalent dq circuits for controller design of the inner current loop for the shunt branch are:

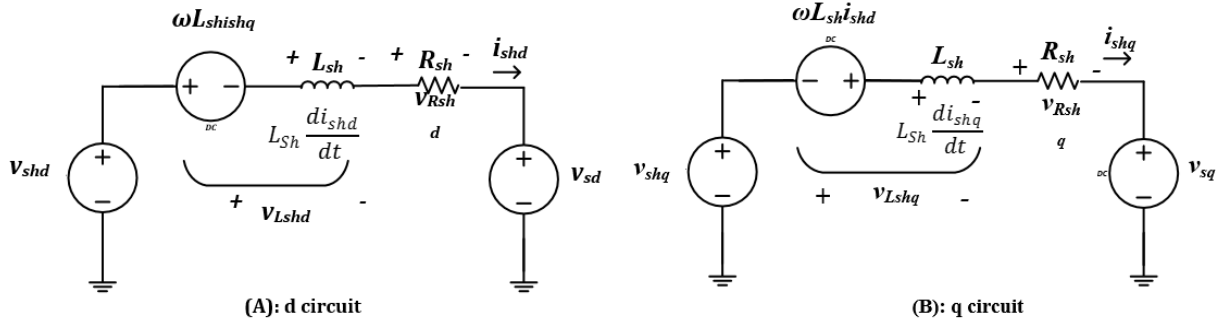


Figure 3-6: The equivalent circuit of the shunt branch (A) d circuit (B) q circuit

The first and last terms of (3.4) and (3.5) are used as feedforward branches to compensate for the variation of the voltage and the effect of the coupling of the d and q currents.

$$v_{shd} = v_{shd1} + v_{sd} + \omega L_{sh} i_{shq} \quad (3.6)$$

$$v_{shq} = v_{shq1} + v_{sq} - \omega L_{sh} i_{shd} \quad (3.7)$$

Where V_{shd1} and V_{shq1} are the voltages of VSC3 required to regulate the current in the RL DC circuit.

- **Control design of the inner current loop of the shunt branch**

With the utilization of the feedforward (FFW) loops, the current controller can be designed considering a decoupled system. The plant of the shunt branch can be represented by an RL circuit, the second and third terms of (3.4) and (3.5). Thus, the transfer function of the inductive branch is given by:

$$G_{sh}(s) = \frac{I_{shd,q}}{V_{shd,q}} = \frac{1/R_{sh}}{s\tau_G + 1} \quad (3.8)$$

Where, τ_{shG} is the time constant of the inner loop plant of the shunt branch and it equal to L_{sh}/R_{sh}

The block diagram for the design of the PI-type controller, assuming unit feedback, becomes:

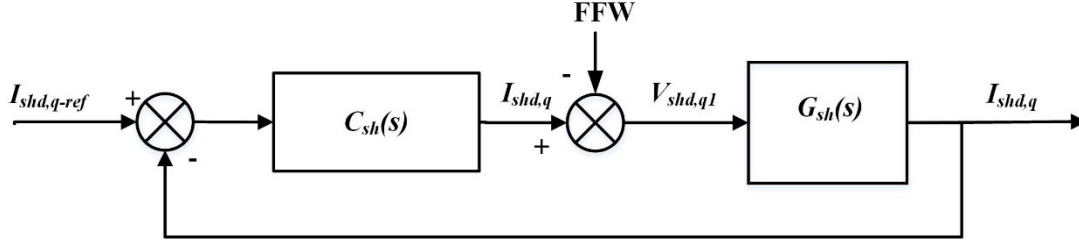


Figure 3-7: The block diagram for the design of the PI-type controller of the shunt branch (inner current loop)

It is assumed that the VSC operates with SPWM and a switching frequency (f_{sw}) of 5 kHz. The PI type 2 controller of the inner current control (C_{sh}) is designed for a crossover frequency (f_c) of 1 kHz (20% f_{sw}), and a phase margin (PM) of 60° .

The transfer function of a PI type 2 controller is:

$$C_{sh}(s) = K_{psh} \left(\frac{1 + s\tau_{sh}}{s\tau_{sh}} \right) \frac{1}{(1 + sT_{psh})} \quad (3.9)$$

For an inductor of the shunt coupling transform of the shunt branch, $L_{sh} = 0.003\text{H}$, and the shunt parasitic resistance, $R_{sh} = 0.1 \Omega$, the parameters of the controller are calculated as $K_{Psh} = 21.14$, $\tau_{sh} = 0.57\text{ms}$, $T_{Psh} = 0.0422 \text{ ms}$. ω in the coupling terms, is equal to $2\pi f$. f is the system frequency (60 Hz). Thus, $\omega = 377 \text{ rda/sec}$.

3.3.2. The Mathematical Model for the Outer Voltage Control Loop of the Shunt Branch (DC Voltage Controller)

As mentioned before, the DC voltage (V_{dc}) is controlled by the q-axis current component of the shunt VSC3 (I_{shq}). Therefore, the mathematical model of the outer voltage loop should result in getting a relationship between V_{dc} and I_{shq} . Figure 3-8 shows the circuit of the DC of the UIPC that will be used to derive the mathematical model for the design of the DC voltage control loop.

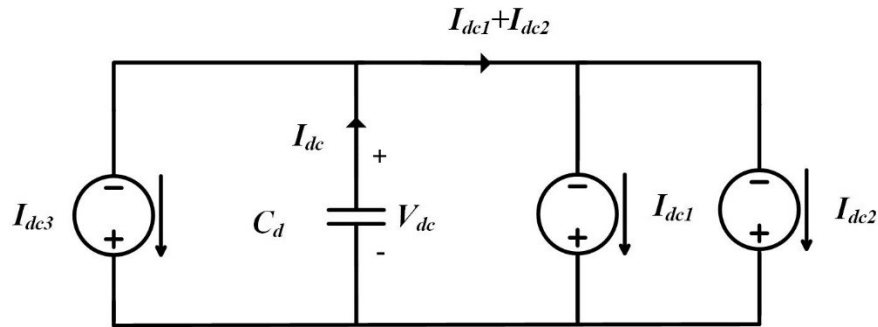


Figure 3-8: The circuit of the DC link

For lossless inverters and coupling transformers, the mathematical model for the DC voltage control loop can be derived by using the relation between the active power of the three branches of the UIPC and the active power in DC link as follows:

$$P_{VSC3-DC} = -(P_{VSC1} + P_{VSC2}) + P_{dc} \quad (3.10)$$

Where P_{VSC1} and P_{VSC2} are the active powers of the series VSC1 and VSC2. They can be expressed as:

$$P_{VSC1} + P_{VSC2} = V_{dc}(I_{dc1} + I_{dc2}) = V_{dc}I_{dc12} \quad (3.11)$$

Where V_{dc} is the DC voltage across the DC capacitor link, and I_{dc12} is the DC current from both series VSCs. The active power that is supplied or absorbed by the DC capacitor link, P_{dc} , can be calculated as:

$$P_{dc} = V_{dc}I_{dc} = C_d V_{dc} \frac{dV}{dt} \quad (3.12)$$

By substituting (3.11), and (3.12), into (3.10), one can get:

$$P_{VSC3-DC} = -V_{dc}I_{dc12} + C_d V_{dc} \frac{dV_{dc}}{dt} \quad (3.13)$$

The active power supplied by VSC3 can be expressed in term of dq-axis in AC side as:

$$P_{VSC3-AC} = \frac{3}{2}(V_{sd}I_{sh} + V_{sq}I_{shq}) \quad (3.14)$$

For the shunt branch, the dq frame system is defined with reference to the input bus of the UIPC (sending end node, V_s). Thus, $v_{sd}=0$ and the above equation becomes:

$$P_{VSC3-AC} = \frac{3}{2}(I_{sq}I_{shq}) \quad (3.15)$$

The relationship between V_{dc} and I_{shq} can be obtained from the power balance equation of the shunt VSC3, where $P_{VSC3-AC} = P_{VSC3-DC}$. By substituting the expressions of $P_{VSC3-AC}$ and $P_{VSC3-DC}$ from (3.13) and (3.15), one can get:

$$\frac{3}{2}(V_{sq}I_{shq}) = -V_{dc}I_{dc12} + C_d V_{dc} \frac{dV_{dc}}{dt} \quad (3.16)$$

$$I_{sh} = -\frac{2}{3} \frac{V_{dc}}{V_{sq}} I_{dc12} + \frac{2}{3} \frac{V_{dc}}{V_{sq}} C_d \frac{dV_{dc}}{dt} \quad (3.17)$$

The first term of the above equation is related to the active power exchanged between the two series VSCs and the shunt VSC3. This term will be used as feedforward branch to compensate

for the variation in the active power of the series VSCs. The second term of the above equation will be used to derive the transfer function for designing the outer DC voltage control loop.

$$I_{sh} = I_{shq1} - \frac{2}{3} \frac{V_{dc}}{V_{sq}} I_{dc12} \quad (3.18)$$

Where I_{shq1} ,

$$I_{shq1} = \frac{2}{3} \frac{V_{dc}}{V_{sq}} C_d \frac{dV_{dc}}{dt} \quad (3.19)$$

- **Design of the DC voltage controller of the shunt branch**

The transfer functions of the DC link can be obtained by introducing the small perturbations for in (3.19) while assuming that V_{sq} is constant [46].

$$I_{shq1} = I_{shq10} + \tilde{i}_{shq1} \text{ and } V_{dc} = V_{dc0} + \tilde{v}_{dc} \quad (3.20)$$

By substituting (3.20) into (3.19), then removing the dc components and products of small perturbations, the transfer function can be expressed as follow:

$$G_{DC}(s) = \frac{V_{dc}(s)}{I_{shq}(s)} = \frac{3}{2} \frac{V_{sq}}{sCV_{dc}} \quad (3.21)$$

Since the control circuit of the shunt branch consists of the inner current control loop and outer voltage control loop, the outer voltage control loop should be designed to be slower than the inner current loop, with a crossover frequency of 10% of the current loop. Therefore, the inner control loop can be represented by the gain feedback element ($H_i(s)$). Figure 3-9 shows the block diagram for the design of the DC voltage control loop.

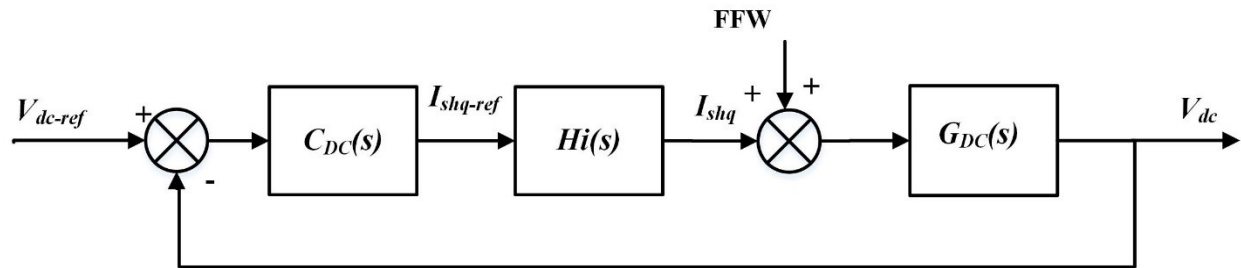


Figure 3-9: The block diagram for the design of DC voltage control

The PI controller of the DC voltage control loop (C_{DC}) is designed for an f_x of 100 Hz (10 times less than f_x of the inner current loop) and a PM of 60° .

The transfer function of the PI controller is given by:

$$C_{DC}(s) = K_{pDC} \left(\frac{1 + s\tau_{DC}}{s\tau_{DC}} \right) \quad (3.22)$$

Considering that the DC link capacitor, C_C , is 2000 μF , the DC bus voltage, V_{dc} , is to be regulated at 25kV, and that V_{sq} is equal to 187.8 kV (From the value of V_S in the case study in Chapter 2), the parameters of the PI controller are calculated as $K_{pDC} = 1.7$, $\tau_{DC} = 5.8\text{ms}$.

The remaining part in the control of the shunt VSC3 is the outer loop control of the AC bus of the UPFC-based UIPC (the sending end node, in this case, V_S). Recall that the AC voltage is controlled by the d-axis component of the shunt VSC3. In this work, the UPFC-based UIPC is assumed to be connected to an infinite bus, or to a strong network ($X_s \approx 0$). Accordingly, the AC voltage is assumed to be constant (equal to its rated value, 1pu) and I_{shd_ref} will be set to zero. In other words, the shunt VSC3 will not inject or absorb reactive power to/from AC bus (V_S).

Since the mathematical models of the shunt branch for the inner and outer control loops are derived, one can show the schematic control diagram of the shunt branch of the UPFC-based UIPC.

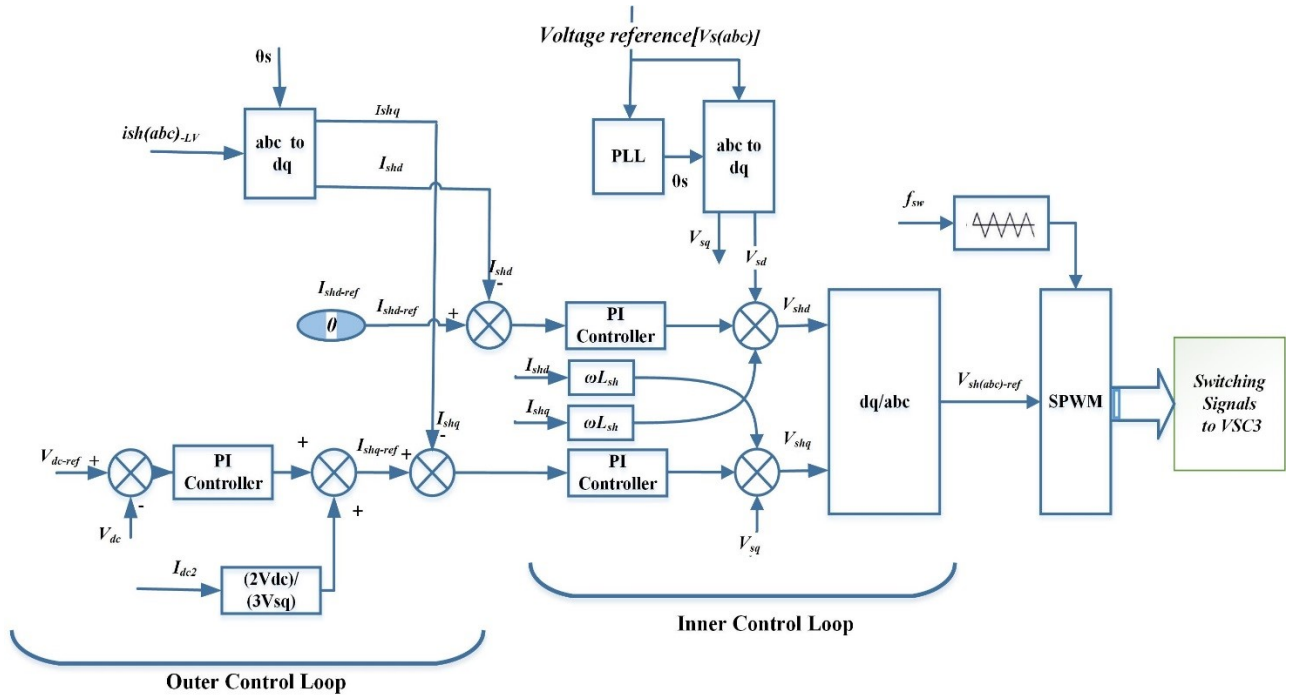


Figure 3-10: Schematic diagram of the outer and inner control block of the shunt VSC3.

3.4. Realizing the Proposed Control Strategy for the Series VSCs of the UPFC-based UIPC

The aim of the UIPC is to control the power flow through the transmission line. By controlling the magnitude and the angle of the transmission line current, one can control the active and reactive power flow in this line. The series VSC1 and VSC2 of the inductive and capacitive branches are used to achieve the desired magnitude and angle of the transmission line, by controlling the current in their respective branches. Recall the proposed approach in this work, which is to calculate the UPFC-based UIPC control variables (V_{injL} , ρ_1 , V_{injC} , and ρ_2) by splitting the real and imaginary parts of the transmission line current among the inductive and capacitive branches as a function of sharing factors, α and β , bounded between 0 and 1. That is,

$$\underline{I}_L = \alpha \times Re(\underline{I}_{TL}) + j\beta \times Im(\underline{I}_{TL}) \quad (3.23)$$

$$\underline{I}_C = (1 - \alpha) \times Re(\underline{I}_{TL}) + j(1 - \beta) \times Im(\underline{I}_{TL}) \quad (3.24)$$

From the above equations, one can note that the suitable control structure for the series VSCs is to be current-controlled, to synthesize the desired reference current in the transmission line. Several methods are available for controlling the currents of a VSC connected to a grid through an inductive impedance [57]. For example, hysteresis current control (HCC), proportional plus integral (PI) control with the synchronous reference frame (dq), and proportional-resonant (PR) control in the abc stationary frame [58, 59]. However, in this particular application, one also needs to control the current in the capacitive branch of the UPFC-based UIPC with a VSC. In such a case, the current shall vary faster than usual, requiring a digital controller with very small steps for using HCC. The task is not much simpler with a PI controller with the synchronous reference frame (dq), where the decoupling of the quantities in the d and q axes is done via feedforward loops. Conversely, in order to achieve a small error in the steady state with a PR controller, one should merely use a high gain at the resonant (grid) frequency. Therefore, this approach has been selected in this Chapter for controlling the current in the inductive and capacitive branches of the UPFC-UIPC.

The next chapter (Chapter 4) will discuss the use of the synchronous reference frame (dq) for controlling the series VSCs, with zero error in steady state. The challenge of synthesizing a current in the capacitive branch of the UIPC with a VSC2 by using the direct current control with the dq frame is addressed by proposing an indirect current control.

3.4.1. Proportional Resonant (PR) Controller

The PR controller in the abc stationary frame has been commonly used to control the current in a VSC connected to a grid through an inductive impedance. The ideal PR controller is derived by converting the ideal synchronous frame PI controller to the abc stationary frame. The ideal PR controller represented by [44]:

$$C_{PR}(s) = K_p + K_i \frac{2s}{s^2 + \omega_o^2} \quad (3.25)$$

Where K_p is the proportional gain term, K_i is the integral gain term, and ω_o is the resonant frequency at the fundamental frequency. The ideal PR controller, achieves infinite gain at the AC frequency, ω_o , as can be seen from Figure 3-11 (A). This will result in a zero steady state error to step reference signal variations. However, implementing the ideal PR controller is not practical since the infinite gain at the grid frequency will make the controller very sensitive to the grid frequency variations. Therefore, it was proposed in the literature to introduce a damping factor to the ideal PR, or widening its bandwidth at the expense of a lower gain at the resonant frequency, leading to a non-ideal PR controller [44]:

$$C_{PR}(s) = K_p + K_i \frac{2\omega_c s}{s^2 + 2\omega_c s + \omega_o^2} \quad (3.26)$$

Where, ω_c is the bandwidth around the resonant frequency, ω_o . Although the gain of the non-ideal PR control at the grid frequency, ω_o , is a finite value, it is still large enough to provide a very small steady state error [60]. Figure 3-11 (B) shows the frequency response for the non-ideal PR controller.

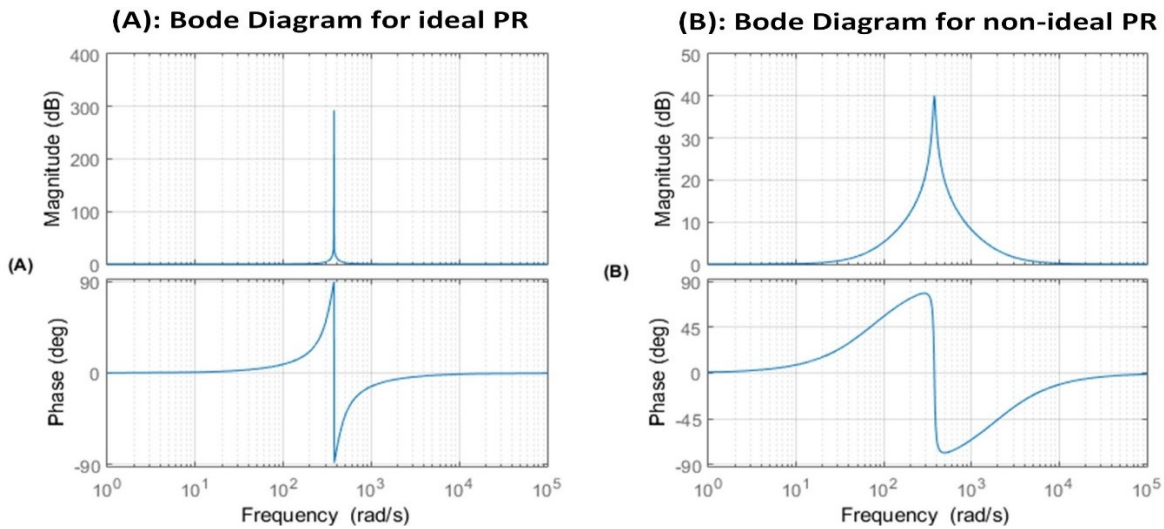


Figure 3-11: Bode Diagram (A) ideal PR controller with, $K_p = 1$, $K_i = 100$, $\omega_o = 2\pi 60$ (rad/s), (B) non-ideal PR controller with $K_p = 1$, $K_i = 100$, $\omega_o = 2\pi 60$, $\omega_c = 10$ (rad/s)

3.4.2. The Mathematical Model of the Series Branches of the UPFC-Based-UIPC in the abc Stationary Frame

In order to design the current controller of the series branches of the UPFC-based UIPC with a PR controller, their stationary frame (abc) mathematical models should be derived. Recall that the UPFC-based UIPC has two series branches, the inductive and the capacitive branches. Thus, two mathematical models need to be presented. Unlike the derivation of the mathematical model in the dq frame (for the shunt branch in the previous section or the series branches for the next Chapter), the mathematical models derivation in the abc stationary frame for both series branches is a simple task.

A. The mathematical model and PR control design of the inductive branch

Figure 3-12 shows the single line diagram of the inductive branch, which is extracted from the UPFC-based UIPC circuit in Figure 3-4.

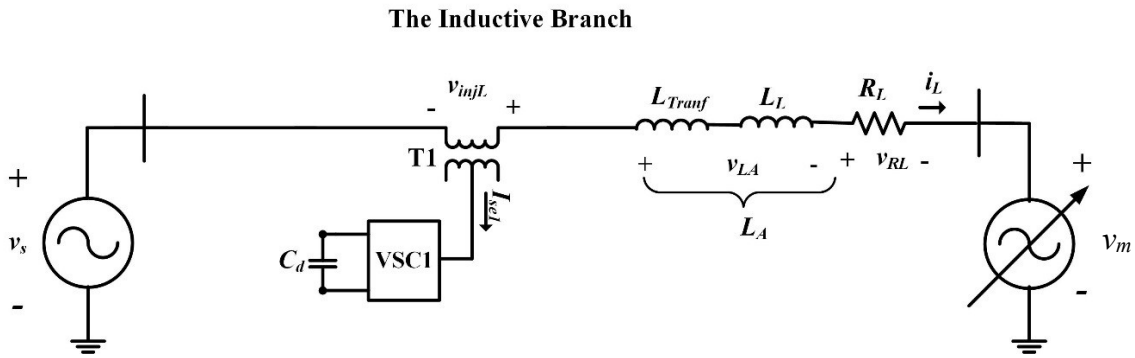


Figure 3-12: The single line diagram of the inductive branch

The equation that represents the 3-phase system of the inductive branch in Figure 3-12 is:

$$[v_{injL}]_{abc} = [v_m]_{abc} - [v_s]_{abc} + L_A \frac{d[i_L]_{abc}}{dt} + R_L [i_L]_{abc} \quad (3.27)$$

Where v_{injL} is a vector with the voltages required to regulate the currents in an RL circuit, and L_A is equal to $L_L + L_{Transf}$. The RL circuit can represent the plant of the inductive branch (the last two terms of (3.27)). Thus, the transfer function of the inductive branch to design the current controller is:

$$[G_L]_{abc}(s) = \frac{[i_L]_{abc}(s)}{[v_{injL}]_{abc}(s)} = \frac{1/R_L}{(R_L/L_A)s + 1} \quad (3.28)$$

Regarding design, the integral gain K_i at the grid frequency, ω_0 , should be set large enough to impose a small steady-state error. The proportional gain, K_p , defines the dynamics of the system and it can be tuned as the PI controller in an equivalent DC system [61]. The bandwidth, ω_c determines the sensitivity to frequency variations in the grid, typically been selected in the range of 5-15 rad/s [60]. The series inductor of the inductive branch, L_A presents an inductance of 0.491 H and equivalent series parasitic resistance, R_L , of 0.1 Ω . In this work, the switching frequency (f_{sw}) is 5 kHz. The bandwidth (f_x) which defines the value of K_p , is set to 20% of f_{sw} (1 kHz). The gain of the loop transfer function (LTF) at the resonance frequency is to be 30 dB. Based on these two target design specifications, the parameters of the PR controllers for the inductive branch are selected as $K_{pL} = 3038$ and $K_{iL} = 5630$.

B. The mathematical model of the capacitive series branch of UPFC-based-UIPC

Figure 3-13 shows the single line diagram of the capacitive branch, which is extracted from the UPFC-based UIPC circuit in Figure 3-4.

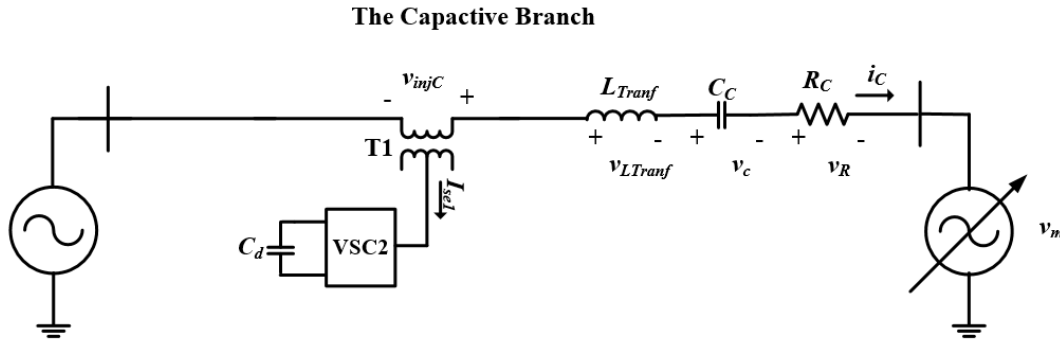


Figure 3-13: The single line diagram of the capacitive branch

The equation that represents the 3-phase system of the capacitive branch in Figure 3-13 is:

$$[v_{injC}]_{abc} = [v_m]_{abc} - [v_s]_{abc} + R_C [i_C]_{abc} + \frac{1}{C_C} \int [i_C]_{abc} dt + L_{Transf} \frac{d[i_C]_{abc}}{dt} \quad (3.29)$$

Where v_{injC} is a vector with the voltages required to regulate the currents in an RLC circuit. The RLC circuit can represent the plant of the capacitive branch, the last three terms of (3.29). Thus, the transfer function of the capacitive branch to design the current controller is given by:

$$[G_C]_{abc}(s) = \frac{[i_C]_{abc}(s)}{[v_{injC}]_{abc}(s)} = \frac{sC_C}{L_{Transf}C_Cs^2 + R_C C_C s + 1} \quad (3.30)$$

The series capacitor of the capacitive branch, C_C , presents a capacitance of 13.9 μF , the series transformer inductor, L_{Tranf} , presents an inductance of 0.0146 H, and the series parasitic resistance, R_C , is 1 Ω . The PR controller of the capacitive branch was designed to have a similar bandwidth (f_x) and consequently, a similar speed of response like the inductive branch. Besides, it should yield a high gain at the resonant frequency for its LTF, and it should be almost equal to the one for the inductive branch. In this work, the switching frequency (f_{sw}) is 5 kHz. f_x , which defines the value of K_p , is set to 20% of f_{sw} (1 kHz). The gain of the LTF at the resonance frequency is to be 30 dB. Based on these two target design specifications, the parameters of the PR controller for the capacitive branch are selected as $K_{pC} = 82.3$ and $K_{iC} = 11557.2$.

3.4.3. Realizing the Current References in abc-Frame for the PR Controllers

The main objective of the UPFC- UIPC is to control the current in the transmission line. The desired current magnitude (I_{TL-des}) and angle (ϕ_{TL-des}) with respect to the receiving end voltage are assumed to be provided by the Transmission System Operator (TSO). This current will be shared by the inductive and capacitive branches of the UIPC, according to the sharing factors, α and β . These are computed off-line, considering the phase angle between the voltages in the sending and receiving ends of the transmission line (δ), as discussed before and stored in a lookup table.

The reference currents for the inductive and capacitive branches of the UIPC, in abc-frame for the PR controllers, are obtained from the lookup table and the reference current for the transmission line as shown in Figure 3-14. The principles behind the logic for the proposed scheme and pertinent equations are discussed below. The approach is based on a dq to abc (Park) transformation, where the dq components are computed from α and β as well as I_{TL-des} and ϕ_{TL-des} for a given δ . It is assumed that the phase angle of the voltage at the receiving end of the transmission line (θ_r) is available and it is used as θ_{ref} for the dq to abc transformation.

As mentioned before, the Park transformation considered in this work is the “original motor notation.” There, the positive d-axis is aligned with the magnetic axis of the field winding, and the positive q-axis leads the d-axis by 90°. In such a case, the d and q components of the grid (reference) voltages are $V_d = 0$ and $V_q = -\sqrt{2} V_{\phi_rms}$.

In order to realize a current with magnitude I_{TL-des} and phase ϕ_{TL-des} with respect to the reference voltage, which provides the angle for the dq to abc (inverse Park) transformation; one

should define the d and q components of the desired transmission line current. This can be done from:

$$I_{TLd_{des}} = \sqrt{2}I_{TL_{des}} \sin(\phi_{TL_{des}}) \quad (3.31)$$

$$I_{TLq_{des}} = -\sqrt{2}I_{TL_{des}} \cos(\phi_{TL_{des}}) \quad (3.32)$$

Since the α and β factors correspond to shares of the real and imaginary components of \underline{I}_{TL} , the d and q components for \underline{I}_L and \underline{I}_C can be obtained from

$$I_{Lq_{ref}} = \alpha I_{TLq_{des}} \quad \& \quad I_{Ld_{ref}} = \beta I_{TLd_{des}} \quad (3.33)$$

$$I_{Cq_{ref}} = (1 - \alpha)I_{TLq_{des}} \quad \& \quad I_{Cd_{ref}} = (1 - \beta)I_{TLd_{des}} \quad (3.34)$$

The above dq references of the current in each branch are converted into the abc-frame, and synchronized with the reference voltage, using the inverse Park transformation as shown in Figure 3-14. There, one can also see the implementation of the current control loop in abc-frame with PR controllers and SPWM.

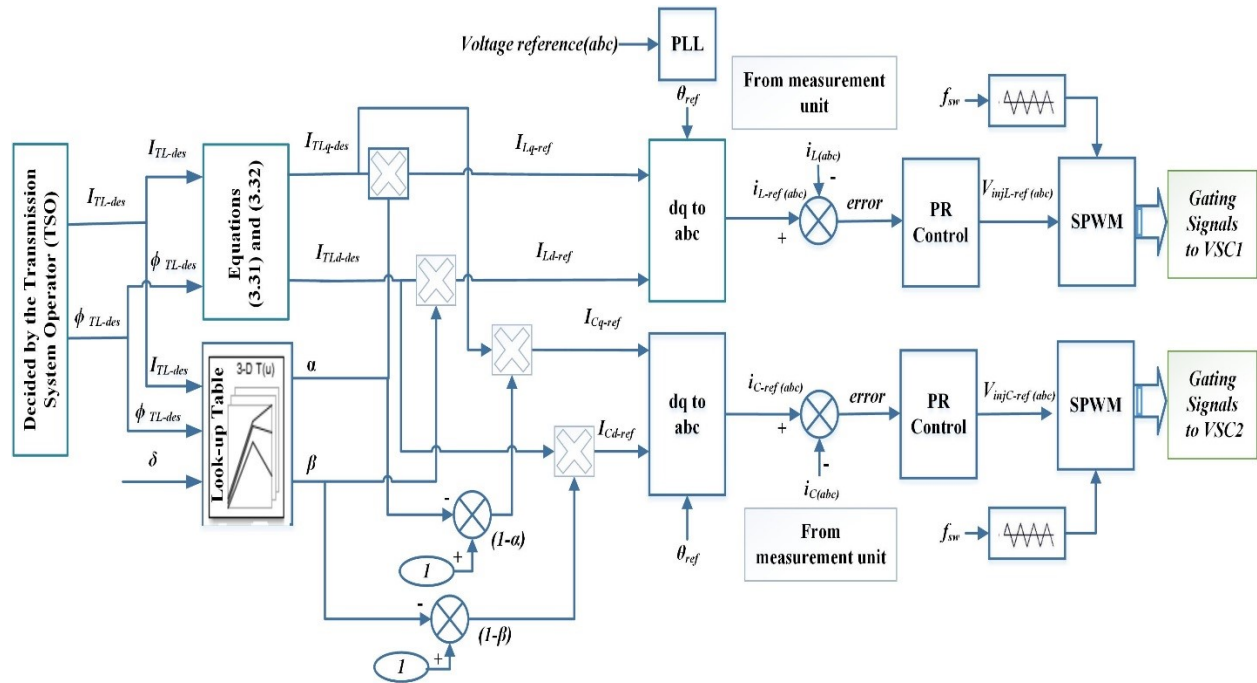


Figure 3-14: Schematic diagram of the proposed control scheme for the UPFC-UIPC with optimal current sharing factors and PR controllers

3.5. Case Study

As mentioned earlier in this chapter, the UPFC-based UIPC is modeled and simulated using PSCAD/EMTDC. The main objective is to verify the proposed control scheme, that is, make the UIPC work as UPFC mode to control the current flow through the transmission line. Furthermore, it will help investigate the performances of the PR current controllers for the series VSCs and the double loop decoupled controller for the shunt VSC, in different cases. The same case study that was considered in Chapter 2 is considered for this chapter (Figure 2-6 and Table 2-1).

The three power factors at the receiving end of the transmission line discussed in Chapter 2 are considered in Chapter 3: UPF with $\phi_{TL} = 0^\circ$, PF/Leading of 0.8 ($\phi_{TL} = 36.87^\circ$) and PF/Lagging of 0.8 ($\phi_{TL} = -36.87^\circ$). However, this chapter considers only two cases (two values) of the desired transmission line current magnitude (I_{TL-des}), which belongs to one current control range. Recall that for Chapter 2, different control ranges of the desired current magnitude, I_{TL-des} , are considered, which are based on the different values of angle δ . They are used to compare the capability and the performances of the SPS-based UIPC and the UPFC-based UIPC for different operating conditions. Since, it was shown that in most cases, the UPFC-based UIPC is more capable than the SPS-based UIPC to impose a desired current in the transmission line, without exceeding the allowed voltage and current values of the VSCs; there is no need to consider all current ranges (all values of angle δ). Instead, only one current range, which is corresponded to angle δ with a value of 15° , is considered.

Using the proposed technique in Chapter 2 to find the control variables of the UPFC-based UIPC, it has been found that the UPFC-based UIPC can achieve a control range from 0 pu to 1 pu for the UPF and leading PF cases, for $\delta=15^\circ$. On the other hand, it was found that the UPFC-based UIPC can achieve control range from 0 pu to 0.8 pu for lagging PF case, for the same value of δ , 15° . The reason behind achieving a lower current control range for PF lagging than other PF cases is because the required voltage from the VSC2 of the capacitive branch is higher than 0.25 pu for PF = 0.8 lagging case. Based on the defined control current range, the two values of I_{TL-des} , which will be considered for each main case (PF case) are: $I_{TL-des} = 0.5$ pu and 1 pu for the first two main cases, and $I_{TL-des} = 0.5$ pu and 0.8 pu for the last main case.

3.6. Simulation Results

The simulation results are divided into parts. The first part will consider the simulation results of the UPFC-based UIPC to study the performance of the PR controllers for both series branches, on both operating conditions, a transient response for a current references variation, and steady state condition. This part considers all PF cases with the two considered values of I_{TL-des} . The second part of the simulation results is to validate the response of the double loop PI decoupled controller of the shunt branch, where only one PF case with the two values of I_{TL-des} is used.

3.6.1. Simulation Results to Investigate the Performance of PR Controllers of the Series Branches

A. UPF Case ($\phi_{TL} = 0^\circ$)

For the UPF case ($\phi_{TL} = 0^\circ$), the UPFC-based UIPC should be controlled to result in the transmission line current to be in phase with the receiving end voltage. As was mentioned before, two values of I_{TL-des} , 0.5pu and 1pu, are considered. Table 3-5 shows the values of the sharing factors, α and β , the calculated currents magnitudes in pu, and angles of the inductive branch (I_L and ϕ_L), and the capacitive branch (I_C and ϕ_C), for the UPF case and the two values of I_{TL-des} .

Table 3-5: Values of α and β , I_L , ϕ_L , I_C , and ϕ_C , for the two considered value of I_{TL-des} for the UPF case

PF case	$\phi_{TL-des} (^\circ)$	$I_{TL-des}(pu)$	α	β	$I_L(pu)$	$\phi_L (^\circ)$	$I_C(pu)$	$\phi_C (^\circ)$
UPF	0	0.5	0.6633	-	0.3317	0	0.1683	0
		1	0.2999	-	0.2999	0	0.7001	0

Figure 3-15 shows the simulation waveforms of phase A, for I_{TL} , I_L , I_C and the reference voltage, V_R and I_{TL} in the UPF case in the steady state condition. As can be seen in the curves in the top of Figure 3-15, I_L and I_C are in phase, among themselves and with the line current, I_{TL} , which is in phase with V_R , and has no imaginary/reactive part. These results match the theoretical values, which are mentioned in Table 3-5. In terms of current magnitudes, based on Table 3-5, I_L should take most of I_{TL} ($I_L = 0.3317$ pu), for $I_{TL} = 0.5$ pu. On the other hand, for $I_{TL} = 1$ pu, I_C should take most of I_{TL} ($I_C = 0.7001$ pu).

Figure 3-15, in the bottom, shows that the waveform of phase A for I_{TL} is almost in phase with the waveform of phase A, for V_R , for both I_{TL-des} values. It also shows that the desired values of I_{TL-des} are achieved with very small error

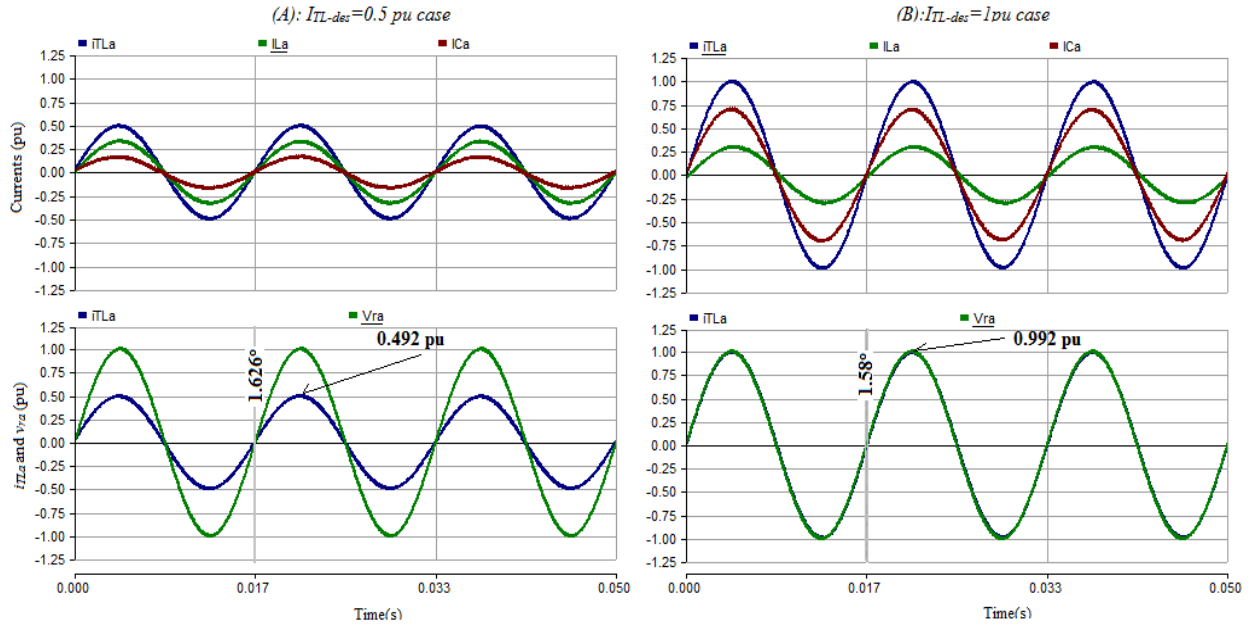


Figure 3-15: Simulation waveforms for UPF case: (A) $I_{TL} = 0.5$ pu (B) $I_{TL} = 1$ pu. Top: I_{TL} , I_L and I_C . Bottom: I_{TL} and V_R

Since the main purpose of the UPFC-based UIPC is to control the active and reactive power flow through the transmission line (achieved by controlling the line current and its angle), it is important to show the active and reactive powers and the power factor at the receiving end side, (P_r , Q_r , PF). Recall that for the UPF case, the active power (P_r) should be equal to 0.5 pu and 1pu for $I_{TL-des} = 0.5$ pu and 1pu, respectively. There is no reactive supplied nor absorbed by the receiving end ($Q_r = 0$ pu) for this case. From Figure 3-16 (A) and (B), one can note that the desired values of P_r , Q_r and PF , are achieved for the UPF case for both current subcases, 0.5pu and 1pu. They are all almost matched to their targeted values with very small errors.

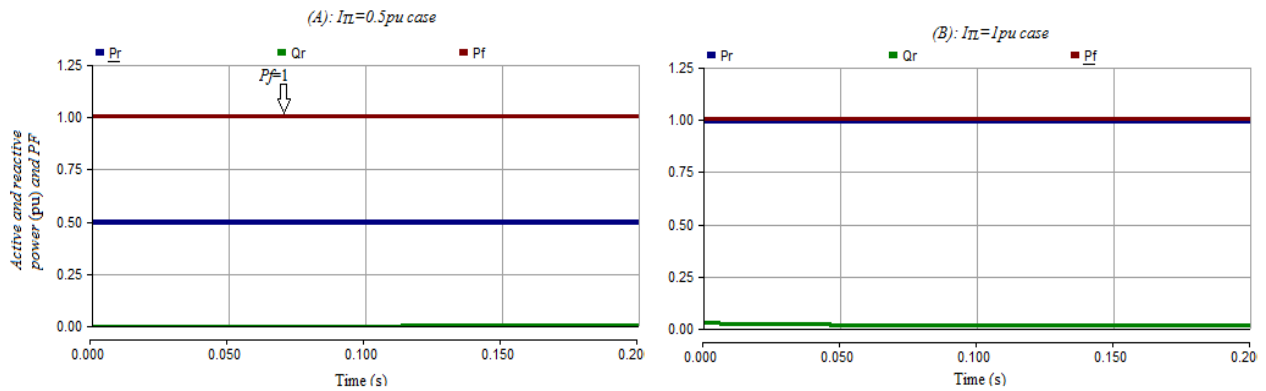


Figure 3-16: the active power (P_r), reactive power (Q_r), and the power factor (PF), at the receiving end side

In order to investigate the performance of the PR current controllers of the inductive and capacitive branches during transient conditions, their actual values should be observed during the step change of their references values to achieve the desired transmission line current. Figure 3-17 shows the reference and actual waveforms for the inductor and capacitor branches of the UPFC-based UIPC when the transmission line reference current is changed from 0.5 to 1 pu. From Figure 3-17 (A), one can note that the PR controller for the inductive branch results in a fast and well-damped dynamic response with a small error in steady state. On the other hand, the PR controller for the capacitive branch results in a low-speed and moderate dynamic response compared to the inductive branch. Nevertheless, the PR controller for the capacitive branch also leads to a small error in steady state.

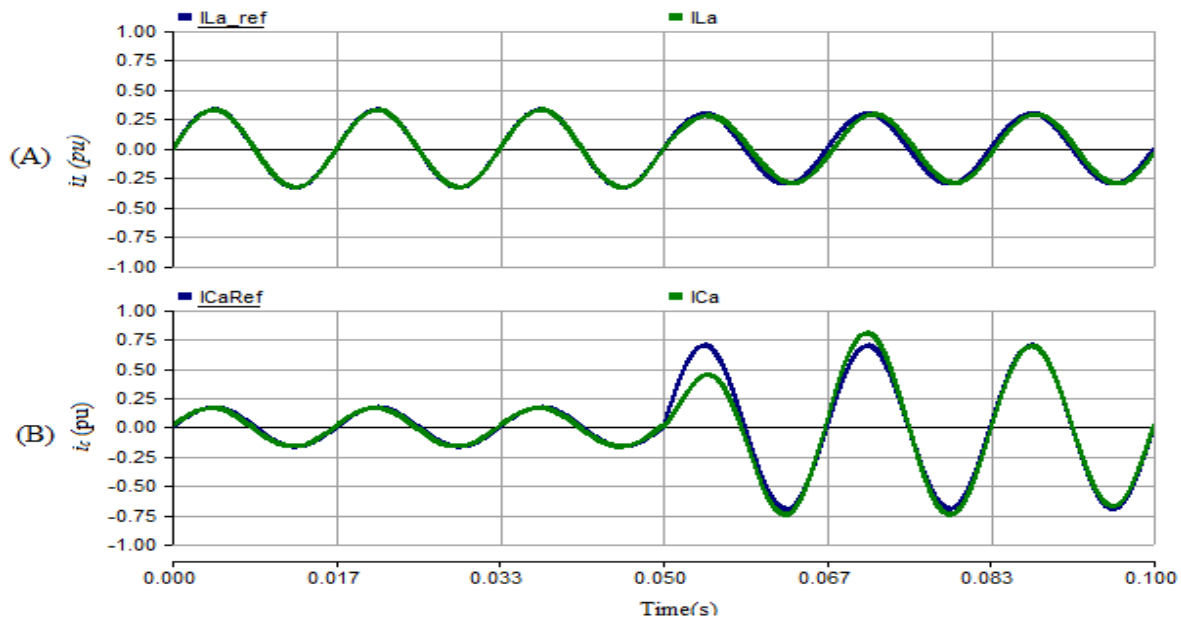


Figure 3-17: The actual and reference current waveforms for phase A of the inductive and capacitive branches, for UPF case

B. Leading PF case (0.8 and $\phi_{TL} = 36.87^\circ$)

For the leading *PF* case with a value equal to 0.8, the UPFC-based UIPC should be controlled to make the transmission line current lead the receiving end voltage by an angle with a value equal to 36.87° . Two values of I_{TL-des} are considered (0.5pu, and 1pu), as in the previous case. Table 3-6 shows the sharing factors, α and β , I_L , ϕ_L , I_C and ϕ_C , for the two considered values of I_{TL-des} in the PF/leading case.

Table 3-6: Values of α and β , I_L , ϕ_L , I_C , and ϕ_C for the two considered values of I_{TL-des} for the PF/leading case

PF case	$\phi_{I_{TL-des}}$	$I_{TL-des}(pu)$	α	β	$I_L(pu)$	$\phi_L(^{\circ})$	$I_C(pu)$	$\phi_C(^{\circ})$
0.8 PF/Leading	36.87 $^{\circ}$	0.5	0.8578	0.0822	0.3440	4.11	0.2811	78.33
		1	0.2878	0	0.2302	0	0.8274	46.48

From Figure 3-18 shows the simulation waveforms of phase A, for I_{TL} , I_L , I_C and the reference voltage, V_R , and I_{TL} in the PF = 0.8 leading case in the steady state condition

Figure 3-18, the top curves, shows the contribution of I_L and I_C to synthesize I_{TL} for $I_{TL} = 0.5pu$ and $1pu$. The contributions of I_L and I_C to I_{TL} are almost equal for the 0.5 pu case. On the other hand, for $I_{TL} = 1 pu$ case, the share of I_C to I_{TL} is much higher than I_L . Here, unlike in the UPF case, the waveforms of I_{TL} , I_L and I_C are not in phase. The magnitudes of these waveforms do correspond to what was expected and listed in Table 3-7. The waveforms of I_{TL} and V_R for the leading PF case are shown, as well, to check if the desired angle of transmission line current is achieved. From Figure 3-18, in the bottom, one can note not only that the magnitudes of I_{TL} present the expected values but also that the angles of I_{TL} present the expected value, which is around 36.87 $^{\circ}$.

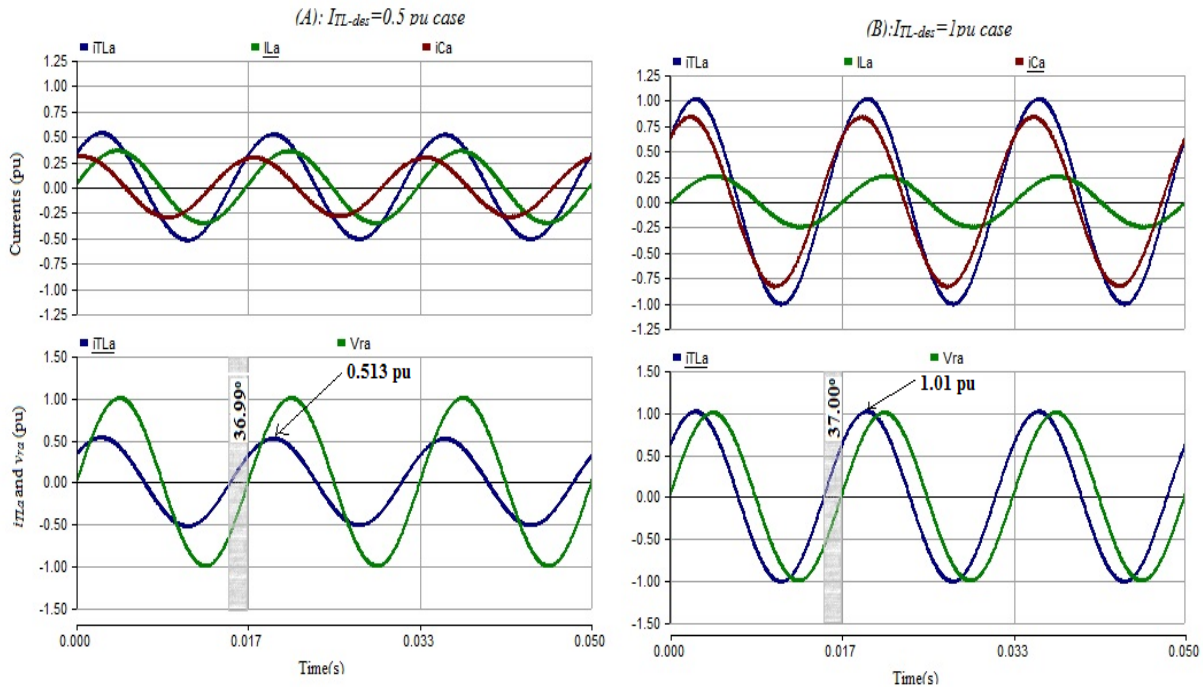


Figure 3-18: Simulation waveforms for PF/Leading case: (A) $I_{TL} = 0.5 pu$ and (B) $I_{TL} = 1 pu$. Top: I_{TL} , I_L , and I_C . Bottom: I_{TL} and V_R

In this case, also, the active and reactive powers and the power factor at the receiving end side, (P_r , Q_r , PF) will be illustrated. Recall that for the PF /leading case, that PF is equal to 0.8, P_r should be equal to 0.4 pu and 0.8 pu for $I_{TL-des} = 0.5$ pu and 1pu, respectively. Finally, for this PF case, there is Q_r supplied by the receiving end and it is equal to 0.3 pu and 0.6 pu for $I_{TL-des} = 0.5$ pu and 1pu, respectively. From Figure 3-19 (A) and (B), one can note that the desired values of P_r , Q_r , and PF , are achieved for the Leading PF case, for both current subcases, 0.5pu and 1pu, with very small errors in the steady state.

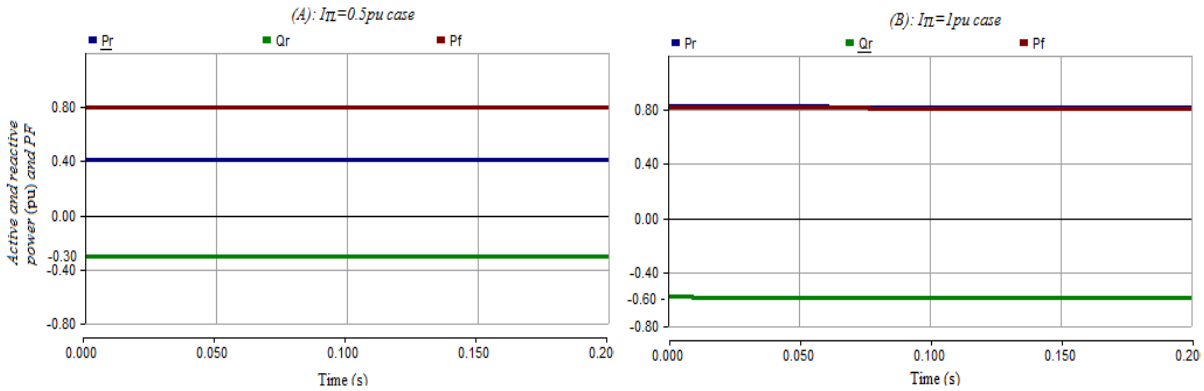


Figure 3-19: the active power (P_r), reactive power (Q_r), and the power factor (PF), at the receiving end side

The performance of the PR current controllers of the inductive and capacitive branches during transient conditions is considered as well in this case. Figure 3-20 shows the reference and actual waveforms for the inductor and capacitor branches of the UPFC-based UIPC when the transmission line reference current is changed from 0.5 to 1 pu for this PF case. As in previous PF case, the PR controller for the inductive branch, Figure 3-20 (A), leads to a fast and well-damped dynamic response with a small error in steady state and the PR controller for the capacitive branch, Figure 3-20 (B), results in a low-speed and moderate dynamic response for the leading PF case. Still, the PR controller for the capacitive branch also leads to a small error in steady state.

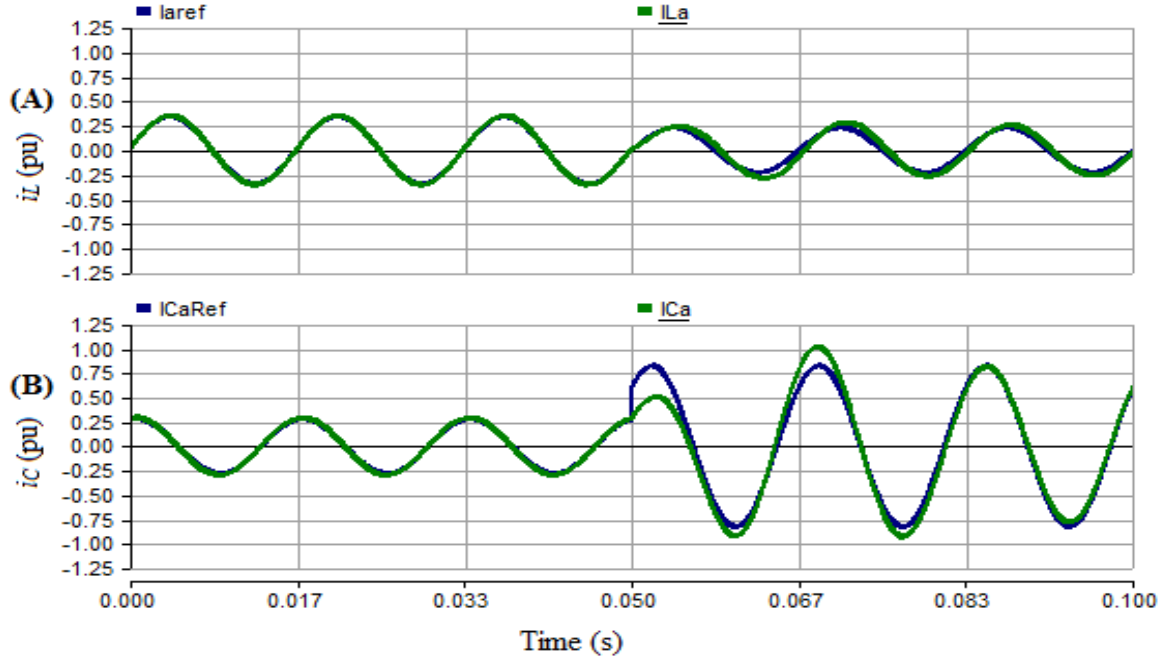


Figure 3-20: The actual and reference current waveforms for phase A of the inductive and capacitive branches, for PF/leading case

C. Lagging PF Case (0.8 and $\phi_{TL} = -36.87^\circ$)

For the lagging PF case with a value equal to 0.8, the UPFC-based UIPC should result in the transmission line current lagging the receiving end voltage by an angle with a value equal to -36.87° (same absolute angle value of the leading PF case with a different sign). As in the two previous PF cases, two values of I_{TL-des} are considered. The first value of I_{TL-des} is the same as in the previous two cases, which is 0.5 pu. However, the second value of I_{TL-des} will be different from the previous two cases. Using the techniques for calculating the control variables of the UPFC-based UIPC that mentioned in Chapter 2, it was found that the maximum current that can be achieved by the UIPC is 0.8 pu for lagging PF with a value of 0.8. Hence, the second considered value of I_{TL-des} is equal to 0.8 pu. Table 3-7 shows the sharing factors, α and β , I_L , ϕ_L , I_C and ϕ_C , for the two considered values of I_{TL-des} in the PF/lagging case.

Table 3-7: Values of α and β , I_L , ϕ_L , I_C , and ϕ_C , for the two considered values of I_{TL-des} for the PF/lagging case

PF case	$\phi_{I_{TL-des}}$	$I_{TL-des}(pu)$	α	β	$I_L(pu)$	$\phi_L(^\circ)$	$I_C(pu)$	$\phi_C(^\circ)$
0.8 PF/Lagging	-36.87°	0.5	0.7324	0	0.2930	0	0.3185	-70.36
		0.8	0.4617	0	0.2955	0	0.5908	-54.33

The simulation results for the lagging PF case do not bring up a big difference from two previous PF cases. It gives even more evidence about the ability of the UPFC-based UIPC to control power flow (transmission line current) for different conditions using the PR controllers. Figure 3-21, the top curves, validates the sharing parts of I_L and I_C to I_{TL} that are mentioned in Table 3-7. Figure 3-21, the bottom curves, show that the magnitudes of I_{TL} present the expected values, 0.5 pu, and 0.8 pu with an error that is equal to and smaller than 5. The angles of I_{TL} , which should be equal -36.87° , are achieved for the two current magnitudes cases (0.5 and 0.8 pu) with errors that are equal to or less than 1%.

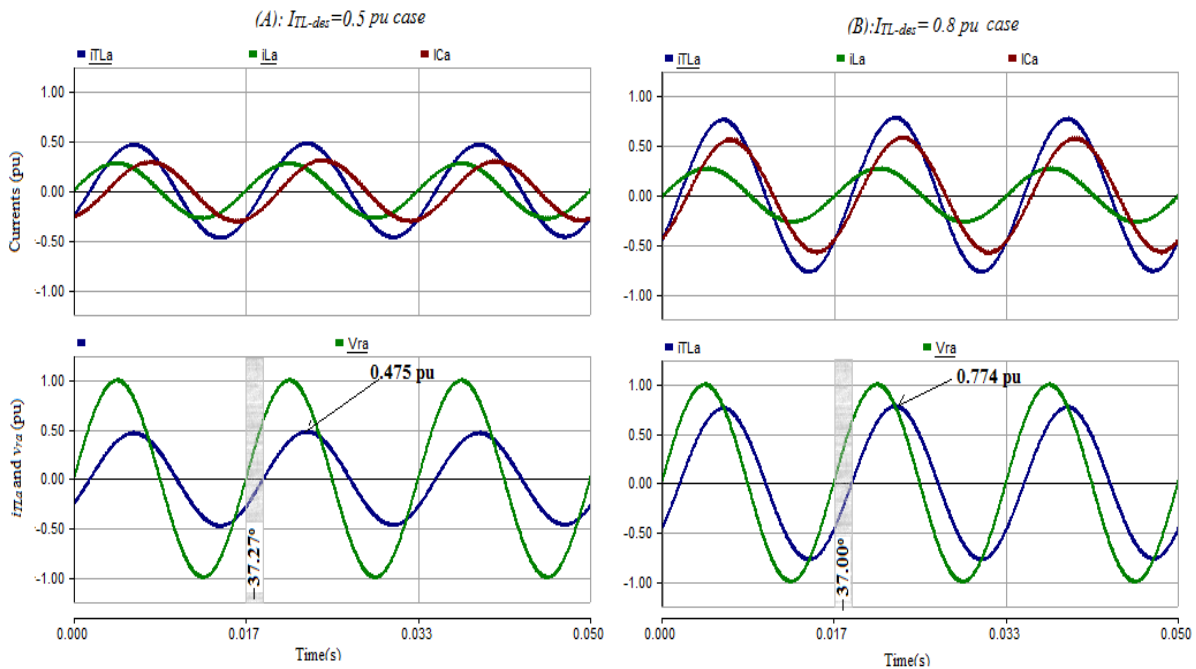


Figure 3-21: Simulation waveforms for PF/Lagging case: (A) $I_{TL} = 0.5$ pu and (B) $I_{TL} = 1$ pu. Top: I_{TL} , I_L , and I_C . Bottom: I_{TL} and V_R

The active and reactive powers and the power factor at the receiving end side, (P_r , Q_r , PF) will be shown for this case. Recall that for the $PF = 0.8$ lagging case, P_r should be equal to 0.4 pu and 0.8 pu for $I_{TL-des} = 0.5$ pu and 1pu, respectively. Q_r for a lagging PF case is absorbed by the receiving end and its equal to 0.3 pu and 0.6 pu for $I_{TL-des} = 0.5$ pu and 1pu, respectively. From Figure 3-24 (A) and (B), one can note that the desired values of P_r , Q_r , and PF , are achieved for the leading PF case, for both current subcases, 0.5pu and 1pu, with very small errors in the steady state.

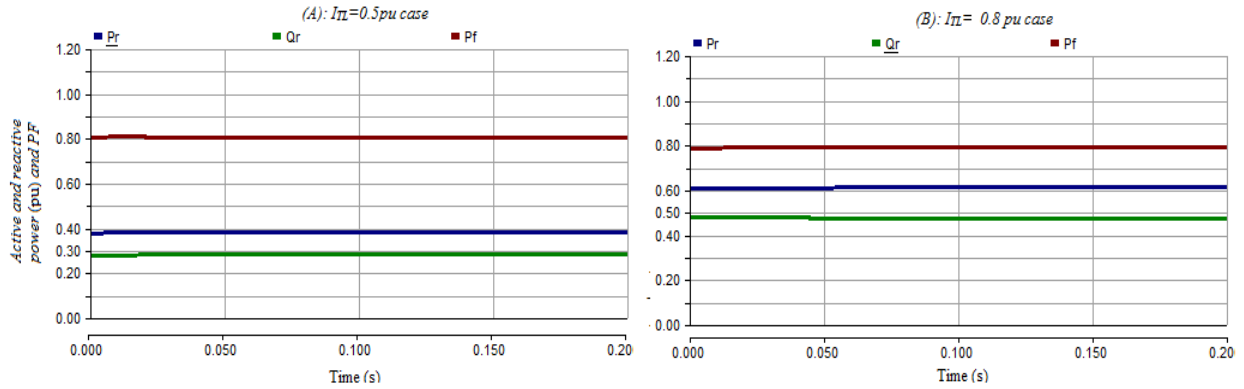


Figure 3-22: the active power (P_r), reactive power (Q_r), and the power factor (P_f), at the receiving end side

The performance of the PR current controllers of the inductive and capacitive branches during transient conditions does not bring up a big difference from two previous PF cases as well.

As can be seen from Figure 3-23 (A), the PR controller for the inductive branch, leads to a fast and well-damped dynamic response with a small error in steady state and the PR controller for the capacitive branch, Figure 3-23 (B), leads to a low-speed and acceptable dynamic response for the leading PF case. Nevertheless, the PR controller for the capacitive branch also leads to a small error in steady state.

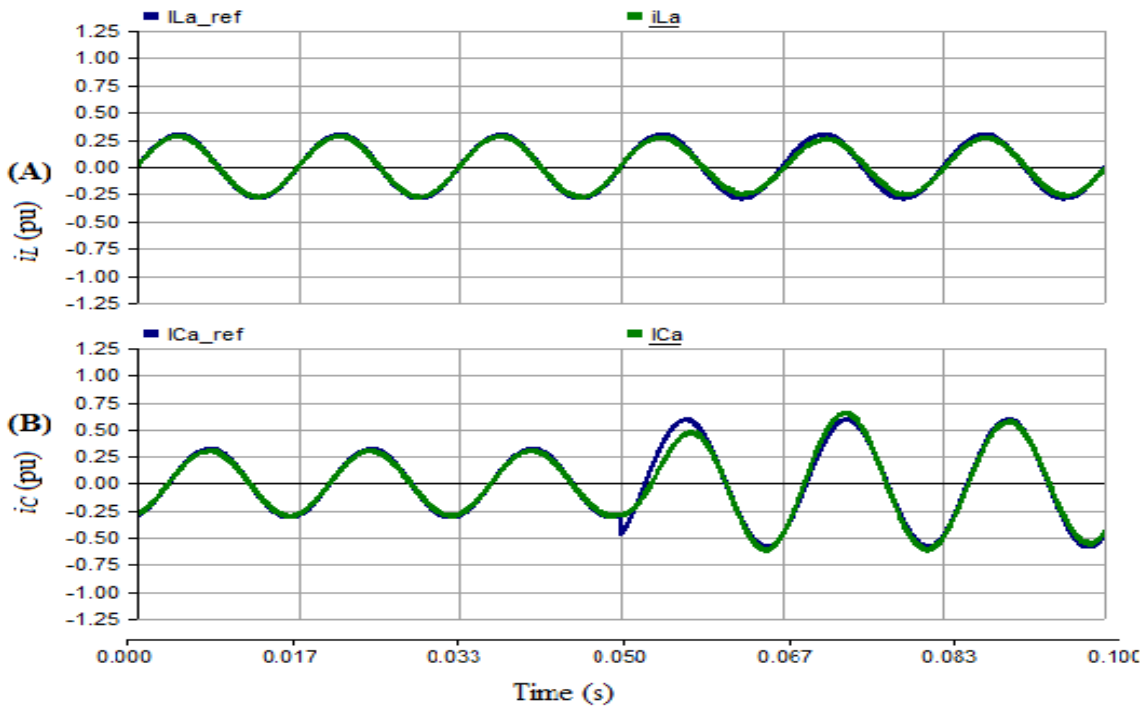


Figure 3-23: The actual and reference current waveforms for phase A of the inductive and capacitive branches, for PF/leading case

3.6.2. Simulation Results to Investigate the Performance of the Shunt Branch Controller

The main task of the shunt VSC is to regulate the common DC bus voltage according to its reference value, thus balancing the active power demanded by both series VSCs. Since the UPFC-based UIPC is assumed to be connected to the infinite bus (as mentioned before), the shunt VSC3 will not inject nor absorb reactive power to/from the sending end node (or to/from the system) to regulate the AC bus voltage (V_s). Therefore, the reference current of the d-axis component ($I_{shd-ref}$) will be set to zero pu. The reference value of the q-axis current component ($I_{shq-ref}$) of the shunt branch will be generated from the outer DC voltage loop and will be fed to the q-axis inner current loop. The performance of the cascaded controller for the shunt branch during transient and steady state conditions will be presented for the previous PF case (0.8 lagging PF).

Figure 3-24 shows the actual and reference currents of the shunt branch (the q and d axis current components in the top, and the AC waveform of phase A, in the middle). It also shows the actual and references DC voltage across the DC capacitor link and (in the bottom). At $t = 0.3s$, the reference value for the transmission line current changes from 0.5pu to 0.8pu. This causes the variations in the currents in the inductive and capacitive branches shown in Figure 3-23 and variations in the active power demanded from the common DC bus. This results in a variation in the current reference of the shunt VSC3 to regulate the DC bus voltage. The dq current controller results in a fast and well-damped dynamic response, with a zero error in the steady state. From Figure 3-24, in the bottom, it can be noted that the DC voltage controller achieves its tasks, maintaining the DC voltage around its reference (1pu), by generating the required q-axis current reference, which is followed by the effective current control loop.

The change of the active power demanded (supplied/absorbed) by the series VSCs due to the change of their current references are discussed in this paragraph along with the active power supplied/absorbed by the shunt VSC3. As shown in Figure 3-8, in Section 3.3.2, if the active powers are supplied from the VSCs to the shunt or the series branches, their sign is minus (-). Thus, active power of VSC3 will always have a different sign from the active power of the two series VSCs (Eq. 3.6) since whatever amount of the active powers those are supplied/absorbed by series VSCs have to be absorbed/supplied by the shunt VSC3.

$$P_{VSC3} = -(P_{VSC1} + P_{VSC2}) + P_{dc}$$

For the steady state condition, $P_{dc} = 0$ pu. Thus: $P_{VSC3} = -(P_{VSC1} + P_{VSC2})$

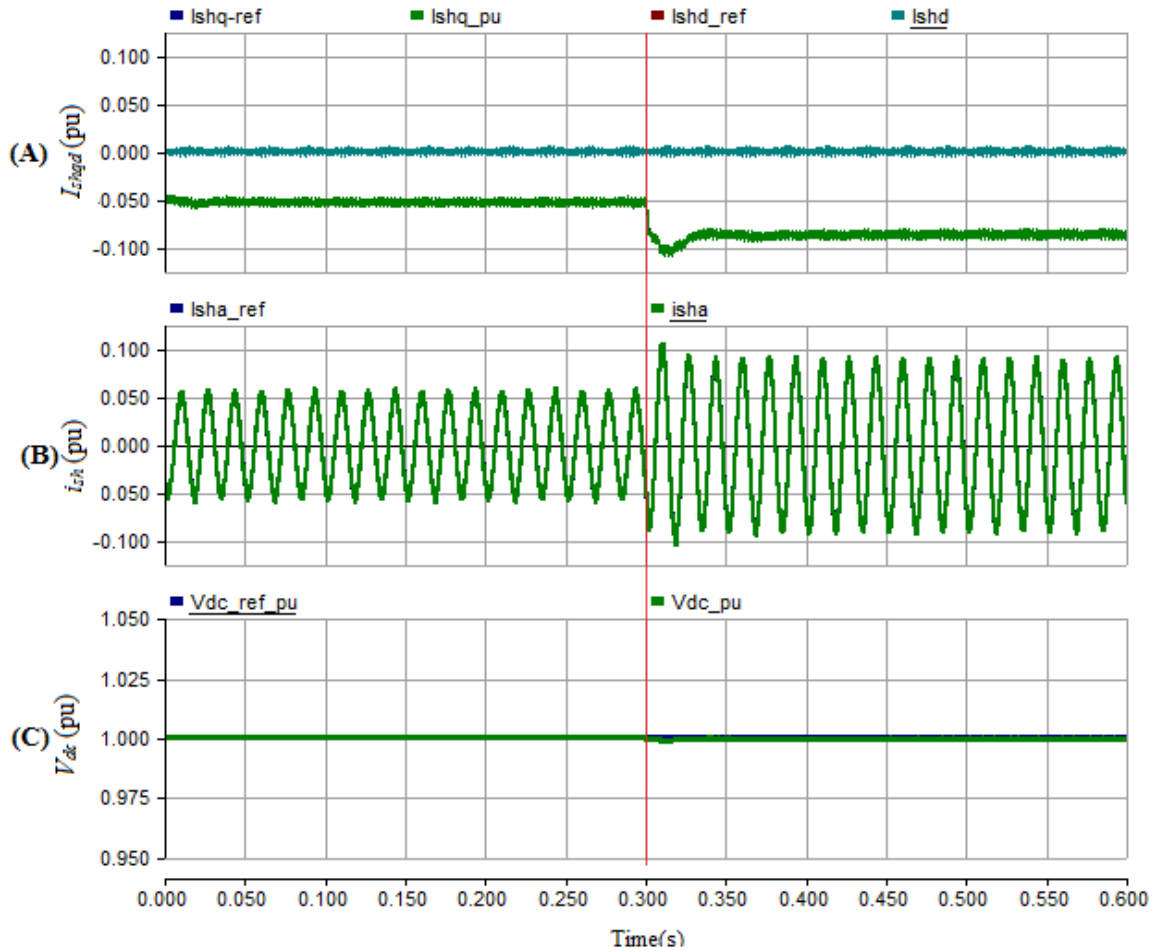


Figure 3-24: (A) The actual and references dq currents of shunt branch, (B) current waveforms for phase A of the shunt branch (C) The actual and reference of the DC voltage across the DC sharing the link, for the lagging PF case

Figure 3-25 shows the active power of the series VSC1 and VSC2 (P_{VSC1} and P_{VSC2}), the negative sum of P_{VSC1} and P_{VSC2} , and the active power of the shunt VSC3 (P_{VSC3}). For the considered PF case (lagging PF), the shunt VSC3 should absorb the active power from the sending end source and supply it to the series VSC1 and VSC2. Therefore, the sign of P_{VSC3} is minus and the signs of P_{VSC1} and P_{VSC2} are positive as shown in Figure 3-25. In Figure 3-25, one can note that at 0.3 sec, the active power demanded by the two series VSCS (P_{VSC1} and P_{VSC2}) is increased when the current references of both series branches are increased to synthesize the desired reference current in the transmission line. As shown in Figure 3-25, bottom curve (P_{VSC3}), the shunt VSC3 is the one responsible for supplying more active power to the series VSCs to satisfy their power demands. Finally, for Figure 3-25, one can note that the negative sum of P_{VSC1} and P_{VSC2} is almost equal to P_{VSC3} .

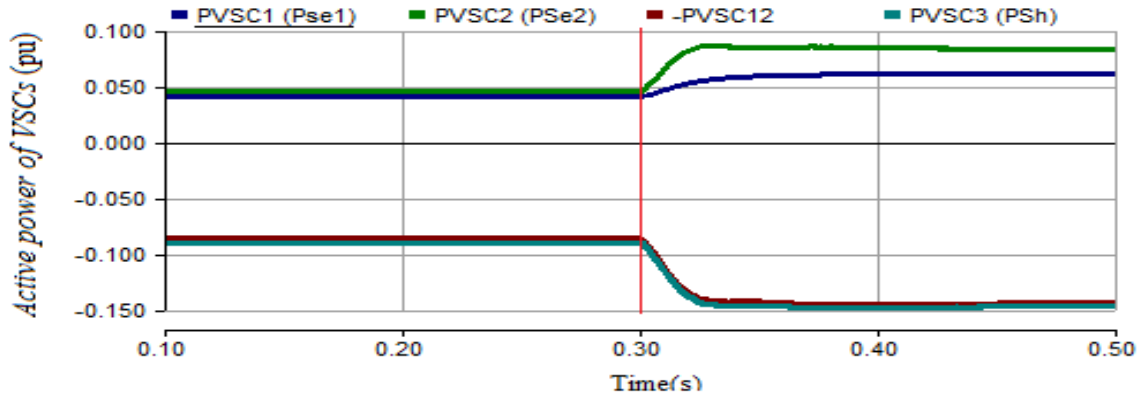


Figure 3-25: The active power; P_{VSC1} and P_{VSC2} , $-(P_{VSC1} + P_{VSC2})$, and P_{VSC3} for DC bus voltage regulation.

3.7. Summary

In this Chapter, PSCAD model was developed to verify the proposed control scheme for the UIPC (UPFC-based UIPC). The double loop PI decoupled control was used to control the current flow through the shunt branch and to regulate the common DC bus voltage. PR controllers were used for controlling the currents flowing through the series branches, to synthesize the desired reference current in the transmission line. The current sharing factors (α and β), which are calculated in Chapter 2, are stored in a lookup table and used to obtain the reference currents of the inductive and the capacitive branches. Then, these current references currents are used as reference signals for the PR current controllers of both series branches.

The performances of these controllers were demonstrated using a simple power system with a UPFC-based UIPC connected in series with a transmission line. Firstly, the simulation results of the series branches were presented to exam the performance of the PR controllers and to prove the concept of UPFC-based UIPC in the time domain. The simulation results for this part proved the ability of the UPFC-based UIPC, to achieve different desired transmission line current, for different PF cases, and also showed that the PR controllers gave a good dynamic response with a very small error in the steady state. Finally, the simulations result of the shunt branch were presented. They showed that the inner current loop of the double loop PI decoupled controller, to control the shunt branch current, resulting in a fast and well-damped dynamic response, with a zero error in the steady state. Moreover, the simulation results indicated that the DC voltage controller (outer voltage loop of the double loop PI decoupled controller) accomplished its tasks, maintaining the DC voltage around its reference by generating the required q-axis current reference.

CHAPTER 4. THE SYNCHRONOUS REFERENCE FRAME (DQ) CONTROLLER

4.1. Introduction

This chapter discusses the use of the synchronous reference frame (dq) for controlling the series VSCs. This technique allows the transformation of ac quantities into dc quantities (d and q) which are projections of the ac quantities on reference frames (d and q) that rotate synchronously to the ac quantities. The synchronous reference frame (dq) scheme with a PI controller is commonly used for controlling grid-connected VSCs [45]. Using the PI controller in dq frame results in zero steady-state error, to a step variation reference signal, since the integrator of the PI controller gives an infinite gain at zero frequency. For the series VSC1, of the inductive branch of the UIPC, and also for the shunt VSC3, of the shunt branch of the UIPC, the design of the PI controller is an easy task since their transfer functions and the equivalent circuit for the controller design are similar to the ones used for the STATCOM and the SCCC [46]. However, for the series VSC2 of the capacitive branch, it is not that simple. This is because the derivation of a transfer function and equivalent circuit of the plant for dq current controller design in the capacitor branch (with a series capacitor) is not straightforward. In this chapter, a dq model for the capacitive branch will be developed and a suitable linear controller will be designed to control the currents flow through the capacitive branch with zero error in steady state. The performance of the system is then verified by means of simulation results.

4.2. The Mathematical Model of the Series Branches of the UPFC-based-UIPC in dq Frame

In order to design the current controller for the series branches of the UPFC-based UIPC with the synchronous reference frame (dq), their dynamic mathematical models should be derived using the synchronous reference frame (dq). Deriving the dq mathematical model allows obtaining the transfer functions that are important for the design of the control loop. Recall that the UPFC-based UIPC has two series branches (inductive and capacitive). Thus, their models are presented (inductive) and developed (capacitive) in the following subsections.

4.2.1. The Mathematical Model for the Inductive Branch of the UPFC-based-UIPC

The mathematical model of the inductive series branch of the UIPC in dq frame for the current control loop is similar to the mathematical model of the shunt branch for the inner current control loop [46]. Thus, the derivation of it will not be included, and only the circuit and the final equations will be presented. The single line diagram of the inductive branch, which is extracted from the UIPC circuit, see Figure 3-4 in Chapter 3, is shown in Figure 4-1:

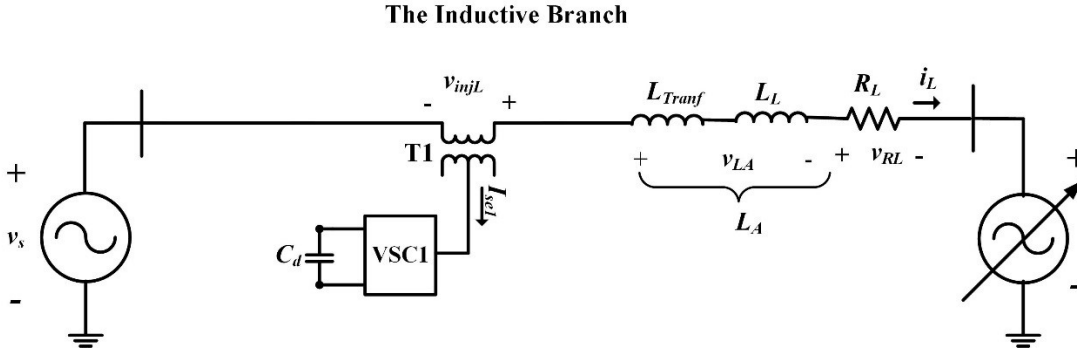


Figure 4-1: The single line diagram of the inductive branch circuit

The two main expressions that represent the series inductive branch in dq model are:

$$v_{injLd} = L_A \frac{di_{Ld}}{dt} + R_L i_{Ld} + v_{md} - v_{sd} + \omega L_A i_{Lq} \quad (4.1)$$

$$v_{injLq} = L_A \frac{di_{Lq}}{dt} + R_L i_{Lq} + v_{mq} - v_{sq} - \omega L_A i_{Ld} \quad (4.2)$$

These can be shown as equivalent dq circuits as in Figure 4-2:

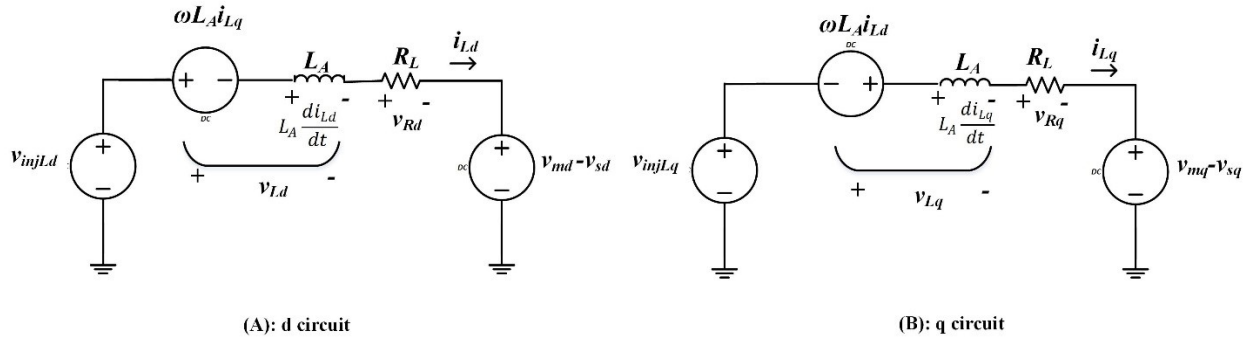


Figure 4-2: The equivalent circuits of the inductive branch (A) The circuit of the d axis (B) The circuit of the q axis.

The third, fourth and last terms of (4.1) and (4.2) are used as feedforward (FFW) branches to compensate the variations of the voltage and the effect of the coupling of d and q currents.

$$v_{injLd} = v_{injLd1} + v_{md} - v_{sd} + \omega L_A i_{Lq} \quad (4.3)$$

$$v_{injLq} = v_{injLq1} + v_{mq} - v_{sq} - \omega L_A i_{Ld} \quad (4.4)$$

Where v_{injLd1} and v_{injLq1} are the voltages required to regulate the currents in the two decoupled RL dc circuits.

- **Design of the current controller for the inductive branch**

With the utilization of the FFW loops, the current controller can be designed considering a decoupled system. The plant of the inductive branch can be represented by an RL circuit, the first and the second terms of (4.1) and (4.2). Thus, the transfer functions or the plant of the inductive branch is given by:

$$G_L(s) = \frac{I_{Ld,q}}{V_{injLd,q}} = \frac{1/R_L}{s\tau_{ind} + 1}, \text{ where } \tau_{ind} = L_A/R_L \quad (4.5)$$

The block diagram for the design of the PI-type controller, assuming unit feedback, becomes:

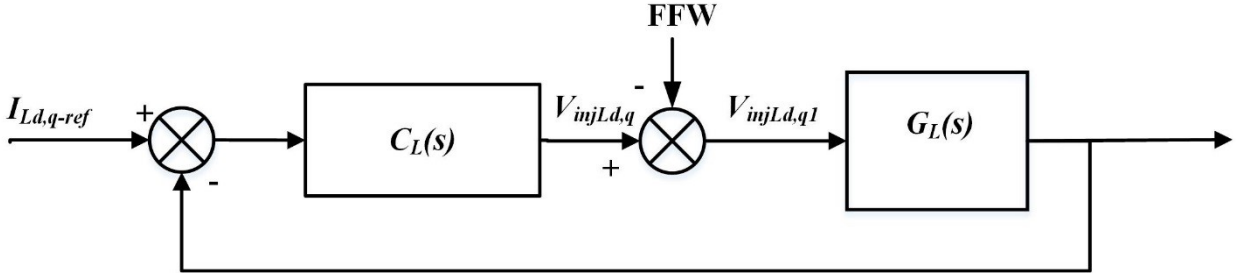


Figure 4-3: The block diagram for the design of the PI-type controller of the inductive branch

The VSC operates with SPWM with switching frequency (f_{sw}) of 5 kHz. The PI type 2 controller of the current control (C_L) is designed at crossover frequency (f_x) of 1kHz (20% of f_{sw}), and a phase margin (PM) of 80° .

The transfer function of a PI type 2 controller is:

$$C_L(s) = K_{pL} \left(\frac{1 + s\tau_L}{s\tau_L} \right) \frac{1}{(1 + sT_{pL})} \quad (4.6)$$

For a series inductor of the inductive branch, $L_A = 0.491$ H, and the series parasitic resistance, $R_L = 0.1 \Omega$, the parameters of the controller are calculated as $K_{pL}=3147.5$, $\tau_L=1.78$ ms, and $T_{pL}=0.0136$ ms. $\omega = 377$ rda/sec

4.2.2. The Mathematical Model of the Capacitive Series Branch of UPFC-based-UIPC

As mentioned before, the mathematical model of the series capacitive branch of the UPFC-based UIPC for the analysis and design of the current control loop has not been presented in the literature. VSCs are typically connected to a power grid via a series inductance, not a series capacitance as in the capacitive branch of the UPFC-based UIPC case. Thus, the derivation of a dynamic model for current control in the capacitive branch and the design of a suitable controller that leads to a zero error in steady state to a step variation in the reference current, are presented in this subsection.

Figure 4-4 shows the single line diagram of the capacitive branch circuit, which was obtained from the UPFC-based UIPC circuit (Figure 3-4 in Chapter 3).

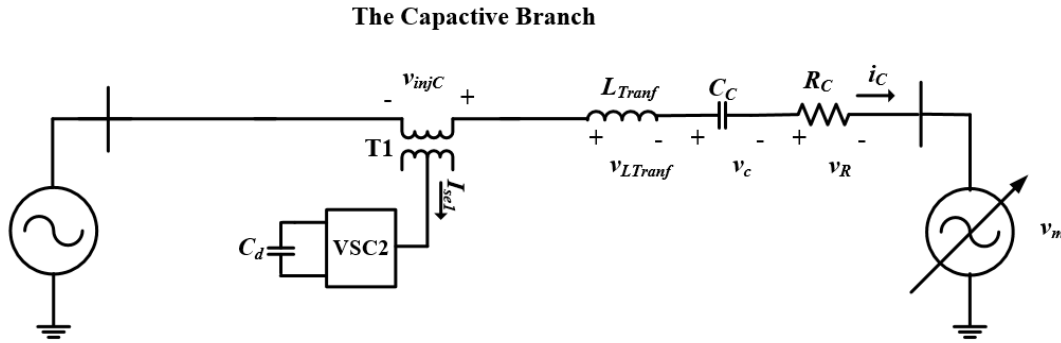


Figure 4-4: The single line diagram of the capacitive branch

The equation that represents the three-phase system of the capacitive branch in Figure 4-4 is:

$$\Delta[v_{branch}]_{abc} = [v_s]_{abc} + [v_{injC}]_{abc} - [v_m]_{abc} = [v_{LTranf}]_{abc} + R_c[i_c]_{abc} + [v_c]_{abc} \quad (4.7)$$

There, one can identify two terms. One concerns the grid plus injected voltages, which will define the current in the capacitive branch, and the other concerns the voltage drops across the capacitive branch impedances. The injected voltage by the series VSC2 is $v_{injC-abc}$, and the grid voltages are v_{sabc} and v_{mabc} . C_c and R_c , are the series capacitor and resistance of the capacitive branch, respectively, while L_{Tranf} , is the leakage inductor of the series coupling transformer.

To derive the mathematical model of the capacitive branch in dq frame, the quantities mentioned in (4.7) have to be transformed from abc frame to dq frame using the Park transformation technique. Recall that the general expression of Park transformation to transform from abc to dq was already mentioned in (3. 3), section 3.3.1.

The dq voltage components across the series capacitor can be calculated as:

$$v_{Cd} = \frac{2}{3} [v_{Ca} \cos \theta_d + v_{Cb} \cos(\theta_d - 120^\circ) + v_{Cc} \cos(\theta_d + 120^\circ)] \quad (4.8)$$

$$v_{Cq} = \frac{2}{3} [v_{Ca} \sin \theta_d + v_{Cb} \sin(\theta_d - 120^\circ) + v_{Cc} \sin(\theta_d + 120^\circ)] \quad (4.9)$$

The dq voltage components of the “voltage sources” are calculated as:

$$\Delta v_{bran-cd} = \frac{2}{3} [\Delta v_{branCa} \cos \theta_d + \Delta v_{branCb} \cos(\theta_d - 120^\circ) + \Delta v_{branCc} \cos(\theta_d + 120^\circ)] \quad (4.10)$$

$$\Delta v_{bran-cq} = \frac{2}{3} [\Delta v_{branCa} \sin \theta_d + \Delta v_{branCb} \sin(\theta_d - 120^\circ) + \Delta v_{branCc} \sin(\theta_d + 120^\circ)] \quad (4.11)$$

The dq current components of the capacitive branch can be expressed by considering that as:

$$[i_C]_{abc} = C_C \frac{d[v_C]_{abc}}{dt}$$

$$i_{Cd} = \frac{2}{3} \left[C_C \frac{dv_{Ca}}{dt} \cos \theta_d + C_C \frac{dv_{Cb}}{dt} \cos(\theta_d - 120^\circ) + C_C \frac{dv_{Cc}}{dt} \cos(\theta_d + 120^\circ) \right] \quad (4.12)$$

$$i_{Cq} = \frac{2}{3} \left[C_C \frac{dv_{Ca}}{dt} \sin \theta_d + C_C \frac{dv_{Cb}}{dt} \sin(\theta_d - 120^\circ) + C_C \frac{dv_{Cc}}{dt} \sin(\theta_d + 120^\circ) \right] \quad (4.13)$$

Applying the derivative operator to the equation of v_{cd} , (4.8), and considering that $\omega = \frac{d\theta_d}{dt}$

,one can get:

$$\begin{aligned} \frac{dv_{Cd}}{dt} + \frac{2}{3} \omega [v_{Ca} \sin \theta_d + v_{Cb} \sin(\theta_d - 120^\circ) + v_{Cc} \sin(\theta_d + 120^\circ)] \\ = \frac{2}{3} \left[\frac{dv_{Ca}}{dt} \cos \theta_d + \frac{dv_{Cb}}{dt} \cos(\theta_d - 120^\circ) + \frac{dv_{Cc}}{dt} \cos(\theta_d + 120^\circ) \right] \end{aligned} \quad (4.14)$$

It can be noted that the second term on the right-hand side of (4.14), is equal to v_{Cq} , multiplied by ω , see (4.9). Thus:

$$\frac{dv_{Cd}}{dt} + \omega v_{Cq} = \frac{2}{3} \left[\frac{dv_{Ca}}{dt} \cos \theta_d + \frac{dv_{Cb}}{dt} \cos(\theta_d - 120^\circ) + \frac{dv_{Cc}}{dt} \cos(\theta_d + 120^\circ) \right] \quad (4.15)$$

By multiplying both sides of ((4.15) with C_C , and considering the expression of i_{cd} in (4.12), one can get:

$$i_{cd} = C_C \frac{dv_{cd}}{dt} + \omega C_C v_{cq} \quad (4.16)$$

Applying the derivative operator to the equation of v_{cq} , (4.9), and considering that $\omega = \frac{d\theta_d}{dt}$,

$$\begin{aligned} \frac{dv_{cq}}{dt} - \frac{2}{3} \omega [v_{ca} \cos \theta_d + v_{cb} \cos(\theta_d - 120^\circ) + v_{cc} \cos(\theta_d + 120^\circ)] \\ = \frac{2}{3} \left[\frac{dv_{ca}}{dt} \sin \theta_d + \frac{dv_{cb}}{dt} \sin(\theta_d - 120^\circ) + \frac{dv_{cc}}{dt} \sin(\theta_d + 120^\circ) \right] \end{aligned} \quad (4.17)$$

It can also be noted for the q axis case that the second term of the right-hand side of (4.17), is equal to v_{cd} multiplied by ω , see (4.8). Thus:

$$\frac{dv_{cq}}{dt} - \omega v_{cd} = \frac{2}{3} \left[\frac{dv_{ca}}{dt} \sin \theta_d + \frac{dv_{cb}}{dt} \sin(\theta_d - 120^\circ) + \frac{dv_{cc}}{dt} \sin(\theta_d + 120^\circ) \right] \quad (4.18)$$

By multiplying both sides of (4.18) with C_C , and considering the expression of i_{cq} in (4.13), one can get:

$$i_{cq} = C_C \frac{dv_{cq}}{dt} - \omega C_C v_{cd} \quad (4.19)$$

(4.16) and (4.19) are key equations that will be considered for the design of the current controller in the capacitive branch. Where, i_{cd} and i_{cq} can be controlled through v_{cq} and v_{cd} , respectively. The derivative terms in (4.16) and (4.19), (dv_{cd}/dt) and (dv_{cq}/dt) can be neglected (null in the steady-state). Thus, one can say that the capacitive branch currents (i_{cd} and i_{cq}) can be indirectly controlled by controlling the voltages across its series capacitor (v_{cq} and v_{cd}).

Accordingly, the derivation of the mathematical models in the dq frame of the capacitive branch should lead to getting expressions (transfer functions), to regulate v_{cd} and v_{cq} via the injected voltages of VSC2 (v_{injcd} and v_{injq}). In this chapter, only the main developed expressions that represent the series capacitive branch in the dq models for voltage control (indirect current control) will be presented. Besides, the equivalent dq circuits of the capacitive branch for controller design will be shown. The rest of the deriving process of the mathematical model in the dq frame for the capacitive branch and validation of its dq circuits will be presented in Appendix A (A1 and A2).

The two main expressions that represent the series capacitive branch in the dq model for voltage controller (indirect current controller) are:

$$v_{injcd} = \underbrace{C_C L_{Tranf} \frac{d^2 v_{Cd}}{dt^2} + R_C C_C \frac{dv_{Cd}}{dt} + (1 + \omega^2 L_{Tranf} C_C) v_{Cd}}_{v_{injcd1}} + R_C \omega C_C v_{Cq} + 2\omega L_{Tranf} i_{Cq} + v_{md} - v_{sd} \quad (4.20)$$

$$v_{injcq} = \underbrace{C_C L_{Tranf} \frac{d^2 v_{Cq}}{dt^2} + R_C C_C \frac{dv_{Cq}}{dt} + (1 + \omega^2 L_{Tranf} C_C) v_{Cq}}_{v_{injcq1}} - R_C \omega C_C v_{Cd} - 2\omega L_{Tranf} i_{Cd} + v_{mq} - v_{sq} \quad (4.21)$$

Based on the equations (4.20) and (4.21), the equivalent dq circuits for controller design are shown in Figure 4-5:

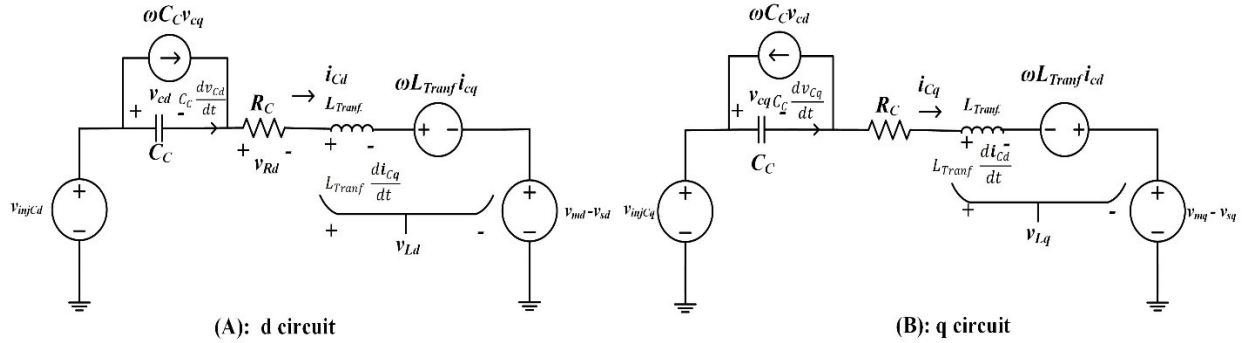


Figure 4-5: (A) The circuit of d axis (B) The circuit of q axis

Further verification of the circuits of the d axis and q axis is included in Appendix A. 2.

The fourth, fifth, sixth and last terms of (4.20) and (4.21) are used as FFW branches to compensate the variations of the voltage and the effect of the coupling of d and q currents. On the other hand, the first three terms of the same equations (v_{injcd1} and v_{injcq1}) are used to get the transfer functions of the plant for designing indirect current control of the capacitive branch.

- **Design of the voltage controller of the capacitive branch**

The voltage controller can be designed considering the coupling between d and q axes and the grid voltages (V_s and V_m) as disturbances, which will be added as FFW branches. The plant of the capacitive branch can be represented by an RLC circuit, the first, the second, and the third terms of (4.20) and (4.21). Thus, the transfer functions of the capacitive branch to design the voltage controller, which will indirectly set the desired capacitive branch currents, is given by:

$$G_C(s) = \frac{V_{Cd,q}(s)}{V_{injCd,q}(s)} = \frac{1}{C_C L_{Tranf} s^2 + R_C C_C s + (1 + \omega^2 L_{Tranf} C_C)} \quad (4.22)$$

The block diagram for the design of the PI-type controller, assuming unit feedback, becomes:

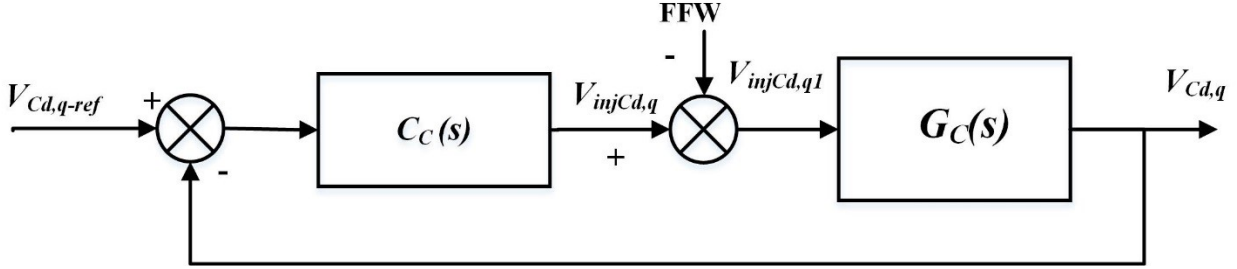


Figure 4-6: The block diagram for the design of the PI-type controller of the inductive branch

It is assumed that the VSC2 of the capacitive branch operates with SPWM at switching frequency (f_{sw}) of 5 kHz. A PI type 3 controller of the indirect current control (C_C) is designed at crossover frequency (f_x) of 1kHz (20% of f_{sw}), and phase margin (PM) of 80°.

The transfer function of a PI type 3 controller is:

$$C_C(s) = K_{pC} \left(\frac{1 + s\tau_C}{s\tau_C} \right) \frac{1}{(1 + sT_{pC})} \frac{(1 + s\tau_C)}{(1 + sT_{pC})} \quad (4.23)$$

For a series capacitor of the capacitive branch, $C_C = 13.9 \mu\text{F}$, the series parasitic resistance, $R_C = 1 \Omega$, the leakage inductor of the series transformer, $L_{Tranf} = 0.0146 \text{ H}$, and $\omega = 377 \text{ rda/sec}$, the parameters of the controller are calculated as $K_{pC} = 0.34$, $\tau_C = 3.34 \text{ ms}$, and $T_{pC} = 0.007 \text{ ms}$. Figure 4-7 shows the Bode plots of the plant (G_C), controller (C_C), and compensated loop transfer function (LTF) of the capacitive branch are shown in the Figure 4-7.

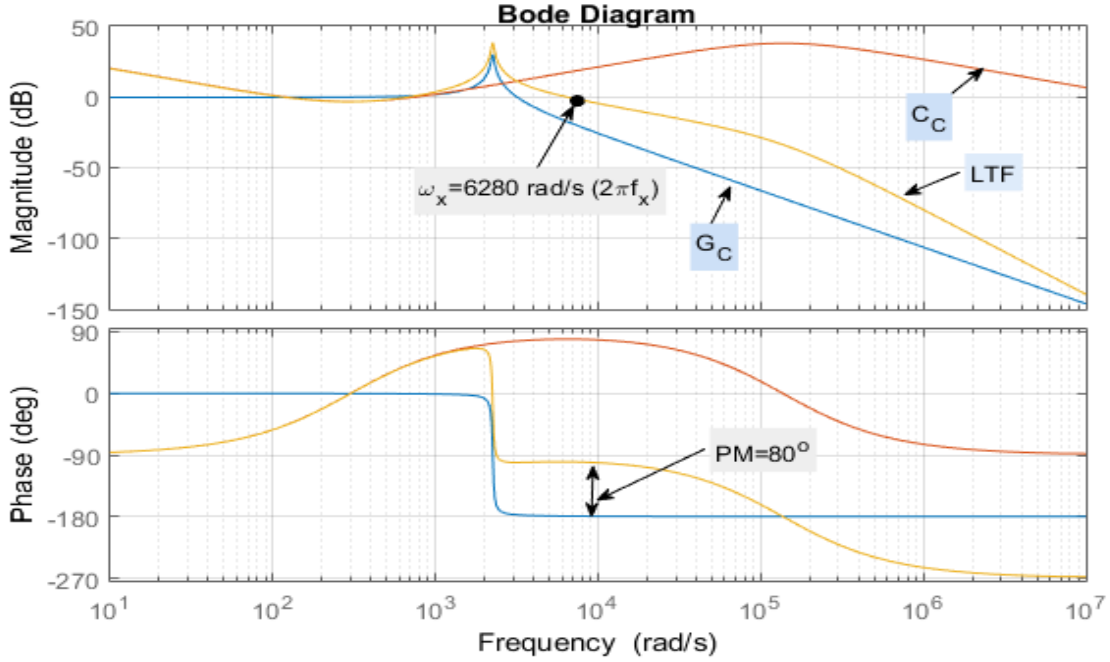


Figure 4-7: Bode plots of the plant, controller, and LTF of the capacitive branch

4.2.3. Realizing the Current and Voltage References for the dq Controllers

The method for obtaining the current references in the synchronous reference frame (dq) for the inductive branch is similar to the case of the PR controllers in Chapter 3. The only difference here is that the dq current references will be used directly as references for the dq current controllers instead of converting them into the abc frame as in the case of the PR controller.

On the other hand, the case of obtaining the references of the dq voltage controller of the capacitive branch will be different since voltage references are required instead of the current references, in the proposed indirect current control scheme. The dq current references that are obtained from factors α and β for the capacitive branch, which was shown in the case of the PR controller in Chapter 3, will be used to obtain the dq voltage references. Recall the relation between RMS current and the dq current components is:

$$\sqrt{2} I_C \angle \phi_C = I_{cq} + jI_{cd} \quad (4.24)$$

The RMS voltage across the series capacitor, C_C , of the capacitive branch (V_c), is equal to RMS current flow through its branch (I_C) multiplying with its impedance (X_C). Thus,

$$\sqrt{2} V_C \angle \delta_{vc} = V_{cq} + jV_{cd} = -jX_C \sqrt{2} I_C \angle \phi_C = -jX_C I_{cq} + +X_C I_{cd} \quad (4.25)$$

From (4.25), the voltage references in the dq frame can be expressed as:

$$V_{cqref} = X_C I_{cdref} \quad (4.26)$$

$$V_{Cdref} = -X_C I_{cqref} \quad (4.27)$$

The two expressions of voltage references in (4.26) and (4.27) can be validated by using the expressions of i_{cd} and i_{cq} , which were presented in the section of the mathematical model derivation of the capacitive branch, Section 4.2.2, equations (4.16) and (4.19).

$$i_{cd} = C_C \frac{dv_{cd}}{dt} + \omega C_C v_{cq} \quad \text{and} \quad i_{cq} = C_C \frac{dv_{cq}}{dt} - \omega C_C v_{cd}$$

Where, $\omega C_C = 1/X_C$. In steady state, the derivative term of the above two equations (for the DC system) is equal to zero. Thus:

$$I_{cd} = \frac{V_{cq}}{X_C} \Rightarrow V_{cq} = X_C I_{cd} \quad \text{and} \quad I_{cq} = -\frac{V_{cd}}{X_C} \Rightarrow V_{cd} = -X_C I_{cq} \quad (4.28)$$

Since the mathematical models, the transfer functions, and the references for dq controllers are defined for the series inductive and capacitive branches of the UIPC, one can show the schematic control diagram of these series branches that corresponds to the implementation of the current control loop in dq-frame with PI-type controllers and SPWM, see Figure 4-8.

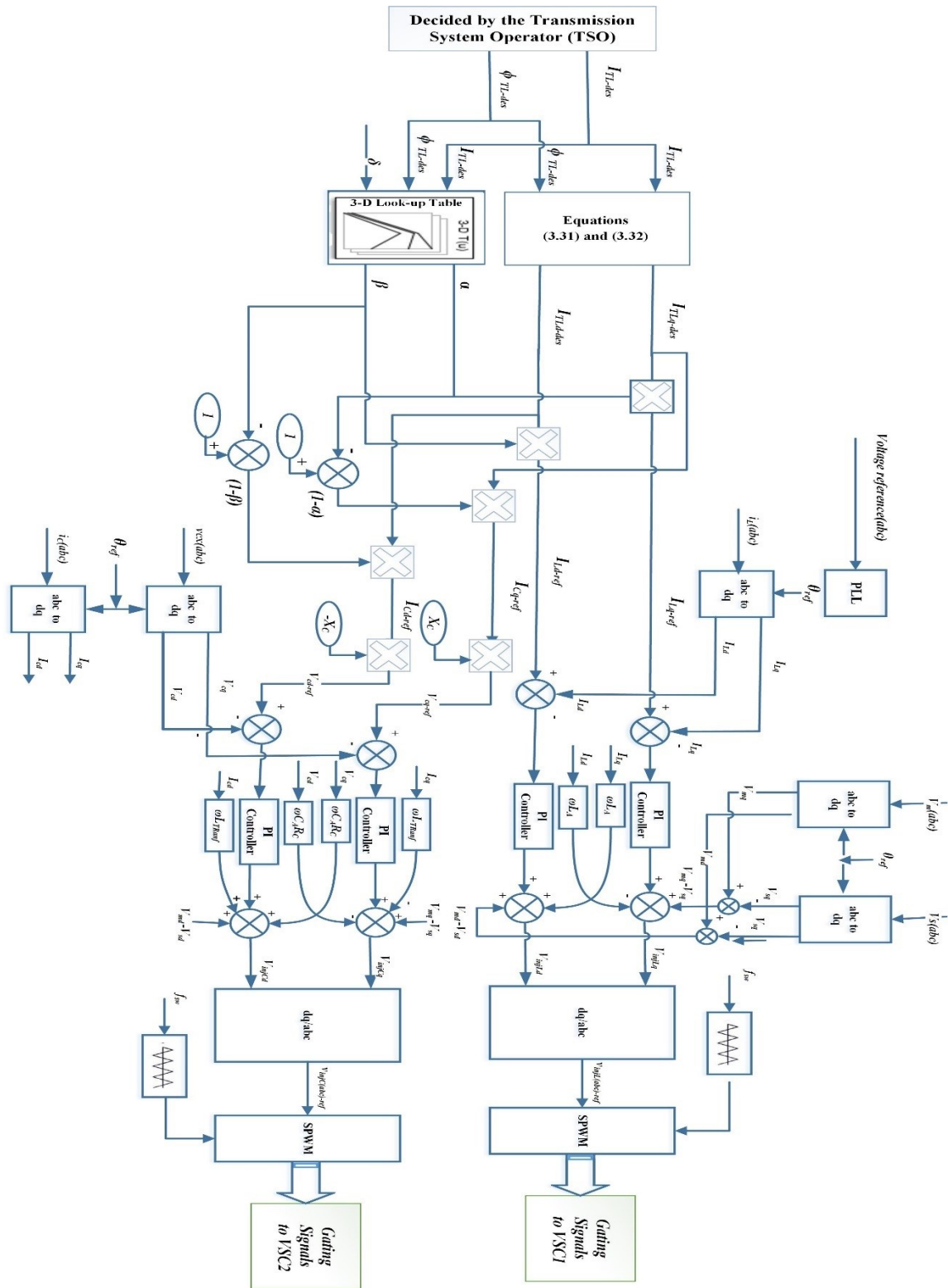


Figure 4-8: The schematic control diagram of the series branches of the UPFC-based-UIPC

4.3. Case Study

The same case study is considered for this Chapter as the one that was used in Chapter 2 and Chapter 3 (Figure 2-6 and Table 2-1). The PSCAD model of the UPFC-based-UIPC that was modeled and used in Chapter 3 is used for this chapter as well. Moreover, the three cases discussed in Chapter 3 are considered in Chapter 4: UPF ($\phi_{TL-des} = 0^\circ$), 0.8 leading PF ($\phi_{TL-des} = 36.87^\circ$) and 0.8 lagging PF ($\phi_{TL-des} = -36.87^\circ$). For each PF case, two values of I_{TL-des} , are considered: $I_{TL-des} = 0.5$ pu and 1 pu for the UPF and leading PF cases, and $I_{TL-des} = 0.5$ pu and 0.8 pu for the lagging PF case.

4.4. Simulation Results

Recall that the series VSCs of both branches have to be controlled to achieve the desired magnitude and angle of the transmission line (I_{TL-des} and ϕ_{TL-des}), while the VSC3, of the shunt branch, has to maintain the DC bus and operates with UPF. Since the used controller structure of the shunt branch is same in this chapter as the one already tested in Chapter 3 (double loop PI decoupled control), the simulation results related to this branch will be not presented. Hence, the simulation results section studies only the performance of the dq controllers for both series branches, on both operating conditions, a steady state and a transient response for a current references variation, for different cases.

4.4.1. Simulation Results of the UPF Case ($\phi_{ITL} = 0^\circ$)

For the UPF case ($\phi_{ITL} = 0^\circ$), the target of the UPFC-based UIPC is to make the transmission line current in phase with the receiving end voltage and to achieve two desired magnitude of transmission line current ($I_{TL-des} = 0.5$ and 1 pu). The sharing factors' values, α and β , the calculated currents magnitudes in pu, and angles of the inductive branch (I_L and ϕ_L), and the capacitive branch (I_C and ϕ_C), for the UPF case and for the two values of I_{TL-des} , were already shown in Chapter 3, Table 3-5, for the case of using the PR controllers. The performance of dq current controller for the inductive branch and the indirect current controller for the capacitive branch in the steady state condition and during transient conditions will be presented.

A. Simulation results in the steady state condition for the Unity PF case (UPF)

Figure 4-9 shows some key waveforms, for phase A, for I_{TL} , I_L , I_C and the reference voltage, V_R , and I_{TL} . The simulation results in term of how I_{TL} is split among I_L and I_C during the steady

state condition for the case of using the dq controllers in Figure 4-9 are similar as the ones presented for the case of using the PR controllers in Figure 3-15, for the same PF case. This is expected since the same method to compute the current sharing factors, α , and β , is used for both, the dq and PR current controllers. The only difference here is in term of the errors in the actual magnitude of the transmission line and series branches currents, and their angle with respect to the reference voltage, V_R in the steady state condition. Recall that the dq current controllers should result in zero error in the steady state. From the bottom curves of Figure 4-9, one can note that errors between the actual current magnitude and its angle from one side (I_{TL} and ϕ_{TL}) and their desired values in another side (I_{TL-des} ϕ_{TL-des}) are extremely small if not zero. Further discussion about the error in actual values of I_{TL} and ϕ_{TL} in the steady state condition, in case of using the dq controllers and their comparison with the PR controller's case, will be presented in a separate section for all PF cases.

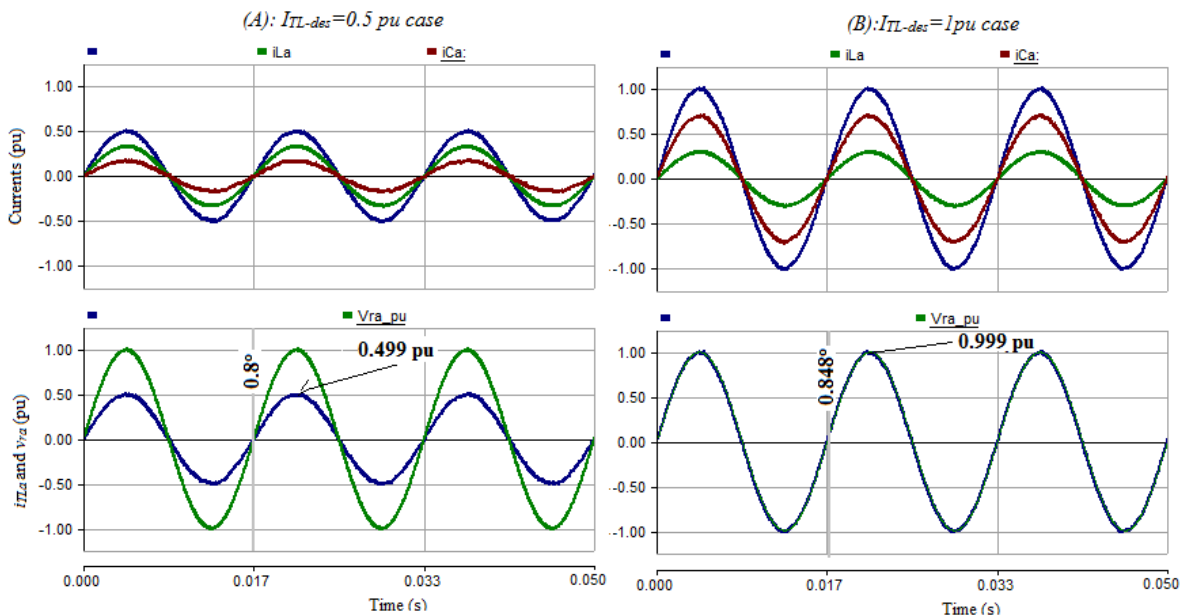


Figure 4-9: Simulation waveforms for UPF case: (A) $I_{TL-des} = 0.5$ pu and (B) $I_{TL-des} = 1$ pu. Top: I_{TL} , I_L , and I_C . Bottom: I_{TL} and V_R .

B. Simulation results of the UPF case in the transient state

In order to investigate the performance of the dq current controller of the inductive branch and the proposed dq voltage controller of the capacitive branch during the transient condition, their actual values should be observed during the step change of their references values to achieve the desired transmission line current. It should be mentioned that for the UPF case, the d-axis of the

inductive current branch and the q-axis of the voltage across the capacitor of the capacitive branch are zero, since no imaginary/reactive part of the transmission line current.

Figure 4-10 (A) shows the transient response of the dq controller of the inductive branch when its reference is changed at 0.3s. Both actual d and q currents (I_{Ld} , and I_{Lq}) follow their references, (0pu and 0.3317 pu for $I_{TL-des} = 0.5$ pu, and 0 pu and 0.299 pu for $I_{TL-des} = 1$ pu), and have zero steady state error. From Figure 4-10 (B), one can see that the dq current controller of the inductive branch leads to a good dynamic response for the AC waveform. It only takes one cycle for the dq current controller to make the inductive branch current reach its steady state value with zero error when its reference is changed from 0.3317pu to 0.299 pu to synthesize I_{TL} (0.5pu & 1pu).

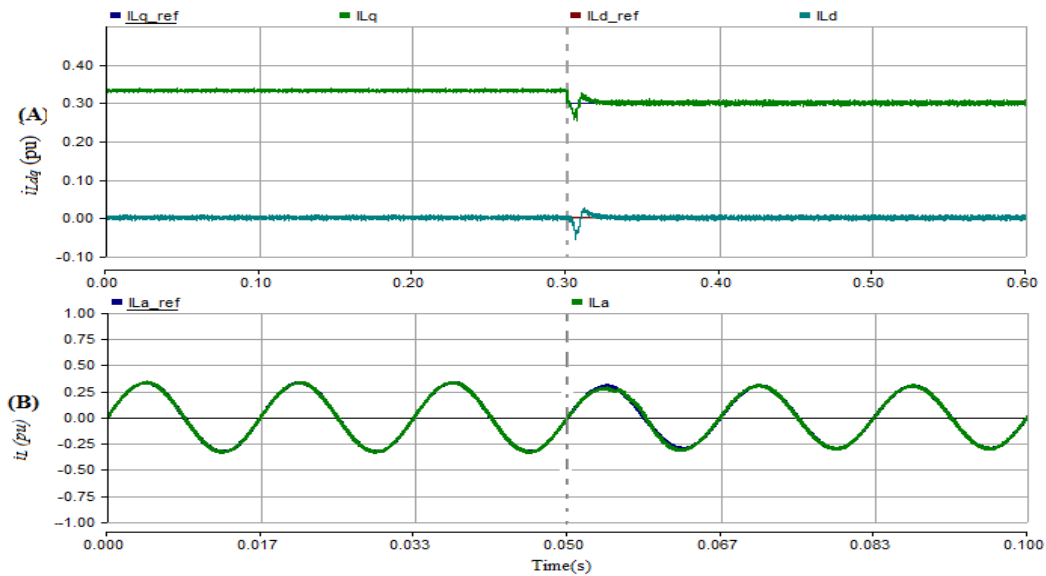


Figure 4-10: (A) the actual and references dq currents, (B) The actual and reference current waveforms for phase A, of the inductive branch for the UPF case.

Let us move to the capacitive branch. Recall that a dq voltage controller is used to regulate the voltage across the series capacitor, and indirectly, the current in the capacitive branch. Therefore, the dq voltages, and AC waveform of phase A, across the series capacitor will be shown to verify the performance of dq voltage controller of the capacitive branch. From Figure 4-11 (A), one can note that the dq voltage controller of the capacitive branch work properly and make the actual d and q voltage components (V_{cd} and V_{cq}) follow their references (0.0604 pu and 0 pu for $I_{TL-des} = 0.5$ and 0.252 pu and 0 pu for $I_{TL-des} = 1$ pu) with zero error in steady-state. The controller has yielded a fast and well behaved response due to a change of the reference signal at 0.3 sec The good performance of the dq voltage controller is evident on the AC voltage waveform of phase A,

across the capacitor (Figure 4-11 (B)). The actual voltage reaches its steady state with zero error, due to a change of the reference signal, in a short time.

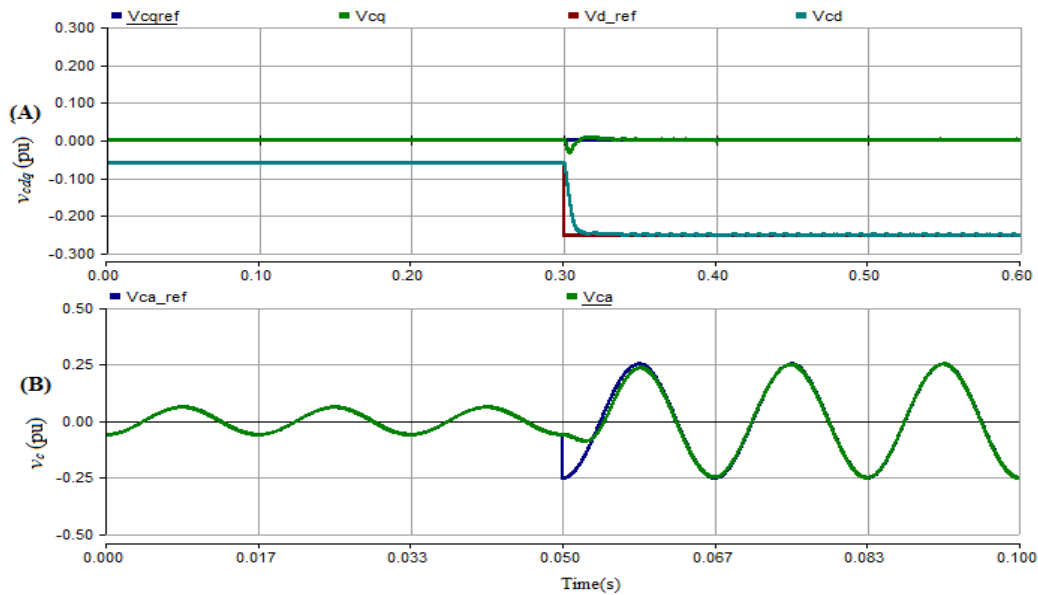


Figure 4-11: (A) the actual and reference dq voltage (B) The actual and reference voltage waveforms for phase A, of the capacitive branch for the UPF case

Since the final goal of using the voltage controller is to synthesize the capacitive branch current to achieve the desired transmission line current (varying from 0.5 to 1 pu in this case), the waveform of the capacitive branch current is shown in Figure 4-12. Although the capacitive branch controller is an indirect current controller based on a voltage control loop, it leads to a good result in the current flow through the capacitive branch as can be seen in Figure 4-12. The indirect dq current controller makes the capacitive branch current reach the steady state value with zero error in a short time, when its required portion is changed from 0.1683pu to 0.7001pu, to make I_{TL} varies from 0.5 to $I_{TL-des}=1$ pu.

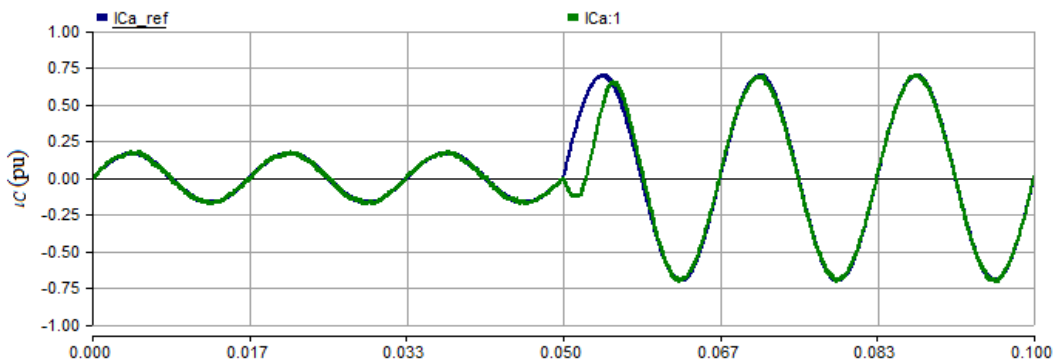


Figure 4-12: The actual and reference current waveforms for phase A of the capacitive branch for UPF case

4.4.2. Simulation Results of the Leading PF Case (0.8 and $\phi_{TL} = 36.87^\circ$)

For the PF=0.8 leading case, the task of the UPFC-based UIPC is to make the transmission line current lead the receiving end voltage by 36.87° and achieve two desired values of transmission line current ($I_{TL-de} = 0.5$ pu, and 1pu). The values of α , β , I_L , ϕ_L , I_C and ϕ_C , for two values of I_{TL-des} for this PF case were given in Table 3-6, for the case of using the PR controllers. Like in the UPF case, the performance of the dq controllers for inductive branch and the capacitive branch in the steady-state condition and during transient conditions will be presented.

A. Simulation results of leading PF case in the steady-state condition

Figure 4-13, shows the simulations results of phase A, for I_{TL} , I_L , I_C , I_C , and the reference voltage, V_R and I_{TL} in the PF=0.8 leading case. The simulation results in term of how I_{TL} is being shared by I_L and I_C , for $I_{TL-des} = 0.5$ pu and 1 pu, for the case of using the dq controllers (Figure 4-13) and for the case of using the PR controllers (Figure 3-18), are similar. For the steady state condition case, the difference between these current controllers is concerning the actual currents magnitudes, and their angle with respect to the reference voltage, V_R . From the bottom curves of Figure 4-13, one can note that errors between the actual current magnitude and its angle from one side (I_{TL} and ϕ_{TL}) and their desired values in another side (I_{TL-des} ϕ_{TL-des}), if are not zero, they are extremely small. This is expected for the dq current controller case.

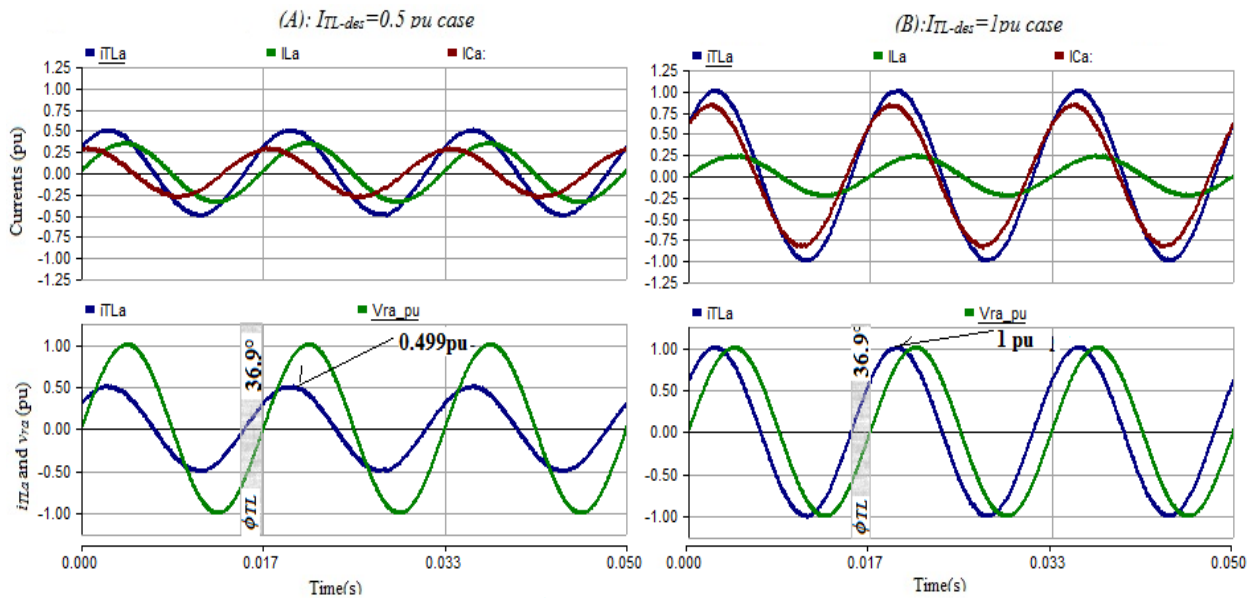


Figure 4-13: Simulation waveforms for Lead PF case: (A) $I_{TL-des} = 0.5$ pu and (B) $I_{TL-des} = 1$ pu. Top: I_{TL} , I_L , and I_C . Bottom: I_{TL} and V_R

B. Simulation results of leading PF case in the transient condition

The performance of the proposed dq controller for both series branches, during the transient response, will be observed during the step change of their reference values for the leading PF case.

Figure 4-14 (A) shows the transient response of the dq controller of the inductive branch when its reference is changed at 0.3s. Both actual d and q currents (I_{Ld} , and I_{Lq}) follow their references ($I_{Ld-ref} = 0.025$ pu and $I_{Lq-ref} = 0.3342$ pu for $I_{TL-des} = 0.5$ pu, $I_{Ld-ref} = 0$ pu and $I_{Lq-ref} = 0.2302$ pu for $I_{TL-des} = 1$ pu), and have zero steady-state error. From Figure 4-14 (B), one can see that the dq current controller of the inductive branch leads to a good dynamic response on the AC waveform for the leading PF case. It only takes one cycle for the dq current controller to make the inductive branch current reaches its steady-state value with zero error when its reference is changed, at 0.05s, from 0.344 pu to 0.2302 pu, to synthesize I_{TL} for $I_{TL-des} = 0.5$ pu and 1pu.

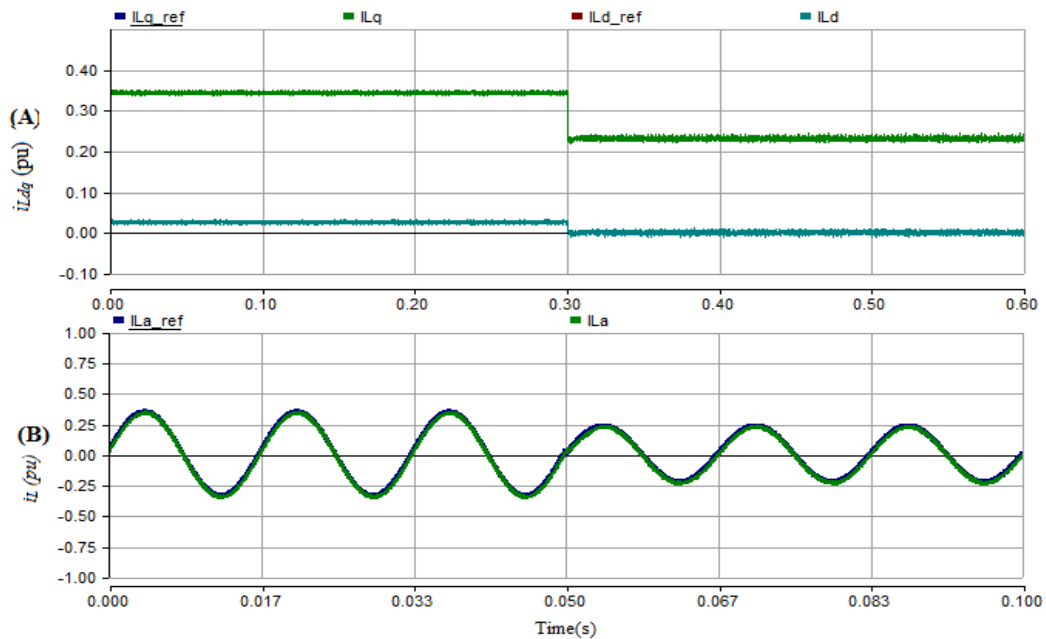


Figure 4-14: the actual and references dq currents, (B) The actual and reference current waveforms for phase A, of the inductive branch for the leading PF case

From Figure 4-15 (A), one can note that the dq voltage controller (indirect current controller), of the capacitive branch, works properly and makes the actual d and q voltages (V_{cd} and V_{cq}), follow their references ($V_{cd-ref} = -0.019$ pu, and $V_{cq-ref} = 0.094$ pu for $I_{TL-des} = 0.5$ pu, $V_{cd-ref} = -0.194$ pu, and $V_{cq-ref} = 0.204$ pu, for $I_{TL-des} = 1$ pu), with zero error in steady state. The controller has yielded a fast and well-behaved response due to a change of the reference signal. The good performance of the dq voltage controller is evident on the AC voltage waveform of phase

A, across the series capacitor as seen in Figure 4-15 (B). The actual voltage reaches its steady state with zero error, due to a change of the reference signal, in a short time.

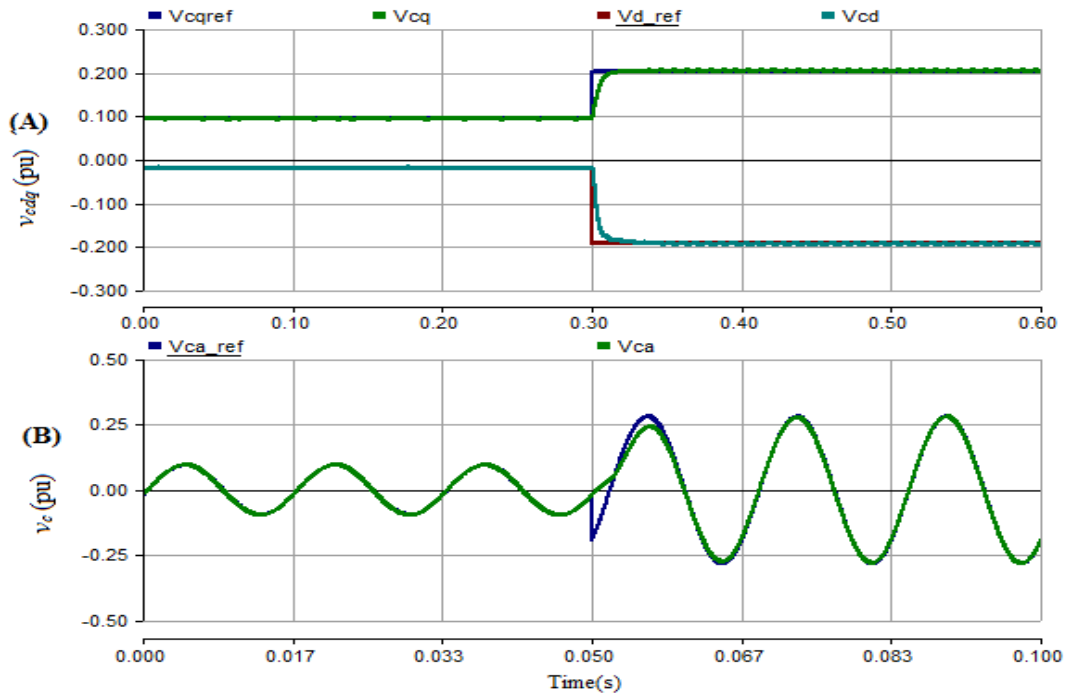


Figure 4-15: (A) the actual and reference dq voltage (B) The actual and reference voltage waveforms for phase A, of the capacitive branch for the PF leading case

The waveform of the capacitive branch current is shown in Figure 4-16. The voltage controller (indirect current controller) makes the capacitive branch share its required portion for I_{TL-des} ($I_c = 0.2811$ pu and 0.8274 pu for $I_{TL-des} = 0.5$ pu and 1 pu), with no error and a good dynamic response.

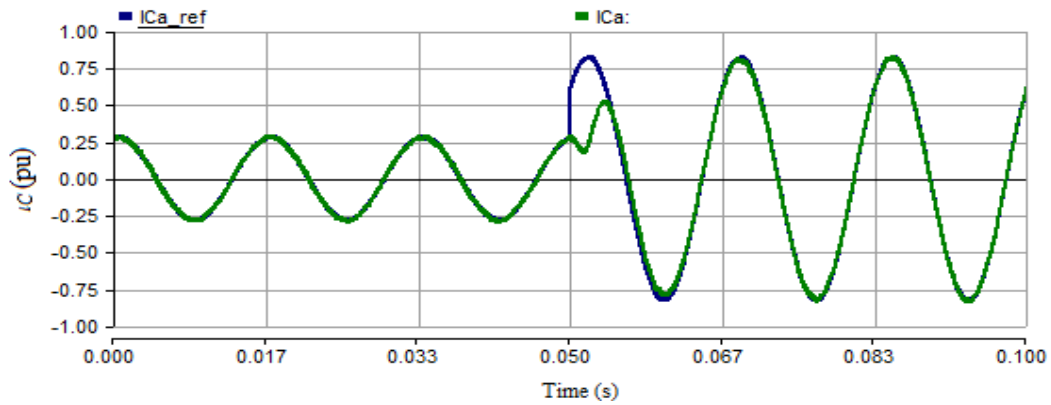


Figure 4-16: The actual and reference current waveforms for phase A of the capacitive branch for leading PF case

4.4.3. Simulation Results of the Lagging PF Case (0.8 and $\phi_{ITL} = -36.87^\circ$)

For the lagging PF case with a value equal to 0.8, the UPFC-based UIPC should result in the transmission line current lagging the receiving end voltage by an angle with a value equal to -36.87° (same absolute angle value of the leading PF case with a different sign). Like in the UPF and leading PF cases, two values of I_{TL-des} will be considered. The first value is the same as in the previous two cases, 0.5 pu. However, the second considered value of I_{TL-des} for this case is equal to 0.8 pu. The reason for considering 0.8 pu instead of 1pu for lagging PF case was mentioned in Chapter 3, for the same PF case. It is due to the extreme limit of the current that the UIPC can achieve, for the PF=0.8 lagging case. Recall also that the sharing factors, α and β , I_L , ϕ_L , I_C and ϕ_C , for the two considered values of I_{TL-des} in the PF =0.8 leading case was shown in Chapter 3, Table 3-7, for the case of using the PR controllers.

Similar to the UPF and leading PF cases, the performance of the dq current controllers for inductive and capacitive branches in the steady state condition and the transient condition will be presented.

A. Simulation results of lagging PF case in the steady-state condition

Figure 4-17 shows the simulation waveforms of phase A, for I_{TL} , I_L , I_C and the reference voltage, V_R , and I_{TL} in the PF = 0.8 lagging case in the steady state condition. By comparing the results for dq controller case (Figure 4-17) with the one were presented for the PR controller case (Figure 3-21), one can note the results of both controller cases are similar in term of how the inductive and capacitive branches share their required portion for $I_{TL-des} = 0.5$ pu and 0.8 pu. However, there is a small difference between the results for the dq controller case and the results for the PR controller case, in terms of the steady state values of current magnitudes and their angles. For the dq current controller case of this chapter, one can note that the waveforms of Figure 4-17 do correspond to what was expected and listed in Table 3-7 with almost zero error in the steady state condition.

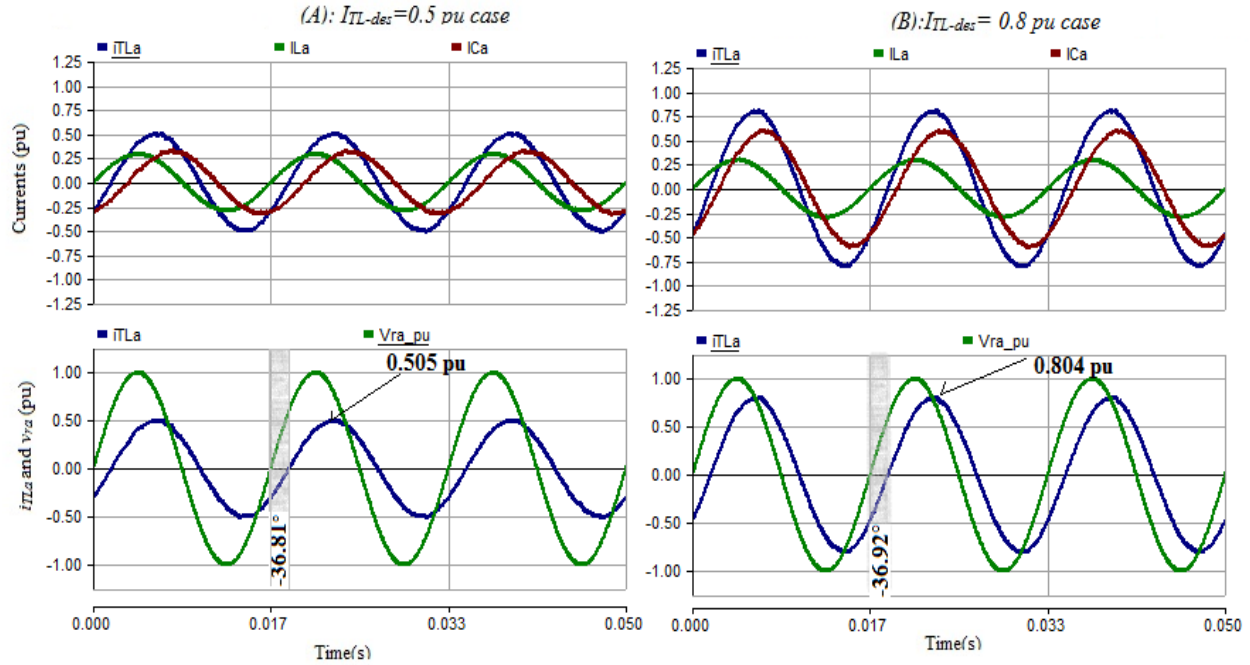


Figure 4-17: Simulation waveforms for lagging PF case: (A) $I_{TL-des} = 0.5$ pu and (B) $I_{TL-des} = 1$ pu. Top: I_{TL} , I_L , and I_C . Bottom: I_{TL} and V_R

B. Simulation results of lagging PF case in the transient condition

The performance of the proposed dq controllers of the inductive and the capacitive branches during the transient response will be observed during the step change of their reference values for the lagging PF case as in previous two cases. Figure 4-18 (A) shows the transient response of the dq controller of the inductive branch when its reference is changed at 0.3s. Both actual d and q currents (I_{Ld} , and I_{Lq}) follow their reference signals ($I_{Ld-ref} = 0$ pu and $I_{Lq-ref} = 0.293$ pu for $I_{TL-des} = 0.5$ pu and $I_{Ld-ref} = 0$ pu and $I_{Lq-ref} = 0.295$ pu for $I_{TL-des} = 1$ pu) and have zero steady state error. From Figure 4-18 (B), one can see that the dq current controller of the inductive branch leads to a good dynamic response on the AC waveform for the lagging PF case. It takes less than a half cycle for the dq current controller to make the inductive branch current reach its steady-state value with zero error, when its references are changed from 0.293 pu to 0.295 pu, to synthesize I_{TL} for $I_{TL-des} = 0.5$ pu and 1pu.

Figure 4-19 (A) shows that the dq voltage controller (indirect current controller) of the capacitive branch works properly and makes the actual d and q voltage components follow their references ($V_{cd-ref} = -0.038$ pu and $V_{cq-ref} = -0.108$ pu for pu for $I_{TL-des} = 0.5$ pu and $V_{cd-ref} = -0.124$ pu and $V_{cq-ref} = -0.172$ pu for $I_{TL-des} = 1$ pu) with zero error in steady state, as in previous two PF cases. The controller has yielded a fast and well-behaved response due to a change of the reference

signal. The good performance of the dq voltage controller is evident on the AC voltage waveform of phase A, across the capacitor, as can be seen in Figure 4-19 (B). The actual voltage reaches its steady state with zero error in one cycle following a change in its reference signal.

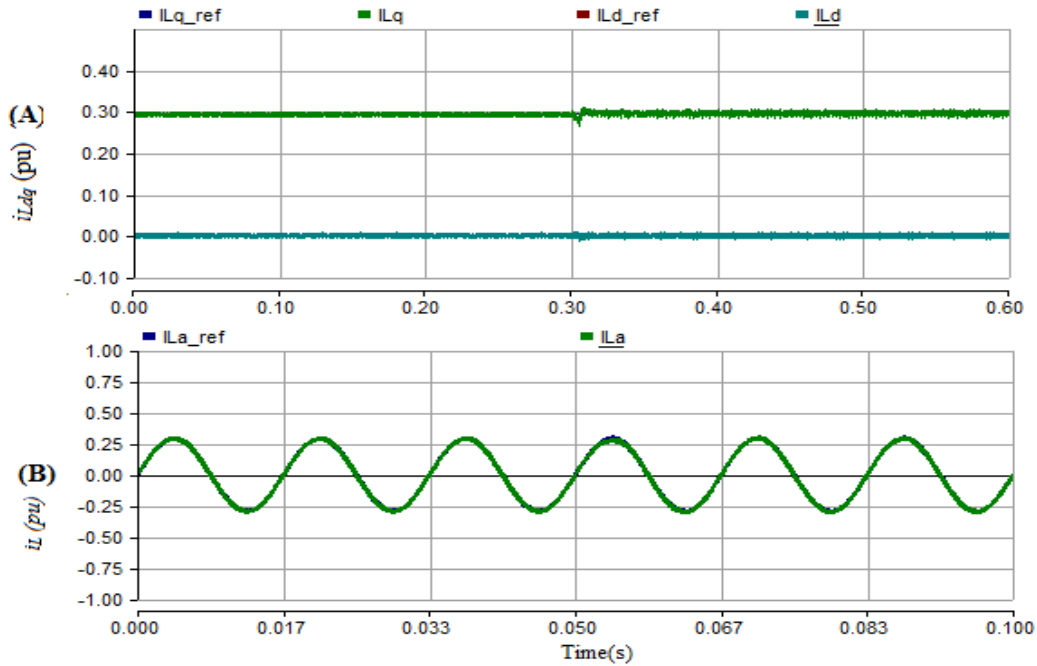


Figure 4-18: the actual and references dq currents, (B) The actual and reference current waveforms for phase A, of the inductive branch for the lagging PF case

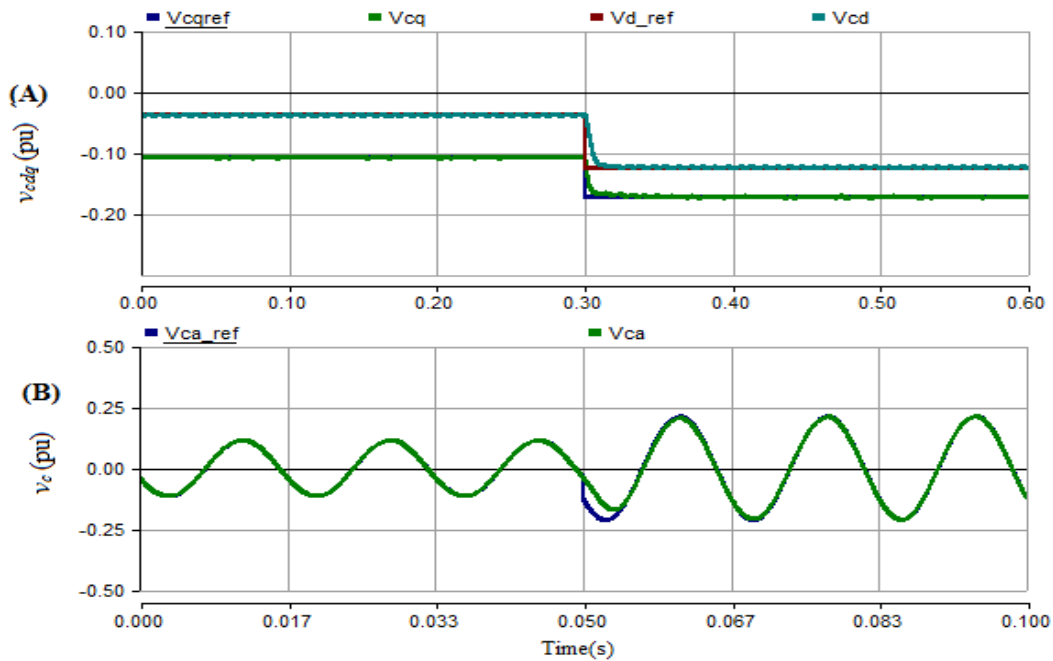


Figure 4-19: (A) The actual and reference dq voltage (B) The actual and reference voltage waveforms for phase A, of the capacitive branch for the PF lagging case

Figure 4-20 shows the waveform of the capacitive branch current. The indirect current controller makes the capacitive branch share its required portion for I_{TL-d} ($I_c=0.3185$ pu and 0.5908 pu for $I_{TL-des}=0.5$ pu and 0.8 pu) with no error in steady state and with a good dynamic response.

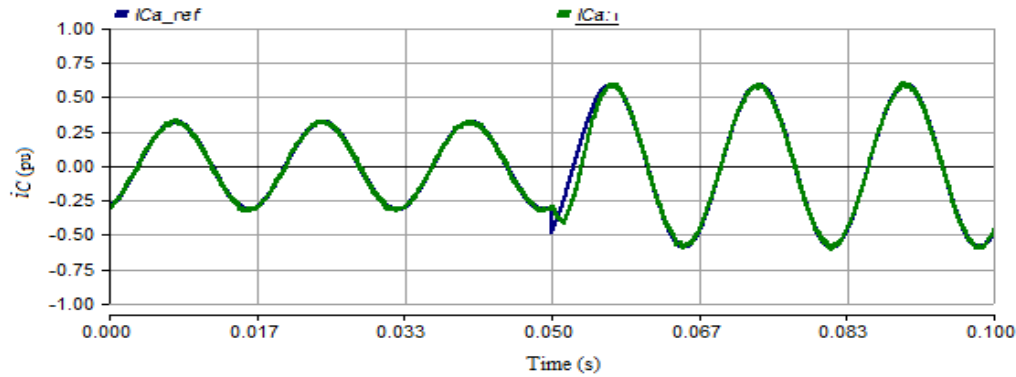


Figure 4-20: The actual and reference current waveforms for phase A of the capacitive branch for lagging PF case

4.4.4 Comparison of the Simulation Results of the UPFC-based UIPC Between the PR Controller and dq Controller in the Steady State Condition

The purpose of this section is to validate the key advantage of using the dq controllers over the PR controller, which is to achieve a zero error in the steady state, to a step variation of the reference signal. Hence, a brief comparison of the simulation results of the UPFC-based UIPC in the steady state, for both controller cases those were presented in Chapter 3 and Chapter 4, are discussed. This comparison will show errors in the actual values of the transmission line magnitude and its angle (I_{TL} and ϕ_{TL}) with respect to their desired values (I_{TL-des} and ϕ_{TL-des}), see Table 4-1.

From Table 4-1, one can note that error values between the actual values of current magnitude and its angle (I_{TL-act} and ϕ_{TL-act}) in the steady state condition and their desired (references), for dq controller case, do not exceed 0.2% for all PF cases. Since this error value (0.2 %) is very small value, it can be neglected (≈ 0). Thus, one can say that the using the dq controllers to control the currents of the inductive branch directly and control the capacitive branch indirectly lead to zero error in the steady state for all PF and I_{TL-des} cases. On the other hand, the PR controller presents errors in the steady state values of I_{TL-act} . However, the error values are small in most cases. The worst case was when the PF is lagging with a value 0.8 and $I_{TL-des}=0.5$ pu. It presents an error with 5.2%.

Table 4-1: Comparison of errors values for the PR controllers and for dq controllers in different values of I_{TL} and ϕ_{TL}

PF case	$\phi_{ITL-des} (^{\circ})$	$I_{TL-des}(pu)$	Control type	$I_{TL-act}(pu)$	Error	$\phi_{ITL-act} (^{\circ})$	Error (%)
UPF	0	0.5	PR	0.492	1.6%	1.626	-
			dq	0.499	0.2% ($\approx 0\%$)	0.8	-
		1	PR	0.990	1%	1.58	-
			dq	0.999	0.1% ($\approx 0\%$)	0.84	-
PF = 0.8/ leading	36.87	0.5	PR	0.511	2.2%	36.99	0.325% ($\approx 0\%$)
			dq	0.499	0.2% ($\approx 0\%$)	36.9	0.08 % ($\approx 0\%$)
		1	PR	1.012	1.2%	37	0.35% ($\approx 0\%$)
			dq	1	0%	36.9	0.08 % ($\approx 0\%$)
PF = 0.8/ lagging	-36.87	0.5	PR	0.474	5.2%	-37.27	1%
			dq	0.5	0%	-36.81	0.163% ($\approx 0\%$)
		0.8	PR	0.773	3.3%	-37	0.35% ($\approx 0\%$)
			dq	0.799	0.125% ($\approx 0\%$)	-36.92	0.13% ($\approx 0\%$)

4.5. Summary

This chapter addressed the use of the synchronous reference frame (dq) controller for controlling the inductive and capacitive branches of the UIPC, to achieve zero error in steady-state for step variations in the reference signals. A review of the dynamic mathematical model in the dq frame for the inductive branch, for current control design, was presented. Then, a mathematical model in the dq frame for the capacitive branch for designing a control loop was proposed in this work. The model of the plant is complex, and it is difficult to achieve current control with a VSC using a linear PI-type controller and feedforward decoupling branches. Therefore, a scheme based on an indirect current control, based on the control of the capacitor voltage of the other axis, was proposed. The impact of the variations in the capacitive voltage in the same axis, not controlled, is minimized by using a relatively slow (low bandwidth) voltage control loop.

The three cases discussed in Chapter 3 were considered in Chapter 4, for verifying the performance of the proposed dq control scheme for the UPFC-based UIPC, in the steady state and

transient conditions. In the steady state condition, the actual current of each branch follows its reference with zero steady-state error, thus leading to the transmission line current (I_{TL}) with the desired magnitudes and phase with respect to the receiving end voltage. For the transient responses, the dq current controller of the inductive branch and the proposed indirect current control via dq voltage controller, for the capacitive branches, presented good dynamic responses following step changes in their references values to achieve the desired transmission line current. In all cases, it was noted that both controllers required less than one cycle to reach their actual values in the steady state condition.

CHAPTER 5. THE EXPERIMENTAL IMPLEMENTATION OF THE UPFC-BASED UIPC

5.1. Introduction

In the previous two chapters, the proposed (UPFC-based) UIPC was simulated with PSCAD to validate the numerical results that were obtained in Chapter 2. Besides, the good performance of the PR and dq controllers for the series VSCs and the double loop PI decoupled control for the shunt VSC was demonstrated by simulation. In this chapter, the primary objective will be to verify the proposed control scheme for the UIPC (UPFC-based UIPC), which makes use of all features of the dual UPFC, to control the current flow through the transmission line with a reduced scale prototype. This chapter starts with the description of some modifications of the electric circuit of the UPFC-based UIPC and “transmission system” that are carried out in the experimental set-up to facilitate its realization. Then, the experimental results of the UIPC for the same cases that were considered in the simulations results of the previous chapters will be presented.

5.2. The Modification of the Electric Circuit with the UIPC

The electrical system used for the theoretical study in previous chapters was a simple two-node transmission system with the UPFC-based UIPC connected at the sending end, as shown in Figure 5-1. The system voltage was 230 kV, the rated frequency was 60 Hz, and the three-phase base power was 100 MVA. In this chapter, the system is scaled-down and slightly modified to be more appropriate for laboratory scale experimental verification.

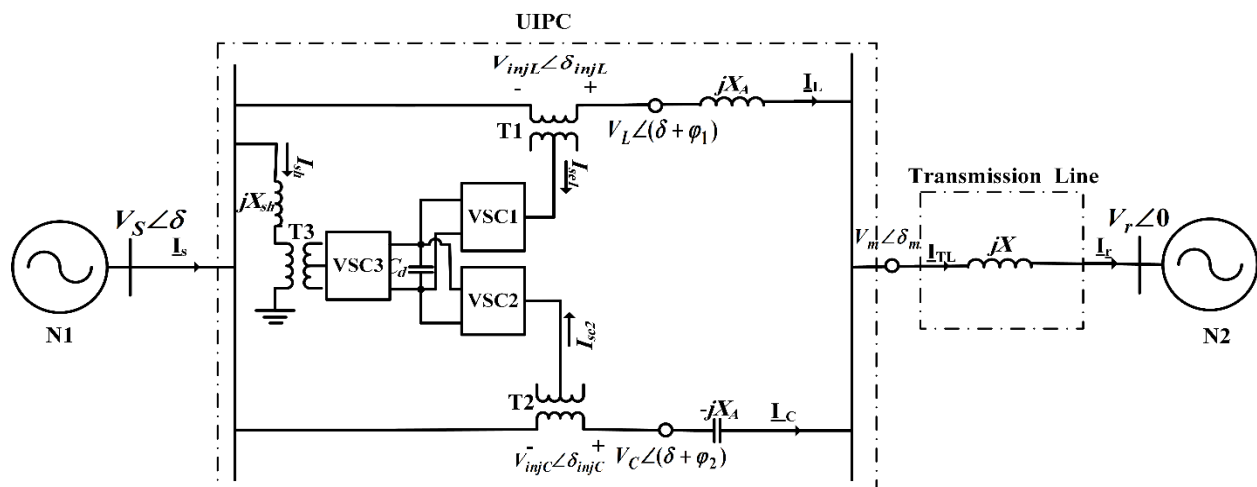


Figure 5-1: The 2-node transmission system with the UIPC connected at the sending end

5.2.1. The Scaled-Down System for Experimental Verification

In the scaled-down system, the base voltage was reduced to 220V and the apparent power to 1kVA. The grid frequency remained at 60 Hz. However, the two-source three-phase system was converted into a single-source three-phase system, as shown in Figure 5-2. There, the single three-phase source represents the voltage difference between the sending and receiving ends of the transmission line, \underline{V}_{RS} . It can be defined by:

$$\underline{V}_{RS} = \underline{V}_R - \underline{V}_S = V_R \angle 0^\circ - V_S \angle \delta = V_{RS} \angle \delta_{RS} \quad (5.1)$$

Assuming that $V_R = V_S$, the magnitude, and angle of \underline{V}_{RS} can be expressed as:

$$V_{RS} = 2V_R \sin\left(\frac{\delta}{2}\right) \quad (5.2)$$

$$\delta_{RS} = \left(\frac{\delta}{2} - 90^\circ\right) \quad (5.3)$$

Since angle δ is variable, so are the magnitude of the voltage difference (V_{RS}) and angle (δ_{RS}) with respect to the receiving end voltage (Table 5-1). Note that the voltage between the point of connection of the UIPC and transmission line (\underline{V}_{ms}) to the ground of \underline{V}_{RS} is lower than, and does not correspond to, the voltage \underline{V}_m in the actual two-source system. The same statement applies to the voltages at the connection points between the series VSCs and the series reactance of the inductive (\underline{V}_{LS}) and capacitive (\underline{V}_{CS}) branches of the UIPC. Conversely, the injected voltages (\underline{V}_{injL} and \underline{V}_{injC}) and the currents (\underline{I}_L , \underline{I}_C , and \underline{I}_{TL}) are the same. These are the key quantities to demonstrate that the system does behave as desired.

It should be pointed out for the single source system that the UPFC-based UIPC still employs the two series branches (VSC1 and VSC2, their series coupling transformers, and their series reactance) those are responsible for controlling the current in the inductive and capacitive branches, thus in the transmission line. This is the main aspect particular to the proposed control strategy for the UIPC. However, the shunt branch (VSC3 and the shunt transformer), was replaced by a three-phase diode bridge rectifier and controlled bleeding resistance (PWM controlled switch and resistance), to keep the DC bus voltage constant. The reason behind emulating the shunt branch by three-phase diode bridge rectifier and controlled bleeding resistance is that the original shunt branch cannot be connected since there is no more a source at the sending end for the single source system. Figure 5-2 shows the equivalent single-source system used in the experimental set-up.

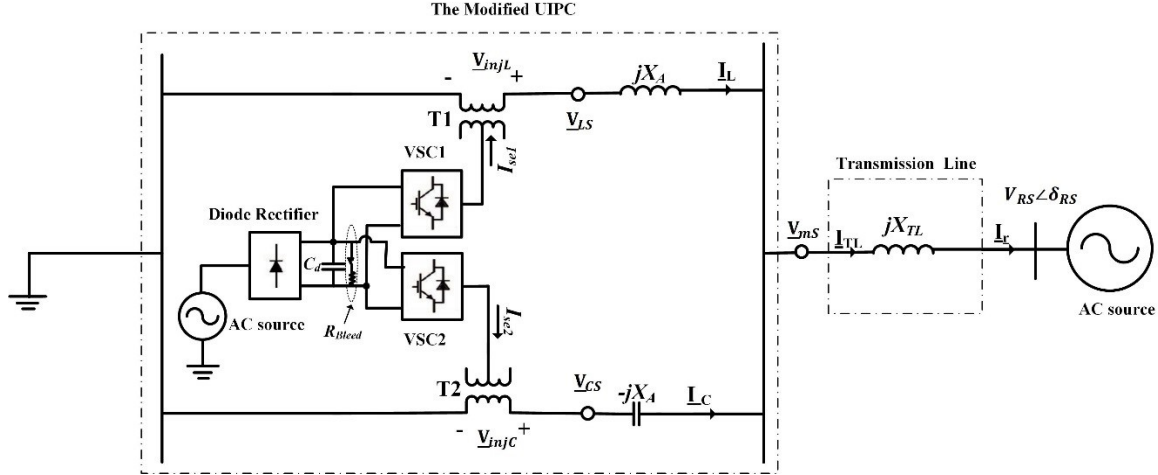


Figure 5-2: The equivalent single-source system used in the experimental set-up

Table 5-1: parameters of the single source system

S_{base}	$V_{base}(L-L)$	$V_s(1-ph)$	$V_r(1-ph)$	δ	$V_{RS}(L-L)$	$V_{RS}(1-ph)$	δ_{RS}
1000 VA	220 V	127 V	127 V	0°	0 V	0 V	-90°
				5°	19.19 V	11.08 V	-87.5°
				10°	38.34 V	22.14 V	-85°
				15°	57.43 V	33.16 V	-82.5°

5.2.2. Redefining the Reference Voltage to \underline{V}_{RS}

It was mentioned before that in the actual power system with a sending end and a receiving end, the reference current for the transmission line should be referred to the voltage at the receiving end. In the case of the single-source system used in this work for the experimental studies, the transmission line current will be created using the locally measured voltage (\underline{V}_{RS}) as the reference. Therefore, to create a transmission line current which would be phase-shifted regarding the receiving end voltage by ϕ_{TL} , based on (5.3), one should take the angle of the single-source system (\underline{V}_{RS}) and subtract by $((\delta/2)-90^\circ)$ to have the angle corresponding to the receiving end, when the sending end leads it by angle δ . This is the one to be used in dq to abc transformation.

5.2.3. The Components of the Experimental Set-up:

As is shown in Figure 5-3, the main elements of the experimental set-up are: the series transformers, the series UIPC inductors (L_A), the series UIPC capacitors (C_A), the inductor that

emulates the transmission line impedance (L_{TL}), the DC link capacitor (C_{dc}), the controlled bleeding resistance (R_{bleed}) and the three-phase voltage sources converters (VSCs).

In this work, six (120V:69V, 200VA) single-phase transformers were used to realize the two three-phase series transformers. They are arranged in the step-up mode, thus being able to carry 1 pu of current (2.624 A.) The maximum injected voltage, per design specification, is 0.25 pu (31.75V), which can be realized with a DC bus voltage regulated at 170 V and SPWM, in the linear region. In this experiment, the DC bus voltage was realized with a three-phase diode rectifier and a switching bleeding resistance, so that the DC bus can supply and absorb active power to/from the series VSCs. The size of R_{bleed} is chosen to be 158 Ω . R_{bleed} is designed to consume the active power that is supplied by both series VSCs in the worst case, which was the leading PF case when $I_{TL-des} = 1$ pu. The values of the passive elements, L_A , C_A and L_{TL} that are used in the experimental set-up are 61mH, 115 μ F, and 32mH, respectively.

The three-phase VSCs used in this work are STEVAL-IPM15B motor control power boards based on the SLLIMM™ 2nd series of IGBT IPMs [62]. Their rated DC voltage and power are 400 V and 1.5 kW. The DC bus capacitor is 3 mF, and no low-pass switching harmonic filters were used in this case. Nevertheless, the current harmonics in the transmission line, inductive and capacitive branches of the UIPC are very small as will be shown in the experimental results. Figure 5-3 shows the three-phase diagram of the experimental set-up.

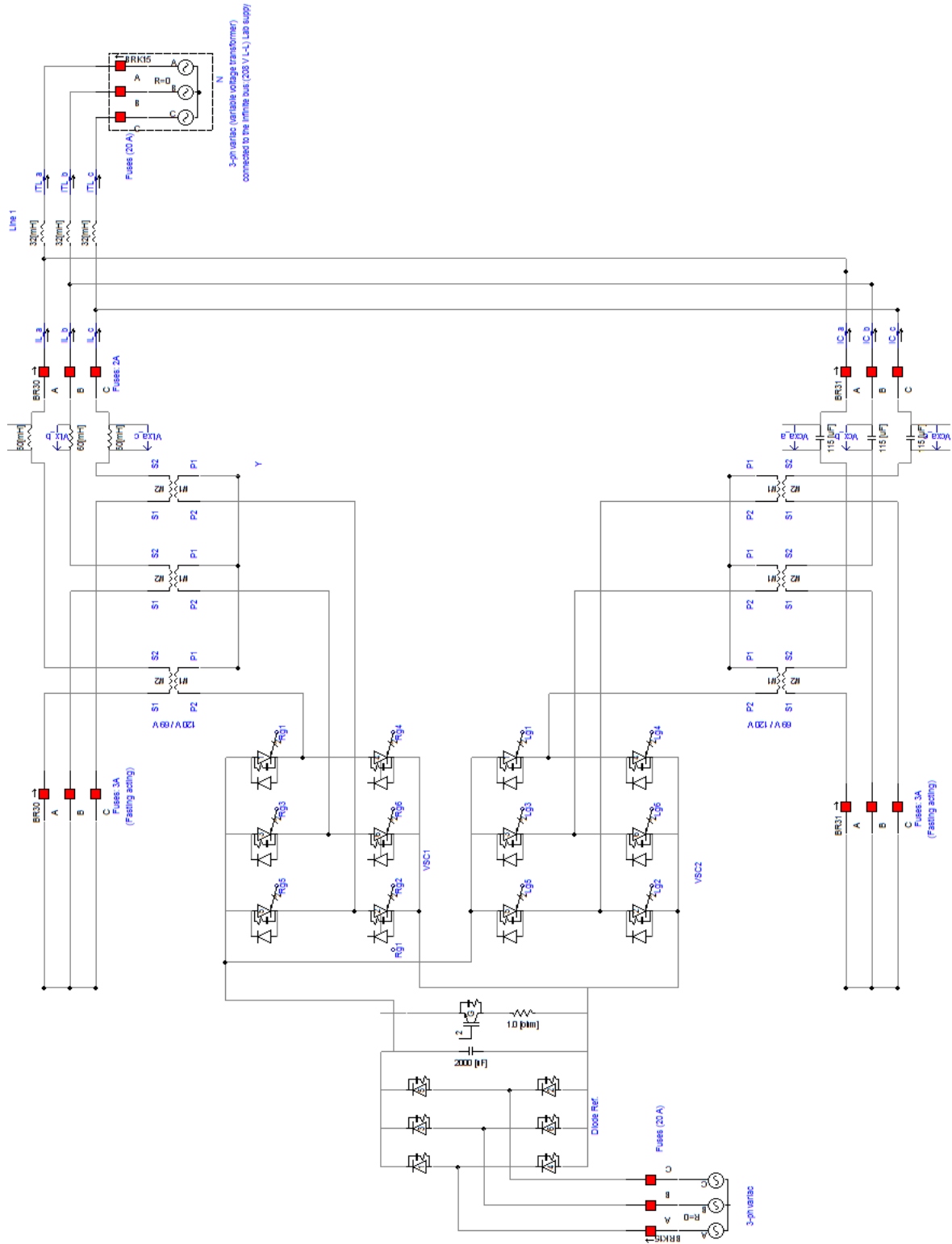


Figure 5-3: The layout of the experimental set-up

Figure 5-4 shows the picture for the experimental set-up.

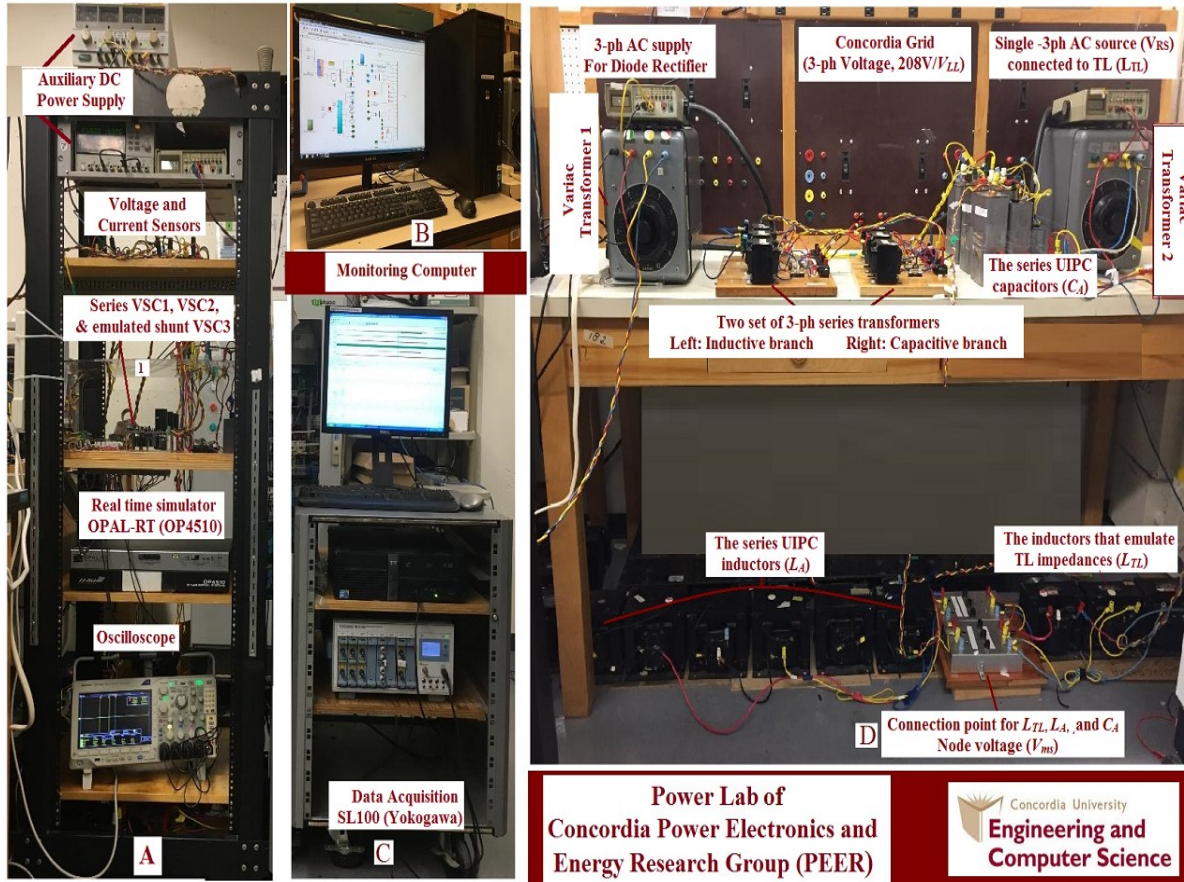


Figure 5-4: The picture of the experimental set of the porotype of the UIPC based UIPC

The picture of the series VSC 1 and VSCs and the emulated shunt VSC3, marked as # 1, in Figure 5-4 (A) is shown in Figure 5-5.

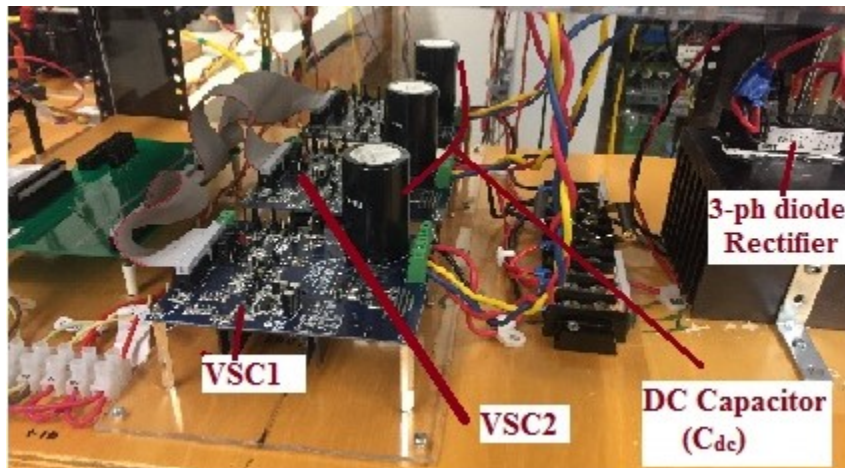


Figure 5-5: The series VSC 1 and VSCs and the emulated shunt VS

5.3. Control Strategy for the Series VSCs of the UPFC-UIPC

As discussed in the previous chapters, the series branches are to be current-controlled to synthesize the desired reference current in the transmission line. In Chapter 3, the proportional-resonant (PR) controllers were used for controlling the currents through the inductive and the capacitive branches. In order to achieve a small error in the steady state with a PR controller, one should *merely* use a high gain at the resonant (grid) frequency. Recall the non-ideal (practical) PR controller [44] is defined as:

$$C_{PR}(s) = K_p + K_i \frac{2 \omega_c s}{s^2 + 2\omega_c s + \omega_o^2} \quad (5.4)$$

Where K_p is the proportional gain, K_i is the integral gain and ω_o is the resonant frequency at the fundamental frequency. ω_c is the bandwidth around the AC frequency, ω_o [60].

In terms of design, the integral gain K_i at the grid frequency, ω_o , should be set large enough to impose a small steady-state error. The proportional gain K_p defines the dynamics of the system and can be tuned as the PI controller in an equivalent DC system [61]. The bandwidth, ω_c determines the sensitivity to frequency variations in the grid, typically been selected in the range of 5-15 rad/s [60]. The PR controllers of both branches were designed to have a similar bandwidth (f_x) and consequently, a similar speed of response. Besides, they should yield equally high gains at the resonant frequency for their loop transfer functions (LTFs), for a small steady-state error. In this work, the switching frequency (f_{sw}) is 5 kHz. The bandwidth (f_x) which defines the value of K_p , is set to 20% of f_{sw} (1 kHz). The gain of the LTF at the resonance frequency is to be 30 dB. Based on these two target design specs, the parameters of the PR controllers for the inductive and capacitive branches are selected as $K_{pL} = 330$ and $K_{iL} = 400$ for the inductive branch, and $K_{pC} = 25$ and $K_{iC} = 800$, for the capacitive one. For both, $\omega_o = 377$ rad/s and $\omega_c = 15$ rad/s.

The reference currents in the abc-frame for the PR controllers in the experimental set up will be obtained from the sharing factors, α and β , in the same manner, which has been mentioned in Chapter 3. Recall that α and β are computed off-line, considering the phase angle between the voltages in the sending and receiving ends of the transmission line (δ), as discussed before, and stored in a lookup table.

Figure 5-6 shows the implementation of the current control loop in abc-frame with PR controllers and SPWM.

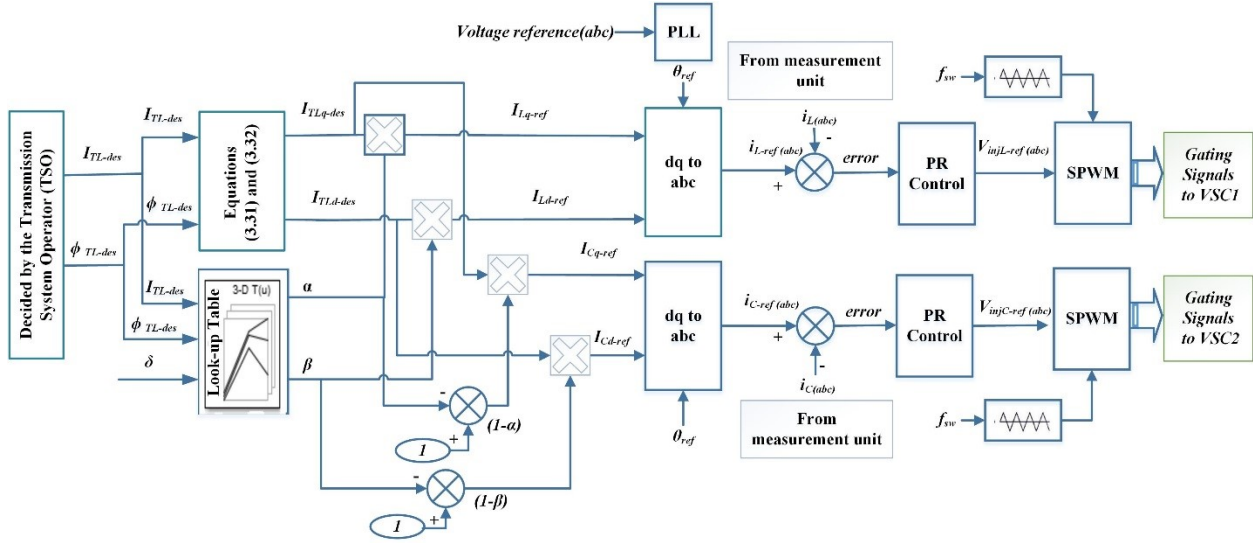


Figure 5-6: Schematic diagram of the proposed control scheme for the UPFC-UIPC with optimal current sharing factors and PR controller

The proposed control scheme of the UIPC, shown in Figure 5-6, was realized by a digital simulator from OPAL-RT (OP4510). It includes the conversion of the reference current into dq, reading of the sharing factors (α and β) from the lookup table for a given δ , generation of the reference currents for the inductive and capacitive branches in abc-frame, implementation of the PR controller and the generation of the gating signals of the VSCs with SPWM. Since Opal-RT works with MATLAB/Simulink, the MATLAB/ Simulink software will be used to get simulation results for the scaled-down system that is used in this chapter. Then, these simulation results will be compared with experimental results.

5.4. Simulation and Experimental Results

The main purpose of this Chapter is to demonstrate the effectiveness and feasibility of the proposed control strategy of the UPFC-UIPC, shown in Figure 5-2 experimentally. It is based on splitting the reference current for the transmission line among the inductive and capacitive branches and enforcing these currents with suitable control loops.

As mentioned before, the proposed scheme requires a lookup table with the values of the optimized α and β factors as a function of the transmission line angle (δ) and magnitude and phase of the desired transmission line current. Figure 5-7 shows, as an illustration, the lookup table for the following conditions: The magnitude of the transmission line current (I_{TL-des}) is assumed to be variable from 0 to 1pu, with steps of 0.1pu. The transmission line angle (δ) can vary from 0° to

15°, with steps of 5°. The phase angle of the transmission line current with respect to the voltage in the receiving end (ϕ_{TL-des}) can be 0° for unity power factor (UPF), the power factor of 0.8 leading ($\phi_{TL-des} = 36.87^\circ$) and 0.8 lagging ($\phi_{TL-des} = -36.87^\circ$). Table 5-2 depicts the values of α and β corresponding to the selected case studies presented in this study: $\delta = \delta_{max} = 15^\circ$, leading to $V_{RS} = 57.43$ V and $\delta_{RS} = -82.5^\circ$ for the single-source system. The values of α and β in Table 5-2 are for transmission line currents of 0.5 and 1 pu and current angles (ϕ_{TL-des}) for operation with PF = 1, 0.8 leading and 0.8 lagging.

Figure 5-7: Lookup table with the optimization results (α and β) considering different cases (values of δ , I_{TL-des} , and ϕ_{TL-des}).

Table 5-2: values of the sharing factors α and β for the desired current magnitudes and angles (I_{TL} and Φ_{TL})

I_{TL-des} Φ_{TL-des}	0.5pu		1pu	
	α	β	α	β
0°	0.778	-	0.501	-
36.87°	0.925	0.352	0.574	0.273
-36.87°	0.920	0.115	0.564	0.044

To validate several aspects of the proposed technique, simulation results for the scaled down two-source system for the UPF case with a transient response for a current reference

variation will be presented. Then, for the experimental set-up with the single-source system, the equivalent transient response will be shown to validate the response of the proposed PR controllers. Finally, for subsequent cases, experimental results with the single-source system, only steady-state results are presented. Recall that the schematic diagram shown in Figure 5-6 can also be used for the single-source system, but the reference angle for the dq to abc transformation should be the angle of the single-source system (\underline{V}_{RS}) subtracted by $((\delta/2)-90^\circ)$.

5.4.1. UPF Case

- **Simulation Results**

The two-source system is used for performance verification using simulation. Figure 5-8 shows some key waveforms, for phase A, concerning the operation of the UIPC with the proposed (UPFC-based) control scheme. The curves on the top show how I_{TL} is split among I_L and I_C for $I_{TL} = 0.5$ pu (left) and 1 pu (right). For UPF, they should all be, and are, in phase, since \underline{I}_{TL} , being in phase with \underline{V}_R , has no imaginary/reactive part. Based on Table 5-2, factor α , I_L should take most of I_{TL} for $I_{TL} = 0.5$ pu. Conversely, for $I_{TL} = 1$ pu, I_L and I_C should split I_{TL} virtually equally. The curves in the bottom show the waveforms of I_{TL} and V_R . The magnitudes of I_{TL} present the expected values and are almost in phase with the receiving end voltage.

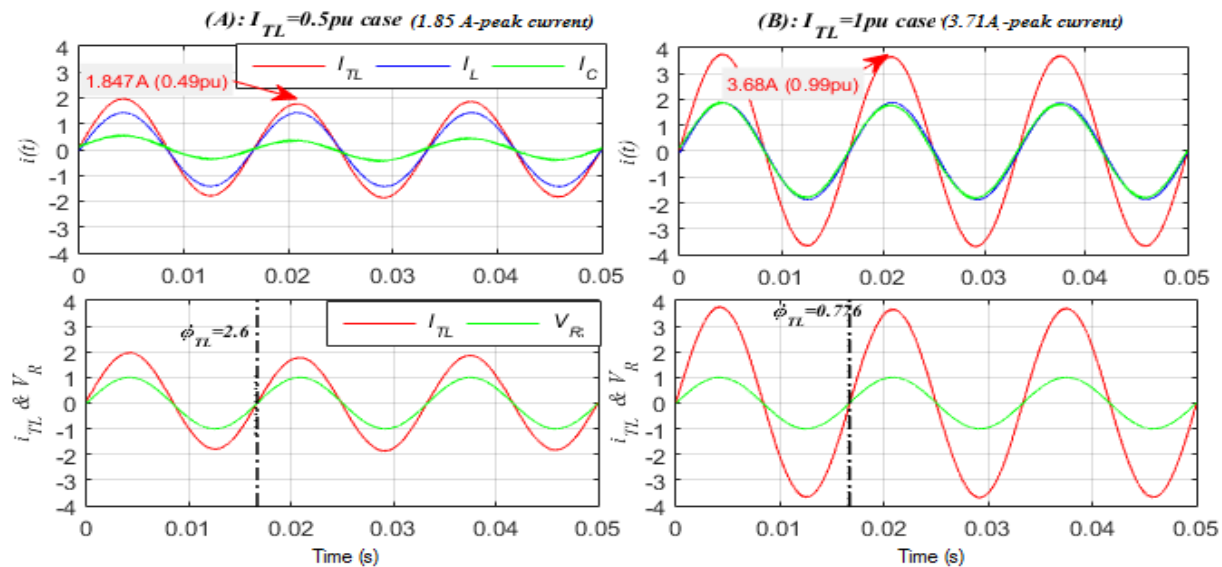


Figure 5-8: Simulation waveforms for UPF: (A) $I_{TL} = 0.5$ pu and (B) $I_{TL} = 1$ pu. Top: I_{TL} , I_L , and I_C . Bottom: I_{TL} and V_R .

Figure 5-9 shows the reference and actual waveforms for the inductor and capacitor branches of the UPFC-based UIPC when the transmission line reference current is changed from

0.5 to 1 pu. There, one can see that the PR controller leads to a fast and well-damped dynamic response with a small error in steady state.

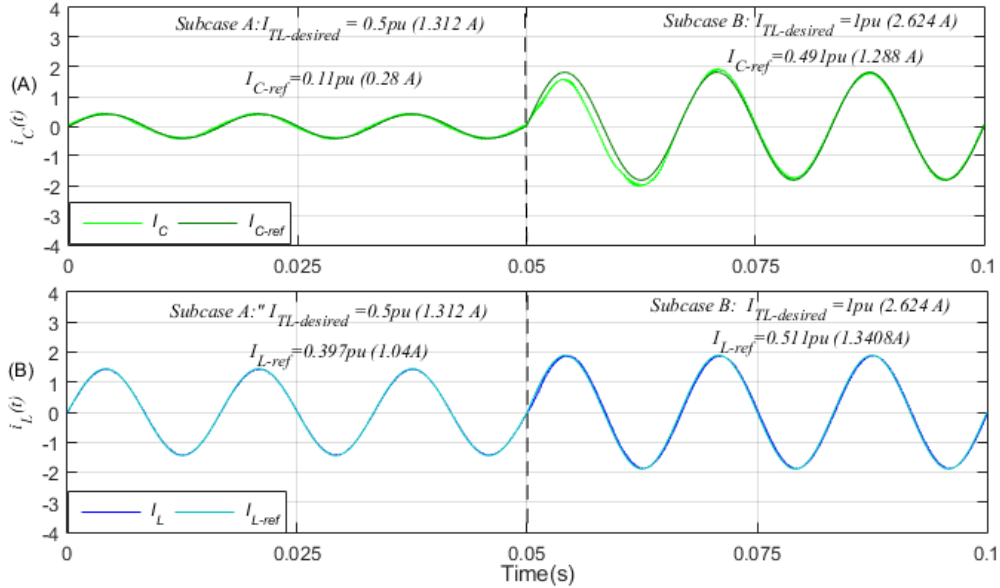


Figure 5-9: Actual and reference current waveforms of (A) The capacitive branch (B) the inductive branch for UPF case and I_{TL-des} varying from 0.5pu to 1pu.

• Experimental Results

The single-source system is then used for performance verification by experimentation. In such a case, \underline{V}_R is not available, and the transmission line current should be synchronized to \underline{V}_{RS} , and leading it by an angle $\phi'_{TL} = \phi_{TL} - \delta_{RS}$, the latter defined in (5.3) is equal to -82.5° for $\delta = 15^\circ$, that is used in the simulation and experimental studies.

Figure 5-10 shows, on the top, how I_{TL} is split among I_L and I_C for $I_{TL} = 0.5$ and 1pu. These experimental waveforms are very similar to the simulated ones shown in Figure 5-8 with the two-source system. At the bottom, one sees the waveforms of I_{TL} and V_{RS} . As expected, the former leads the latter by approximately 82.5° . By inspection, one can see that the harmonic distortion of the waveforms is negligible.

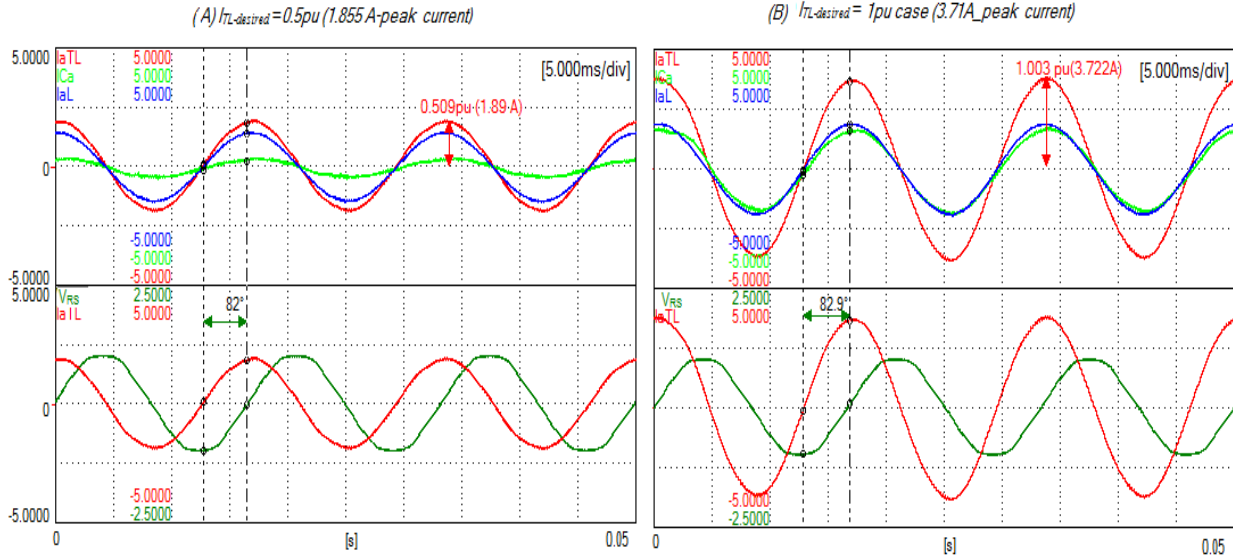


Figure 5-10: Experimental waveforms for UPF: (A) $I_{TL} = 0.5 \text{ pu}$ and (B) $I_{TL} = 1 \text{ pu}$. Top: I_{TL} (red), I_L (blue) and I_C (green). Bottom: I_{TL} (red) and V_{RS} (green).

The transient response of the experimental system to a variation of the transmission line reference current from 0.5 to 1 pu is shown in Figure 5-11. As in the simulation case for the two-source system, the currents in the inductive and capacitive branches of the UPFC-UIPC follow the reference values fast and accurately.

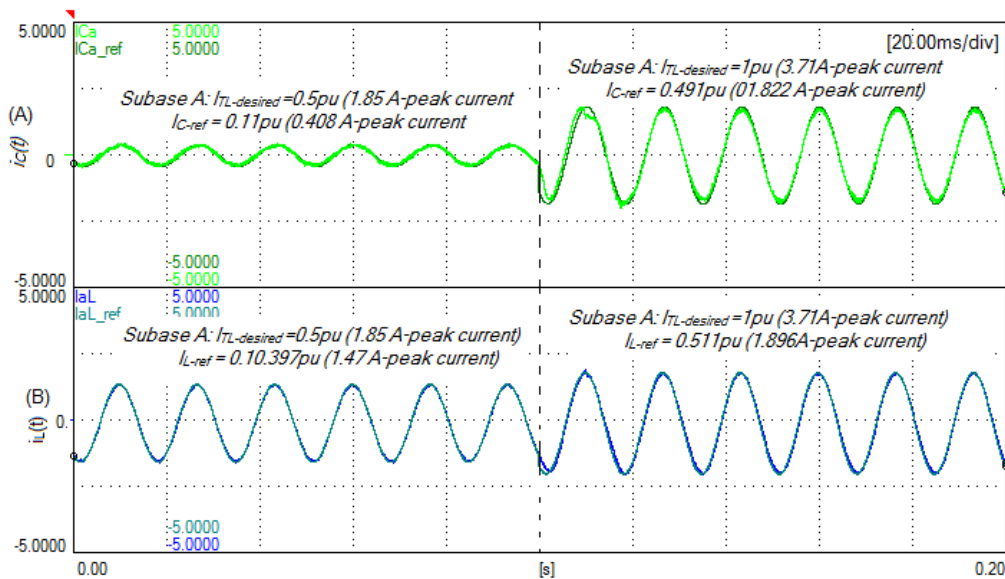


Figure 5-11: Actual and reference current waveforms of (A) the capacitive branch (B) the inductive branch for UPF case and I_{TL_des} varying from 0.5pu to 1pu.

5.4.2. Leading PF Case

A power factor of 0.8 leading was selected for this case study. In the two-source system, the transmission line current (\underline{I}_{TL}) should lead the receiving end voltage (\underline{V}_R) by $\phi_{TL} = 36.87^\circ$. However, for the experimental investigation with a single-source system and $\delta = 15^\circ$, \underline{I}_{TL} should lead the single-source voltage (\underline{V}_{RS}) by $\phi'_{TL} = 119.37^\circ = 36.87^\circ + 82.5^\circ$.

Figure 5-12 shows experimental results for this case where, on the top, one can see how I_{TL} is split among I_L and I_C for $I_{TL} = 0.5$ (left) and 1 pu (right). With \underline{I}_{TL} presenting real and imaginary components, the verification of the realization of factors α and β based on the magnitudes of I_L and I_C is not evident as for UPF. Nonetheless, for relatively high-power factors, the real component of \underline{I}_{TL} should be much larger than the imaginary one. Therefore, for high values of α , I_L should be larger than I_C . Based on Table 5-2, this is what happens for $I_{TL} = 0.5$ pu and is observed in the top left curves. Conversely, for $I_{TL} = 1$ pu $\alpha \sim 0.5$ and the magnitudes should be more similar. For small values of β , $I_C > I_L$. Regarding the phase of \underline{I}_{TL} , based on the waveforms at the bottom, one sees that the phase angle between \underline{I}_{TL} and \underline{V}_{RS} is very close to 119.37° , as expected, for $I_{TL} = 0.5$ and 1 pu.

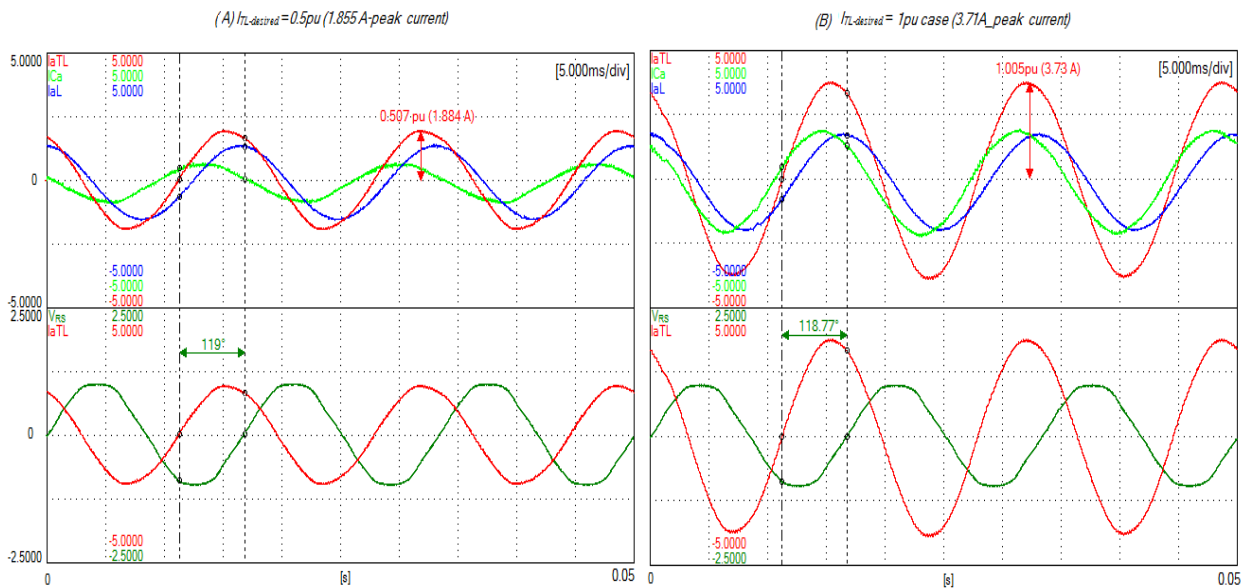


Figure 5-12: Experimental waveforms for: (A) $I_{TL} = 0.5$ pu and (B) $I_{TL} = 1$ pu. Top: I_{TL} (red), I_L (blue) and I_C (green). Bottom: I_{TL} (red) and V_{RS} (green).

5.4.3. Lagging PF Case

The value of 0.8 was also selected for investigating the operation with lagging power factors. In the two-source system, the transmission line current (I_{TL}) should lag the receiving end voltage (V_R), thus $\phi_{TL} = -36.87^\circ$. However, for the experimental investigation with a single-source system and $\delta = 15^\circ$, I_{TL} should lead the single-source voltage (V_{RS}) by $\phi'_{TL} = 45.63^\circ = -36.87^\circ + 82.5^\circ$. Like in the leading power factor case, only experimental results are presented.

Figure 5-13 shows the same key waveforms presented for the other case studies. On the top, one can see how I_{TL} is split among I_L and I_C for $I_{TL} = 0.5$ (left) and 1 pu (right). $I_L > I_C$ for $I_{TL} = 0.5$ pu because $\alpha > 0.9$. Conversely for $I_{TL} = 1$ pu since $\alpha \sim 0.5$ and β is very small, $I_C > I_L$. Finally, based on the waveforms at the bottom, one sees that the phase angle between I_{TL} and V_{RS} is very close to 45.63° , as expected, for $I_{TL} = 0.5$ and 1 pu.

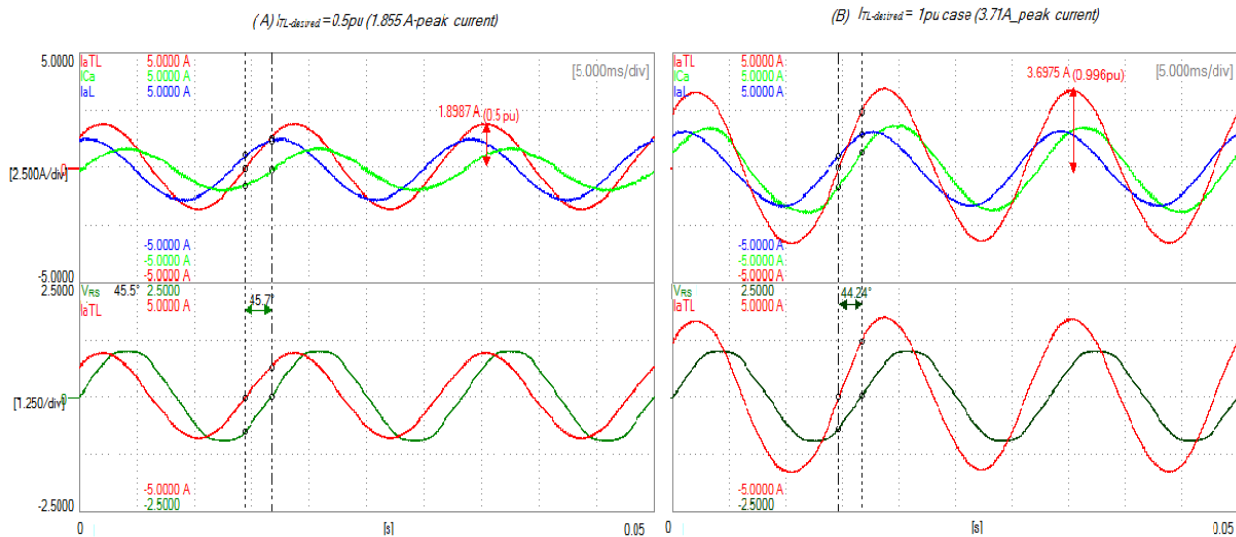


Figure 5-13: Experimental waveforms for: (A) $I_{TL} = 0.5$ pu and (B) $I_{TL} = 1$ pu. Top: I_{TL} (red), I_L (blue) and I_C (green). Bottom: I_{TL} (red) and V_{RS} (green)

5.5. Summary

The focus in this chapter was to test the effectiveness of the proposed scheme (the UPFC-based UIPC) experimentally. The electric circuit with the UIPC was modified to allow a simpler realization of the experimental set-up. In order to control the current with VSCs in the inductive, and capacitive branches, the PR controllers were used with SPWM. The experimental results showed that the desired transmission line current can be synthesized and that the PR controllers yield a fast and well damped dynamic response with a small error in steady state.

CHAPTER 6. CONCLUSION AND THE FUTURE WORK

6.1. Conclusion

In recent years, new techniques for power flow control in transmission lines have been developed and used to get the maximum benefit of the existing power transmission system and to avoid building new transmission lines. Among these techniques are the Flexible AC Transmission System (FACTS) devices. One of the FACTS devices that were reported in the literature is the Interphase Power Controller (IPC), which has a very important characteristic, namely active power regulation in a transmission line with highly variable transmission angles. However, the basic IPC lacked essential features that are required, especially in the modern transmission system, like the speed of response, continuous variation of the control variables. This is due to limitations of its main components, mechanical phase shifting transformers (PSTs). Therefore, it was proposed in the literature to replace the PSTs of the basic IPC with power electronic devices leading to a new generation of IPC, the static IPC.

Three types of static IPC have been reported in the literature: The Thyristor Controlled-based IPC (TC-based IPC), the SSSC-based IPC, and the unified IPC (UIPC). The latter has been the focus of this work because it meets all the expected performance characteristics listed above. It employs a power electronics topology known as dual modified unified power flow controller (Dual-UPFC) instead of mechanical PSTs. The UPFC topology can work in different operation modes. It can work as a shunt source/sink of reactive power, a series source/sink of reactive power, a static phase shifter (SPS) or a combination of them all (multi-functional mode or UPFC mode). In the literature, only the operation mode when the dual UPFC in the UIPC application worked as the SPS was considered, which is essentially the basic PST with continuous phase angle variations. This control strategy was called as SPS-based UIPC in this work. Although the SPS-based UIPC overcomes many limitations of the basic IPC or other electronics IPC types, it does not maximize the power control range for a given rated installed capacity of dual UPFC. Therefore, the scope of this research work has been turned to explore the advantages of making the UIPC work as a multi-functional power flow controller to adjust the power flowing through the transmission lines, to regulate the voltage at its local bus, and to mitigate the impact of potential short-circuit faults in transmission lines. The proposed multi-functional power flow control scheme was named as UPFC-based UIPC.

To study the performance and test the capability of the proposed UIPC (UPFC-based UIPC), Chapter 2 presented a comparison between it and the basic approach of the UIPC that was reported in the literature (SPS-based UIPC). It started with a review of the UIPC and its main component, the dual UPFC, and how it works in the SPS mode, to form the SPS-based UIPC, and in the multi-functional (UPFC) mode, to form the UPFC-based UIPC. The mathematical models in the steady state, control limits, and the methods for calculating the control parameters for both UIPC types were discussed. The increases complexity and flexibility of the computation of the four control parameters of the UPFC-based UIPC, as opposed to two of the SPS-based UIPC, was solved with a simple approach. The simple approach is to employ a current control scheme where the real and imaginary parts of the transmission line current were split among the inductive and capacitive branches as a function of sharing factors, α , and β . Then, the use of optimization techniques was proposed to calculate α and β and to minimize the apparent power required from the series connected VSCs, to realize a given transmission line current.

The performance of the UPFC-based UIPC was compared with the SPS-based UIPC by using a simple case study. Results obtained from MATLAB code showed the voltage, current and apparent power of both UIPCs to control the transmission line current to different desired values for different values of angle δ , and for different target values of power factors at the receiving end. It was shown that in most cases, the UPFC-UIPC had to inject lower voltages and conduct lower currents in the two branches than in the SPS-UIPC, thus resulting in much lower apparent power required to impose a desired current in the transmission line. This was shown for the system operating with UPF at the receiving end as well as for PF = 0.8, leading and lagging.

Since it was shown in Chapter 2 that the UPFC-based UIPC has greater capability than the SPS-based UIPC, Chapter 3 focused solely on the former. It presented a simulation verification to validate the proposed control scheme for the UIPC (UPFC-based UIPC). A simulation model of the UPFC-based UIPC was developed using PSCAD/EMTDC. The double loop PI decoupled control scheme in dq-frame was used to control the current flow through the shunt branch and to regulate the DC bus voltage of the dual UPFC. Then, PR controllers were used for regulating the currents flowing through the inductive and capacitive series branches, and synthesize the desired reference current in the transmission line. A logic to obtain the reference currents in abc-frame for the PR controllers from the optimization results was indicated. It was based on a dq to abc (Park) transformation, where the dq components were computed from sharing factor α and β (computed

off-line by the method mentioned in Chapter 2, and stored in the lookup table), and the desired reference current for the transmission line.

The performance of the UPFC-based UIPC with the proposed control loops was demonstrated using a simple power system. The simulation results were divided into two parts: For the series branches, and for the shunt branch. It considered three power factors at the receiving end of the transmission line: Unity power factor (UPF) with $\phi_{ITL} = 0^\circ$, PF/Leading of 0.8 ($\phi_{ITL} = 36.87^\circ$) and PF/Lagging of 0.8 ($\phi_{ITL} = -36.87^\circ$). For each main cases, two values of the desired transmission line current, I_{TL-des} , were considered. The simulation results for the series branches part showed that the PR controllers of both series branches gave good dynamic responses following step changes in their references currents. Besides, the PR controllers resulted in the expected calculated current values of both branches with a small error in the steady state.

Regarding the effectiveness of the control loop of the shunt branch, the case where the reference transmission line current with a PF of 0.8 lagging case has its magnitude changed from 0.5 pu to 0.8 pu was considered. The simulation results showed that the inner shunt branch current loop of the double loop PI decoupled controller, resulted in a fast and well-damped dynamic response, with a zero error in the steady state. Moreover, the simulation results indicated that the outer DC bus voltage loop of the double loop PI decoupled controller accomplished its tasks, maintaining the DC voltage around its reference (1pu), by generating the required q-axis current reference for the inner loop.

Chapter 4 discussed the use of the linear PI-type controller with the synchronous reference frame (dq) for controlling the inductive and capacitive branches of the UIPC. The main purpose of this technique was to achieve a zero error in steady state for step variations in the reference signals. Chapter 4 started with a review of the mathematical model in the dq frame for the inductive branch for the design of current control. It is well known in the literature and it is similar to the models of FACTS devices such as the STACOM and the SSSC. Then, a mathematical model in the dq frame for the capacitive branch for designing a control loop was proposed in this work. The model of the plant is complex, and it is difficult to achieve current control with a VSC using a linear PI-type controller and feedforward decoupling branches. Therefore, a scheme based on an indirect current control, based on the control of the capacitor voltage of the other axis, was

proposed. The impact of the variations in the capacitive voltage in the same axis, not controlled, is minimized by using a relatively slow (low bandwidth) voltage control loop.

For verifying the performance of the proposed dq control scheme for the UPFC-based UIPC, the three cases discussed in Chapter 3 were considered in Chapter 4. The performances of the dq controller for the three cases were considered in the steady state and transient conditions. In the steady state conditions, the actual current of each branch follows its reference with zero steady-state error, thus leading to the transmission line current (I_{TL}) with the desired magnitudes and phase with respect to the receiving end voltage (V_R).

For the transient responses, the dq current controller of the inductive branch and the proposed indirect current control via dq voltage controller, for the capacitive branches, presented good dynamic responses following step changes in their references values to achieve the desired transmission line current. In all cases, it was noted that both controllers required less than one cycle to reach their actual values in the steady state condition.

Chapter 5 presented the implementation and tested the effectiveness of the proposed scheme (UPFC-based UIPC) experimentally. The electric circuit with the UPFC-based UIPC was modified to allow a simpler realization of the experimental set-up. In order to control the current with VSCs in the inductive, and capacitive branches, the PR controllers were used with SPWM. The experimental results showed that the desired transmission line current can be synthesized and that the PR controllers yield a fast and well damped dynamic response with a small error in steady state.

The general conclusion of this thesis, is that a novel control scheme for the Unified Interphase Power controller (UIPC) was proposed to control the current flow through the transmission line for different control ranges. Consequently, the active and reactive powers are controlled in more flexible and efficient way. The task was achieved by using smaller rated Voltage Source Converters (VSCs) of the (UPFC-based) UIPC than the VSCs of the conventional (SPS-based) UIPC. The results of the reduction of the power ratings of the VSCs, will lead to design a proposed (UPFC-based) UIPC with small size and at low cost.

6.2. Future Work

Future work suggestions related to this study are as follow:

1. Use a prototype of the UPFC-based UIPC with the actual configuration. The modified prototype of the UPFC-based UIPC (using one source and emulating the shunt VSC3 by 3-phase diode rectifier and controlled bleeding resistance) is good enough to test its concept to achieve the desired transmission line current by controlling their series branches. If the actual configuration of the UPFC-based UIPC is considered, one can not only test the shunt branch controller but also implement and test the SPS-based UIPC experimentally.
2. Test the capability of the UPFC-based UIPC to reverse active power direction. In the considered cases, the UPFC-based-UIPC is tested only to control the active power flow from the sending end to the receiving end of the transmission line. That is the same direction of the active power flow of the uncompensated transmission line case.
3. Use a meshed power network to test the UPFC-based UIPC in more practical environments. For the considered case study for this work, only a simple power system with two buses was used. Indeed, this simple system was fair enough to determine and prove that the UPFC-based UIPC has a great capability to control the power flow. It also was good enough to investigate the performance of using the PR controllers with the stationary frame (abc) and the PI controller with the synchronous reference frame (dq). However, in reality, the power transmission systems are more complex than the considered study case. Therefore, it is suggested as future work to use the meshed network, which consists of many buses and corresponds to the existing power transmission systems.
4. Investigate the UIPC problems followed by an opening on one side (sending end side or transmission line side). Besides, consider testing the proposed (UPFC-based) UIPC during the fault condition.

REFERENCES

- [1] K.K. Sen and M.L. Sen, Introduction to FACTS controllers: theory, modeling, and applications, Hoboken, N.J.: IEEE Press, 2009, pp. 521.
- [2] U. Häger, C. Rehtanz, N. Voropai, and SpringerLink, Monitoring, control and protection of interconnected power systems, Heidelberg: Springer, 2014,
- [3] A. Zahedi, "A review of drivers, benefits, and challenges in integrating renewable energy sources into electricity grid," Renewable and Sustainable Energy Reviews, vol. 15, pp. 4775-4779, 2011.
- [4] C. Hitaj, "Renewable Power Effects on Electricity Transmission Congestion and Emissions," Dept.of Agricultural & Resource Economics, University of Maryland, College Park, MD, 2012.
- [5] R.H. Miller and J.H. Malinowski, Power system operation, New York: McGraw-Hill, 1994, pp. 271.
- [6] A. Gomez-Exposito, "Electric energy systems: analysis and operation," 2008.
- [7] A. Hernandez, M. Rodriguez, E. Torres, and P. Eguia, "A review and comparison of FACTS optimal placement for solving transmission system issues," Renewable Energy and Power Quality Journal (RE&PQJ), vol. 11, 2013.
- [8] E. m. Yap, M. Al-Dabbagh and P. C. Thum, "Applications of FACTS Controller for Improving Power Transmission Capability," in TENCON 2005 - 2005 IEEE Region 10 Conference, pp. 1-6, 2005.
- [9] G.G. Karady, "Environmental Impact of Transmission Lines," Electric Power Generation, Transmission and Distribution, 2007.
- [10] S. SAIF, M.F. ALAM and H. ALI, "SHORT CIRCUIT CURRENT CALCULATION AND PREVENTION IN HIGH VOLTAGE POWER NETS," 2014.
- [11] Y. Sang and M. Sahraei-Ardakani, "The link between power flow control technologies: Topology control and FACTS," in Power Symposium (NAPS), 2017 North American, pp. 1-6, 2017.
- [12] A. Edris, "Proposed terms and definitions for flexible AC transmission system (FACTS)," IEEE Trans.Power Del., 1997.

- [13] G. Migliavacca, Advanced technologies for future transmission grids, Springer Science & Business Media, 2012,
- [14] K. Padiyar, "FACTS controllers in power transmission and distribution," 2007.
- [15] N.G. Hingorani and L. Gyugyi, Understanding FACTS :concepts and technology of flexible AC transmission systems, New York: IEEE Press, 2000, pp. 432.
- [16] Brochu, Jacques, Marceau,Richard J., Interphase power controllers, [Montréal]: Polytechnic International Press, 1999, .
- [17] J. Lemay, J. Brochu , and F. Beaugard, "Interphase Power Controllers - complementing the family of FACTS controllers," J. can Rev., vol. vol. 34, pp. pp.9-12, 2000.
- [18] F. Beaugard, J. Brochu, G. Morin and P. Pelletier, "Interphase power controller with voltage injection," IEEE Trans.Power Del., vol. 9, pp. 1956-1962, 1994.
- [19] J. Brochu, P. Pelletier, F. Beaugard and G. Morin, "The interphase power controller: a new concept for managing power flow within AC networks," IEEE Trans.Power Del., vol. 9, pp. 833-841, 1994.
- [20] K. Habashi, J. Lombard, S. Mourad, P. Pelletier, G. Morin, F. Beaugard and J. Brochu, "The design of a 200 MW interphase power controller prototype," IEEE Trans.Power Del., vol. 9, pp. 1041-1048, 1994.
- [21] G. Sybille, Y. Haj-Maharsi, G. Morin, F. Beaugard, J. Brochu, J. Lemay and P. Pelletier, "Simulator demonstration of the interphase power controller technology," IEEE Trans.Power Del., vol. 11, pp. 1985-1992, 1996.
- [22] J. Brochu, F. Beaugard, G. Morin, J. Lamay, P. Pelletier and S. Kheir, "The IPC technology- a new approach for substation updating with passive short-circuit limitation," IEEE Trans.Power Del., vol. 13, pp. 233-240, 1998.
- [23] J. Brochu, F. Beaugard, J. Lemay, G. Morin, P. Pelletier and R. S. Thallam, "Application of the interphase power controller technology for transmission line power flow control," IEEE Transactions on Power Delivery, vol. 12, pp. 888-894, 1997.
- [24] J. Lemay, P. Berube, M. M. Brault, M. Gvozdanovic, M. I. Henderson, M. R. Graham, G. E. Smith, R. F. Hinners, L. R. Kirby, F. Beaugard and J. Brochu, "The Plattsburgh Interphase Power Controller," in Transmission and Distribution Conference, 1999 IEEE, pp. 648-653 vol.2, 1999.
- [25] A. Patel, H. Patel, R. Joshi, and M. Patel, "Phase-Shifting Transformer,."

- [26] J. Verboomen, D. Van Hertem, P. H. Schavemaker, W. L. Kling and R. Belmans, "Phase shifting transformers: principles and applications," in 2005 International Conference on Future Power Systems, pp. 6 pp.-6, 2005.
- [27] R. KORAB and R. OWCZAREK, "Application of phase shifting transformers in the tie-lines of interconnected power systems," *Przełąd Elektrotechniczny*, vol. 91, pp. 166--170, 2015.
- [28] W. Seitlinger, "Phase shifting transformers discussion of specific characteristics," in Cigré session, pp. 12-306, 1998.
- [29] W. Kling, D. Klaar, J. Schuld, A. Kanters, C. Koreman, H. Reijnders, and C. Spoorenberg, "Phase shifting transformers installed in the Netherlands in order to increase available international transmission capacity," in Cigré Session, pp. C2-207, 2004.
- [30] J. Faiz and B. Siahkolah, "Differences between conventional and electronic tap-changers and modifications of the controller," *Power Delivery, IEEE Transactions On*, vol. 21, pp. 1342-1349, 2006.
- [31] D. Dohnal, "On-load tap-changers for power transformers," *Maschinenfabrik Reinhausen GmbH Falkensteinstrasse 8 93059 Regensburg*, 2013.
- [32] J. Li, N. Yan, Y. Yue and H. You, "Designing of PI controller of the thyristor controlled interphase power controller for improving transient stability of power system," in *Electrical and Control Engineering (ICECE), 2011 International Conference on*, pp. 2154-2157, 2011.
- [33] M. Mohammadi and G. Gharehpetian, "Study of power system stability using thyristor controlled-interphase power control," in *Proceedings of the 7th WSEAS international conference on Automatic control, modeling and simulation*, pp. 208-214, 2005.
- [34] A. Samadi and S. Farhangi, "Analysis, control and modeling of cascaded multilevel converter-based IPC," in *Industrial Electronics, 2008. IECON 2008. 34th Annual Conference of IEEE*, pp. 3213-3218, 2008.
- [35] M. Farnad, S. Farhangi, S. Afsharnia and G. Gharehpetian, "Application of voltage source converter in interphase power controller for power flow control and fault limitation," in *Industrial Electronics, 2008. IECON 2008. 34th Annual Conference of IEEE*, pp. 2301-2306, 2008.
- [36] M. Farnad, S. Farhangi, S. Afsharnia and G. Gharehpetian, "Modelling and simulation of voltage source converter-based interphase power controller as fault-current limiter and power flow controller," *IET Generation, Transmission & Distribution*, vol. 5, pp. 1132-1140, 2011.
- [37] J. Pourhossein, G. Gharehpetian and S. Fathi, "Static Inter-Phase Power Controller (SIPC) modeling for load flow and short circuit studies," *Energy Conversion and Management*, vol. 64, pp. 145-151, 2012.

- [38] M. Firouzi, G.B. Gharehpetian and B. Mozafari, "Power flow control and short circuit current limitation of wind farms using unified inter-phase power controller," *IEEE Trans.Power Deliv*, vol. 32, pp. 62-71, 2017.
- [39] J. Pourhossein, G. B. Gharehpetian and S. H. Fathi, "Unified Interphase Power Controller (UIPC) Modeling and Its Comparison With IPC and UPFC," *IEEE Transactions on Power Delivery*, vol. 27, pp. 1956-1963, 2012.
- [40] M. Alizadeh, N. Khodabakhshi-Javinani, G. Gharehpetian and H. Askarian-Abyaneh, "Performance analysis of distance relay in presence of unified interphase power controller and voltage-source converters-based interphase power controller," *Generation, Transmission & Distribution, IET*, vol. 9, pp. 1642-1651, 2015.
- [41] M. Ramamoorthy and L. Toma, "Phase Shifting Transformer: Mechanical and Static Devices," *Advanced Solutions in Power Systems: HVDC, FACTS, and Artificial Intelligence*, vol. 52, pp. 409, 2016.
- [42] X. Zhang, C. Rehtanz and B. Pal, *Flexible AC transmission systems :modelling and control*, Berlin: Springer, 2006, pp. 383.
- [43] R. Pandey and A. Kori, "Real and reactive power flow control using flexible ac transmission system connected to a transmission line: A Power Injection Concept," *International Journal of Advanced Research in Computer Engineering & Technology (IJARCET)*, vol. 1, pp. pp: 252-256, 2012.
- [44] D.N. Zmood and D.G. Holmes, "Stationary frame current regulation of PWM inverters with zero steady-state error," *IEEE Transactions on Power Electronics*, vol. 18, pp. 814-822, 2003.
- [45] L. Liu, Y. Zhang, P. Zhu, Y. Kang and J. Chen, "Control scheme and implement of a unified power flow controller," in *Electrical Machines and Systems, 2005. ICEMS 2005. Proceedings of the Eighth International Conference on*, pp. 1170-1175, 2005.
- [46] S. Round, Q. Yu, L. Norum and T. Undeland, "Performance of a unified power flow controller using a dq control system," 1996.
- [47] Q. Li, "Analysis, Design, and Laboratory Evaluation of a Distributed Unified Power Flow Controller Concept," 2006.
- [48] L. Gyugyi, "Unified power-flow control concept for flexible AC transmission systems," in *Generation, Transmission and Distribution, IEE Proceedings C*, pp. 323-331, 1992.
- [49] K.K. Sen, "Analysis of FACTS Controllers and their Transient Modelling Techniques," in *Transient Analysis of Power Systems*, John Wiley & Sons, Ltd, 2015, pp. 195-247.
- [50] D.G. Luenberger, *Linear and nonlinear programming*, New York: Springer, 2008, pp. 546.

- [51] C. Lopez, MATLAB optimization techniques, Apress, 2014.
- [52] O. Anaya-Lara and E. Acha, "Modeling and analysis of custom power systems by PSCAD/EMTDC," IEEE Trans.Power Del., vol. 17, pp. 266-272, 2002.
- [53] E.U. Guide, "Manitoba HVDC Research Centre Inc," Winnipeg, MB, Canada, 2003.
- [54] Y. Gao, Y. Zhang and Y. Kang, "Control design and analysis of UPFC shunt converter," in Industrial Technology, 2005. ICIT 2005. IEEE International Conference on, pp. 536-540, 2005.
- [55] G.C. Sousa, F.N. Martins, J.P. Rey and J.A. Bruinsma, "An autonomous induction generator system with voltage regulation," in Power Electronics and Drive Systems, 2001. Proceedings., 2001 4th IEEE International Conference on, pp. 94-98, 2001.
- [56] C. Ong, Dynamic simulation of electric machinery: using MATLAB/SIMULINK, Prentice hall PTR Upper Saddle River, NJ, 1998, .
- [57] C. Schauder, L. Gyugyi, M. Lund, D. Hamai, T. Rietman, D. Torgerson and A. Edris, "Operation of the unified power flow controller (UPFC) under practical constraints," IEEE Trans.Power Del., vol. 13, pp. 630-639, 1998.
- [58] M. Kazmierkowski and M. Dzieniakowski, "Review of current regulation methods for VS-PWM inverters," in Industrial Electronics, 1993. Conference Proceedings, ISIE'93-Budapest., IEEE International Symposium on, pp. 448-456, 1993.
- [59] N. Geddada, S.B. Karanki and M.K. Mishra, "Synchronous reference frame based current controller with SPWM switching strategy for DSTATCOM applications," in Power Electronics, Drives and Energy Systems (PEDES), 2012 IEEE International Conference on, pp. 1-6, 2012.
- [60] D. Zammit, C.S. Staines, M. Apap and J. Licari, "Design of PR current control with selective harmonic compensators using Matlab," Journal of Electrical Systems and Information Technology, vol. 4, pp. 347-358, 2017.
- [61] R. Teodorescu, F. Blaabjerg, M. Liserre and P.C. Loh, "Proportional-resonant controllers and filters for grid-connected voltage-source converters," IEE Proceedings-Electric Power Applications, vol. 153, pp. 750-762, 2006.
- [62] Data Sheet, "STEVAL-IPM15B motor control power board based on the SLLIMM™ 2nd series of IGBT IPMs," 2016.

APPENDICES

Appendix A. Derivation of Mathematical Model of the Capacitive Branch in dq frame

A1. Derivation of the Mathematical Model of the Capacitive branch in dq frame

Figure A.1 shows the single line diagram of the capacitive branch circuit, which was obtained from the UPFC-based UIPC circuit (Figure 3-4 in Chapter 3).

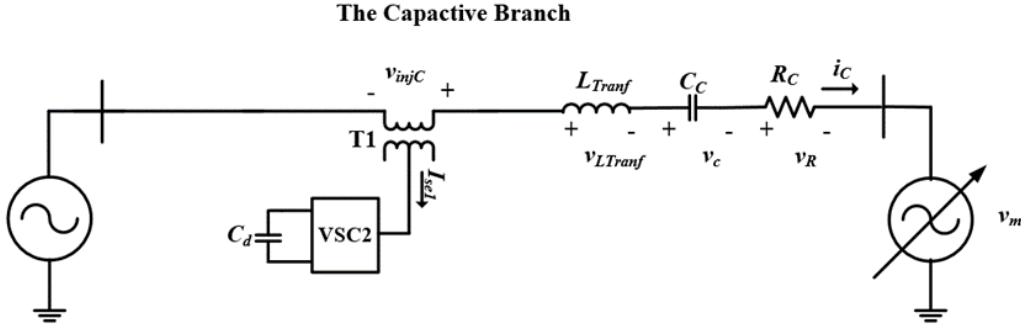


Figure A.1: The single line diagram of the capacitive branch

$$\Delta[v_{branch}]_{abc} = [v_s]_{abc} + [v_{injC}]_{abc} - [v_m]_{abc} = [v_{LTranf}]_{abc} + R_C[i_c]_{abc} + [v_C]_{abc} \quad (A.1)$$

The injected voltage by the series VSC2 is $v_{injC-abc}$, and the grid voltages are v_{sabc} and v_{mabc} . C_C and R_C , are the series capacitor and resistance of the capacitive branch, respectively, while L_{Tranf} , is the leakage inductor of the series coupling transformer. Recall the dq quantities that were shown in Chapter 4.

$$v_{Cd} = \frac{2}{3} [v_{Ca} \cos \theta_d + v_{Cb} \cos(\theta_d - 120^\circ) + v_{Cc} \cos(\theta_d + 120^\circ)] \quad (A.2)$$

$$v_{Cq} = \frac{2}{3} [v_{Ca} \sin \theta_d + v_{Cb} \sin(\theta_d - 120^\circ) + v_{Cc} \sin(\theta_d + 120^\circ)] \quad (A.3)$$

$$\Delta v_{bran-cd} = \frac{2}{3} [\Delta v_{branCa} \cos \theta_d + \Delta v_{branCb} \cos(\theta_d - 120^\circ) + \Delta v_{branCc} \cos(\theta_d + 120^\circ)] \quad (A.4)$$

$$\Delta v_{bran-cq} = \frac{2}{3} [\Delta v_{branCa} \sin \theta_d + \Delta v_{branCb} \sin(\theta_d - 120^\circ) + \Delta v_{branCc} \sin(\theta_d + 120^\circ)] \quad (A.5)$$

$$i_{Cd} = \frac{2}{3} \left[C_C \frac{dv_{Ca}}{dt} \cos \theta_d + C_C \frac{dv_{Cb}}{dt} \cos(\theta_d - 120^\circ) + C_C \frac{dv_{Cc}}{dt} \cos(\theta_d + 120^\circ) \right] \quad (A.6)$$

$$i_{Cq} = \frac{2}{3} \left[C_C \frac{dv_{Ca}}{dt} \sin \theta_d + C_C \frac{dv_{Cb}}{dt} \sin(\theta_d - 120^\circ) + C_C \frac{dv_{Cc}}{dt} \sin(\theta_d + 120^\circ) \right] \quad (A.7)$$

$$\frac{dv_{cd}}{dt} + \omega v_{cq} = \frac{2}{3} \left[\frac{dv_{ca}}{dt} \cos \theta_d + \frac{dv_{cb}}{dt} \cos(\theta_d - 120^\circ) + \frac{dv_{cc}}{dt} \cos(\theta_d + 120^\circ) \right] \quad (\text{A.8})$$

$$i_{cd} = C_c \frac{dv_{cd}}{dt} + \omega C_c v_{cq} \quad (\text{A.9})$$

$$\frac{dv_{cq}}{dt} - \omega v_{cd} = \frac{2}{3} \left[\frac{dv_{ca}}{dt} \sin \theta_d + \frac{dv_{cb}}{dt} \sin(\theta_d - 120^\circ) + \frac{dv_{cc}}{dt} \sin(\theta_d + 120^\circ) \right] \quad (\text{A.10})$$

$$i_{cq} = C_c \frac{dv_{cq}}{dt} - \omega C_c v_{cd} \quad (\text{A.11})$$

Recall that (A.9) and (A.11) are key equations that will be considered for the design of the current controller in the capacitive branch. Here, i_{cd} and i_{cq} can be controlled through v_{cq} and v_{cd} , respectively. The derivative terms in (A.9) and (A.11), (dv_{cd}/dt) and (dv_{cq}/dt) can be neglected (null in the steady-state). Thus, one can say that the capacitive branch currents (i_{cd} and i_{cq}) can be indirectly controlled by controlling the voltages across its series capacitor (v_{cq} and v_{cd}).

Accordingly, the dynamic mathematical models in the dq frame should lead to getting transfer functions (expressions) to regulate v_{cd} and v_{cq} via the injected voltages of VSC2 (v_{injcd} and v_{injq}). To get the final expressions that represent the series capacitive branch in dq model for voltage control (indirect current control), the expression in abc stationary frame of (A.1) should be redefined to make v_{injC} is only a function of one state variable, v_c , instead of two state variables (i_c and v_c) in the previous case.

Recall:

$$[i_c]_{abc} = C_c \frac{d[v_c]_{abc}}{dt} \quad \text{and}$$

$$[v_{LTranf}]_{abc} = L_{Tranf} \frac{d[i_c]_{abc}}{dt} \Rightarrow [v_{LTranf}]_{abc} = C_c L_{Tranf} \frac{d^2[v_c]_{abc}}{dt^2}$$

By substituting the above terms in (A.1), one can get:

$$\Delta[v_{branc}]_{abc} = [v_s]_{abc} + [v_{injC}]_{abc} - [v_m]_{abc} = C_c L_{Tranf} \frac{d^2[v_c]_{abc}}{dt^2} + R_c C_c \frac{d[v_c]_{abc}}{dt} + [v_c]_{abc} \quad (\text{A.12})$$

From (A.12), one can note that the second derivative of the dq voltage components should be obtained to finalize the derivation of the dq mathematical model of the capacitive branch. The first derivative of dq voltages already derived.

- **The second derivative of d component**

Applying the derivative operator to (A.8) and considering that $\omega = \frac{d\theta_d}{dt}$ one can get the expression of the second derivative of v_{cd} as:

$$\begin{aligned} \frac{d^2 v_{cd}}{dt^2} = & \frac{2}{3} \left[\frac{d^2 v_{ca}}{dt^2} \cos \theta_d + \frac{d^2 v_{cb}}{dt^2} \cos(\theta_d - 120^\circ) + \frac{d^2 v_{cc}}{dt^2} \cos(\theta_d + 120^\circ) \right] \\ & - \omega \frac{2}{3} \left[\frac{dv_{ca}}{dt} \sin \theta_d + \frac{dv_{cb}}{dt} \sin(\theta_d - 120^\circ) + \frac{dv_{cc}}{dt} \sin(\theta_d + 120^\circ) \right] - \omega \frac{dv_{cd}}{dt} \end{aligned} \quad (\text{A.13})$$

By substituting (A.10) into (A.13):

$$\frac{d^2 v_{cd}}{dt^2} = \frac{2}{3} \left[\frac{d^2 v_{ca}}{dt^2} \cos \theta_d + \frac{d^2 v_{cb}}{dt^2} \cos(\theta_d - 120^\circ) + \frac{d^2 v_{cc}}{dt^2} \cos(\theta_d + 120^\circ) \right] + \omega^2 v_{cd} - 2\omega \frac{dv_{cd}}{dt} \quad (\text{A.14})$$

- **The second derivative of q component**

Applying the derivative operator to (A.10) and considering that $\omega = \frac{d\theta_d}{dt}$ one can get the expression of the second derivative of v_{cq} component as:

$$\begin{aligned} \frac{d^2 v_{cq}}{dt^2} = & \frac{2}{3} \left[\frac{d^2 v_{ca}}{dt^2} \sin \theta_d + \frac{d^2 v_{cb}}{dt^2} \sin(\theta_d - 120^\circ) + \frac{d^2 v_{cc}}{dt^2} \sin(\theta_d + 120^\circ) \right] \\ & + \omega \frac{2}{3} \left[\frac{dv_{ca}}{dt} \cos \theta_d + \frac{dv_{cb}}{dt} \cos(\theta_d - 120^\circ) + \frac{dv_{cc}}{dt} \cos(\theta_d + 120^\circ) \right] + \omega \frac{dv_{cd}}{dt} \end{aligned} \quad (\text{A.15})$$

By substituting (A.8) into (A.15):

$$\frac{d^2 v_{cq}}{dt^2} = \frac{2}{3} \left[\frac{d^2 v_{ca}}{dt^2} \sin \theta_d + \frac{d^2 v_{cb}}{dt^2} \sin(\theta_d - 120^\circ) + \frac{d^2 v_{cc}}{dt^2} \sin(\theta_d + 120^\circ) \right] + \omega^2 v_{cq} + 2\omega \frac{dv_{cd}}{dt} \quad (\text{A.16})$$

The next stage of the dq models' derivation is to eliminate the AC components in their equations, (A.14) and (A.16).

From the expression in (A.12), the second derivative in the abc stationary frame can be stated as:

$$\frac{d^2 [v_c]_{abc}}{dt^2} = \frac{\Delta [v_{branc}]_{abc}}{C_C L_{Tranf}} - \frac{R_C C_C}{C_C L_{Tranf}} \frac{d[v_c]_{abc}}{dt} - \frac{[v_c]_{abc}}{C_C L_{Tranf}} = +R_C C_C \frac{d[v_c]_{abc}}{dt} \quad (\text{A.17})$$

For d component:

By substituting (A.17) into (A.14), one can get:

$$\begin{aligned} \frac{d^2 v_{Cd}}{dt^2} = & \frac{2}{3} \left[\frac{\Delta v_{branCa}}{C_C L_{Tranf}} \cos \theta_d + \frac{\Delta v_{branCb}}{C_C L_{Tranf}} \cos(\theta_d - 120^\circ) + \frac{\Delta v_{branCc}}{C_C L_{Tranf}} \cos(\theta_d + 120^\circ) \right] \frac{R_C C_C}{C_C L_{Tranf}} \frac{2}{3} \left[\frac{dv_{Ca}}{dt} \cos \theta_d \right. \\ & \left. + \frac{dv_{Cb}}{dt} \cos(\theta_d - 120^\circ) + \frac{dv_{Cc}}{dt} \cos(\theta_d + 120^\circ) \right] \\ & - \frac{1}{C_C L_{Tranf}} \frac{2}{3} [v_{Ca} \cos \theta_d + v_{Cb} \cos(\theta_d - 120^\circ) + v_{Cc} \cos(\theta_d + 120^\circ)] + \omega^2 v_{Cd} - 2\omega \frac{dv_{Cq}}{dt} \end{aligned} \quad (A.18)$$

By substituting (A.2), (A.4) and (A.8) into (A.18), and multiplying both sides by $C_C L_{Tranf}$, one can get the following:

$$C_C L_{Tranf} \frac{d^2 v_{Cd}}{dt^2} = \Delta v_{bran-cd} - R_C C_C \frac{dv_{Cd}}{dt} - R_C \omega C_C v_{Cq} - v_{Cd} + \omega^2 L_{Tranf} C_C v_{Cd} - 2\omega L_{Tranf} (C_C \frac{dv_{Cq}}{dt}) \quad (A.19)$$

$C_C \frac{dv_{Cq}}{dt}$ in (A.19), can be substituted by its equivalent expression in (A.11), Thus:

$$\begin{aligned} C_C L_{Tranf} \frac{d^2 v_{Cd}}{dt^2} = & \Delta v_{bran-cd} - R_C C_C \frac{dv_{Cd}}{dt} - R_C \omega C_C v_{Cq} - v_{Cd} + \omega^2 L_{Tranf} C_C v_{Cd} - 2\omega^2 L_{Tranf} C_C v_{Cd} \\ & - 2\omega L_{Tranf} i_{Cq} \end{aligned} \quad (A.20)$$

Considering the two coefficients of v_{Cd} of (A.20), it can be simplified as:

$$C_C L_{Tranf} \frac{d^2 v_{Cd}}{dt^2} = \Delta v_{bran-cd} - R_C C_C \frac{dv_{Cd}}{dt} - (1 + \omega^2 L_{Tranf} C_C) v_{Cd} - R_C \omega C_C v_{Cq} - 2\omega L_{Tranf} i_{Cq} \quad (A.21)$$

It should be mentioned that the second coefficient of v_{Cd} exists as a result of applying the second derivative to v_{Cd} . Its value is usually much smaller than 1. Thus, it can be neglected.

For q component:

By substituting (A.17) into (A.18), one can get:

$$\begin{aligned} \frac{d^2 v_{Cq}}{dt^2} = & \frac{2}{3} \left[\frac{\Delta v_{branCa}}{C_C L_{Tranf}} \sin \theta_d + \frac{\Delta v_{branCb}}{C_C L_{Tranf}} \sin(\theta_d - 120^\circ) + \frac{\Delta v_{branCc}}{C_C L_{Tranf}} \sin(\theta_d \right. \\ & \left. + 120^\circ) \right] \frac{R_C C_C}{C_C L_{Tranf}} \frac{2}{3} \left[\frac{dv_{Ca}}{dt} \sin \theta_d + \frac{dv_{Cb}}{dt} \sin(\theta_d - 120^\circ) + \frac{dv_{Cc}}{dt} \sin(\theta_d + 120^\circ) \right] \\ & - \frac{1}{C_C L_{Tranf}} \frac{2}{3} [v_{Ca} \sin \theta_d + v_{Cb} \sin(\theta_d - 120^\circ) + v_{Cc} \sin(\theta_d + 120^\circ)] + \omega^2 v_{Cq} \\ & + 2\omega \frac{dv_{Cd}}{dt} \end{aligned} \quad (A.22)$$

By substituting (A.3), (A.5), and (A.10) into (A.22), and multiplying both sides by $C_C L_{Tranf}$, one can get the following:

$$C_C L_{Tranf} \frac{d^2 v_{Cq}}{dt^2} = \Delta v_{bran-cq} - R_C C_C \frac{dv_{Cq}}{dt} + R_C \omega C_C v_{cd} - v_{cq} + \omega^2 L_{Tranf} C_C v_{cq} + 2\omega L_{Tranf} (C_C \frac{dv_{Cd}}{dt}) \quad (A.23)$$

$C_C \frac{dv_{Cd}}{dt}$ of (A.23) can be substituted by its equivalent expression in (A.9). Thus:

$$C_C L_{Tranf} \frac{d^2 v_{Cq}}{dt^2} = \Delta v_{bran-cq} - R_C C_C \frac{dv_{Cq}}{dt} + R_C \omega C_C v_{cd} - v_{cq} + \omega^2 L_{Tranf} C_C v_{cq} - 2\omega^2 L_{Tranf} C_C v_{cq} + 2\omega L_{Tranf} i_{cd} \quad (A.24)$$

Considering the two coefficients of v_{cq} of (A.24), it can be simplified as:

$$C_C L_{Tranf} \frac{d^2 v_{Cq}}{dt^2} = \Delta v_{bran-cq} - R_C C_C \frac{dv_{Cq}}{dt} - (1 + \omega^2 L_{Tranf} C_C v_{cq}) v_{cq} + R_C \omega C_C v_{cd} + 2\omega L_{Tranf} i_{cd} \quad (A.25)$$

It should be mentioned that the second coefficient of v_{cq} exists because of applying the second derivative to v_{cq} . Its value usually much smaller than 1. Thus, it can be neglected.

The only remaining step for the derivation of a mathematical model of the capacitive branch in dq frame, to substitute $\Delta v_{bran-cd}$ and $\Delta v_{bran-cd}$ of (A.21) and (A.25), respectively by their equivalent expressions. The equivalent expressions of $\Delta v_{bran-cd}$ and $\Delta v_{bran-cd}$ in dq frame can be found by considering the first term of (A.17), which concerns the grid plus injected voltages as:

$$\Delta v_{cd} = v_{sd} + v_{injcd} - v_{md} \quad (A.26)$$

$$\Delta v_{cq} = v_{sq} + v_{injqc} - v_{mq} \quad (A.27)$$

By substituting (A.26) into (A.21) and substituting (A.27) into (A.25), one can get the two expressions for the d and q models of the capacitive branch:

$$v_{injcd} = \underbrace{C_C L_{Tranf} \frac{d^2 v_{Cd}}{dt^2} + R_C C_C \frac{dv_{Cd}}{dt} + (1 + \omega^2 L_{Tranf} C_C) v_{Cd}}_{v_{injcd1}} + R_C \omega C_C v_{cq} + 2\omega L_{Tranf} i_{cq} + v_{md} - v_{sd} \quad (A.28)$$

$$v_{injqc} = \underbrace{C_C L_{Tranf} \frac{d^2 v_{Cq}}{dt^2} + R_C C_C \frac{dv_{Cq}}{dt} + (1 + \omega^2 L_{Tranf} C_C) v_{Cq}}_{v_{injqc1}} - R_C \omega C_C v_{cd} - 2\omega L_{Tranf} i_{cd} + v_{mq} - v_{sq} \quad (A.29)$$

These two expressions for the d and q models of the capacitive branch, (A.28) and (A.29) are showed in Chapter 4 and were used to get the transfer functions for designing a suitable controller with linear PI type to control the current indirectly and to get zero error in the steady state condition.

A2. Mathematical Verification of the dq equivalent circuits

Based on the two expressions for the d and q models of the capacitive branch, (A.28) and (A.29), the equivalent dq circuits for controller design were obtained (Figure 4-5 in Chapter 4). They are shown Figure A.2.

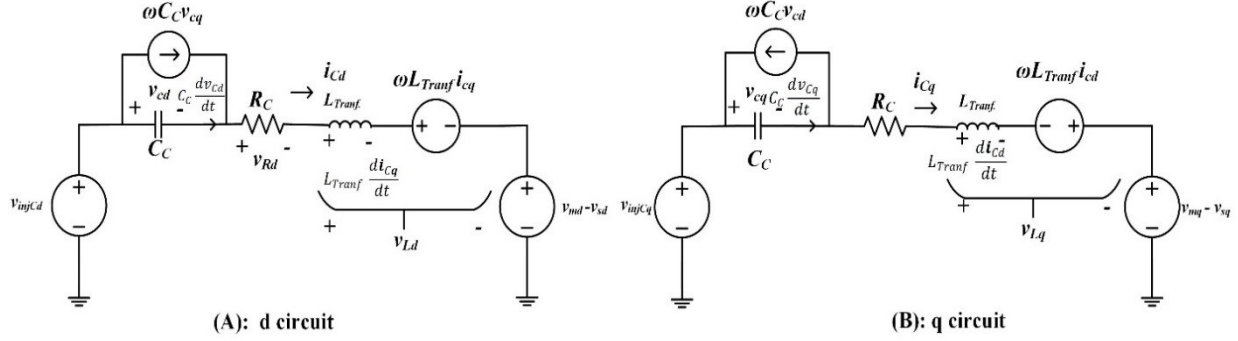


Figure A.2: The equivalent circuits (A) d-axis (B) q-axis.

These two circuits should be verified (the main purpose of this subsection, A2).

The following two equations can express the circuits of Figure A.2:

$$v_{injCd} = v_{Rd} + v_{cd} + v_{Ld} + v_{md} - v_{sd} \quad (\text{A.30})$$

$$v_{injCq} = v_{Rq} + v_{cq} + v_{Lq} + v_{mq} - v_{sq} \quad (\text{A.31})$$

Recall the final expressions in the dq frame for the capacitive branch those are used to obtain the transfer functions to design the indirect current control:

$$v_{injCd} = \underbrace{C_C L_{Tranf} \frac{d^2 v_{Cd}}{dt^2} + R_C C_C \frac{dv_{Cd}}{dt} + (1 + \omega^2 L_{Tranf} C_C) v_{Cd}}_{v_{injCd1}} + R_C \omega C_C v_{Cq} + 2\omega L_{Tranf} i_{Cq} + v_{md} - v_{sd} \quad (\text{A.32})$$

$$v_{injCq} = \underbrace{C_C L_{Tranf} \frac{d^2 v_{Cq}}{dt^2} + R_C C_C \frac{dv_{Cq}}{dt} + (1 + \omega^2 L_{Tranf} C_C) v_{Cq}}_{v_{injCq1}} - R_C \omega C_C v_{Cd} - 2\omega L_{Tranf} i_{Cd} + v_{mq} - v_{sq} \quad (\text{A.33})$$

To prove the derived mathematical models of the capacitive branch in the dq frames, the expression in (A.30) must match the expression in (A.32), and the expression in (A.31) must match the expression in (A.33). The terms in the left-hand side of (A.30) and (A.31) match the same term of (A.32) and (A.33), respectively. The last two terms in the right-hand side of (A.30) and (A.31) matches the last term of (A.32) and (A.33), respectively. However, the other terms in the left-hand side of the equations mentioned above are not matched explicitly. If the derivation of mathematical models in the dq frame is right, the remaining terms of the above equations must be matched implicitly. This main aspect to include this Appendix subsection, A2.

For RLC circuit, the current flowing through L_{Tranf} is equal to the current flowing through C_C . Therefore,

$$v_{L_{Tranf}d} = L_{Tranf} \frac{di_{cd}}{dt} + \omega L_{Tranf} i_{cq} \quad (\text{A.34})$$

$$v_{L_{Tranf}q} = L_{Tranf} \frac{di_{cq}}{dt} - \omega L_{Tranf} i_{cd} \quad (\text{A.35})$$

From the expression of i_{cd} and i_{cq} in (A.9) and (A.11), one can find their derivative:

$$\frac{di_{cd}}{dt} = C_C \frac{d^2 v_{cd}}{dt^2} + \omega C_C \frac{dv_{cq}}{dt} \quad (\text{A.36})$$

$$\frac{di_{cq}}{dt} = C_C \frac{d^2 v_{cq}}{dt^2} - \omega C_C \frac{dv_{cd}}{dt} \quad (\text{A.37})$$

By multiplying both sides of (A.36) and (A.37) by L_{Tranf} , one can get:

$$L_{Tranf} \frac{di_{cd}}{dt} = L_{Tranf} C_C \frac{d^2 v_{cd}}{dt^2} + \omega L_{Tranf} C_C \frac{dv_{cq}}{dt} \quad (\text{A.38})$$

$$L_{Tranf} \frac{di_{cq}}{dt} = L_{Tranf} C_C \frac{d^2 v_{cq}}{dt^2} - \omega L_{Tranf} C_C \frac{dv_{cd}}{dt} \quad (\text{A.39})$$

Equations (A.9) and (A.11) can be rewritten as:

$$C_C \frac{dv_{cd}}{dt} = i_{cd} - \omega C_C v_{cq} \quad (\text{A.40})$$

$$C_C \frac{dv_{cq}}{dt} = i_{cq} + \omega C_C v_{cd} \quad (\text{A.41})$$

By substituting (A.41) into (A.38) and (A.40) into (A.39), one can find:

$$L_{Tranf} \frac{di_{cd}}{dt} = L_{Tranf} C_C \frac{d^2 v_{cd}}{dt^2} + \omega L_{Tranf} i_{cq} + \omega^2 L_{Tranf} C_C v_{cd} \quad (\text{A.42})$$

$$L_{Tranf} \frac{di_{cq}}{dt} = L_{Tranf} C_C \frac{d^2 v_{cq}}{dt^2} - \omega L_{Tranf} i_{cd} + \omega^2 L_{Tranf} C_C v_{cq} \quad (\text{A.43})$$

Then, by substituting (A.42) into (A.34) and (A.43) into (A.35), one can find:

$$v_{L_{Tranf}d} = L_{Tranf} C_C \frac{d^2 v_{cd}}{dt^2} + \omega L_{Tranf} i_{cq} + \omega^2 L_{Tranf} C_C v_{cd} + \omega L_{Tranf} i_{cd} \quad (\text{A.44})$$

$$v_{L_{Tranf}q} = L_{Tranf} C_C \frac{d^2 v_{cq}}{dt^2} - \omega L_{Tranf} i_{cd} + \omega^2 L_{Tranf} C_C v_{cq} - \omega L_{Tranf} i_{cq} \quad (\text{A.45})$$

By taking R_C as common in (A.30) and (A.31), and considering the expression of i_{cd} in (A.9) and the expression of i_{cq} in (A.11), and considering the expression of $v_{L_{Tranf}d}$ and $v_{L_{Tranf}q}$ in (A.44) and (A.45), one can define or highlight the terms of (A.30) and (A.31) as:

$$v_{injcd} = v_{cd} + R_C \underbrace{\left(C_C \frac{dv_{cd}}{dt} + \omega C_C v_{cq} \right)}_{i_{cd}} + \underbrace{C_C L_{Tranf} \frac{d^2 v_{cd}}{dt^2} + \omega^2 L_{Tranf} C_C v_{cd} + \omega L_{Tranf} i_{cq} + \omega L_{Tranf} i_{cd}}_{L_{Tranf} \frac{di_{cd}}{dt}} + \omega L_{Tranf} i_{cd} \quad (\text{A.46})$$

$$+ \underbrace{v_{md} - v_{sd}}_{Grid_volt} \quad v_{injcd} = v_{Rd} + v_{cd} + v_{Ld} + v_{md} - v_{sd} \quad (\text{A.47})$$

$$v_{injCq} = v_{cq} + R_C \underbrace{\left(C_C \frac{dv_{cq}}{dt} - \omega C_C v_{cd} \right)}_{i_{cq}} + \underbrace{C_C L_{Tranf} \frac{d^2 v_{cq}}{dt^2} + \omega^2 L_{Tranf} C_C v_{cq} - \omega L_{Tranf} i_{cd} - \omega L_{Tranf} i_{cd}}_{L_{Tranf} \frac{di_{cq}}{dt}} - \omega L_{Tranf} i_{cd} \quad (\text{A.48})$$

$$+ \underbrace{v_{mq} - v_{sq}}_{Grid_volt} \quad v_{injCq} = v_{Rq} + v_{cq} + v_{Lq} + v_{mq} - v_{sq} \quad (\text{A.49})$$

(A.46) and (4.48) match (A.47) and (A.49), which lead to prove the derived math model and the dq equivalent circuits.